

STATUS OF THESIS

Title of thesis Investigation of Physical and Mechanical Properties of Friction Stir Welding on Aluminum 6092/SiC/25p/T6 Welded Plates

I UMAR BIN PATTHI

hereby allow my thesis to be placed at the Information Resource Center (IRC) of Universiti Teknologi PETRONAS (UTP) with the following conditions:

- 1. The thesis becomes the property of UTP
2. The IRC of UTP may make copies of the thesis for academic purposes only.
3. This thesis is classified as

Confidential

Non-confidential

If this thesis is confidential, please state the reason:

Blank lines for stating reasons for confidentiality.

The contents of the thesis will remain confidential for years.

Remarks on disclosure:

Blank lines for remarks on disclosure.

Signature of Author

Endorsed by Dr Mokhtar Awang, Associate Professor, Mechanical Engineering Department, Universiti Teknologi PETRONAS, Perak. Signature of Supervisor

Permanent address: PT 2413, Desa Seri Iskandar, Bandar Seri Iskandar, 32610 Seri Iskandar, Perak

Assoc. Prof. Dr.Mokhtar Bin Awang

Date : 6/5/12

Date : 6/5/13

UNIVERSITI TEKNOLOGI PETRONAS

INVESTIGATION OF PHYSICAL AND MECHANICAL PROPERTIES OF
FRICTION STIR WELDING ON ALUMINUM 6092/SIC/25P/T6 WELDED
PLATES

by

UMAR BIN PATTHI

The undersigned certify that they have read, and recommend to the Postgraduate Studies Programme for acceptance this thesis for the fulfillment of the requirements for the degree stated.

Dr Mokhtar Awang
Associate Professor
Mechanical Engineering Department
Universiti Teknologi PETRONAS
31750 Tronoh, Perak.

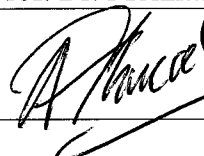
Signature:



Main Supervisor:

Assoc. Prof. Dr. Mokhtar Bin Awang

Signature:

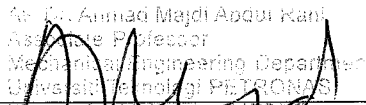


Dr. Faiz Ahmad
Associate Professor
Mechanical Engineering Department
Universiti Teknologi PETRONAS
Bandar Seri Iskandar, 31750 Tronoh,
Perak Darul Ridzuan, Malaysia

Co-Supervisor:

Assoc. Prof. Dr. Faiz Ahmad

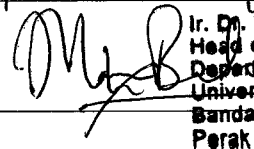
Signature:



Co-Supervisor:

Assoc. Prof. Dr. Ahmad Majdi Bin Abdul Rani

Signature:



Ir. Dr. Masri Baharom
Head of Department/Associate Professor
Department of Mechanical Engineering
Universiti Teknologi PETRONAS
Bandar Seri Iskandar, 31750 Tronoh,
Perak Darul Ridzuan, Malaysia

Head of Department:

Assoc. Prof. Ir. Dr. Masri Bin Baharom

Date:

6/5/13

INVESTIGATION OF PHYSICAL AND MECHANICAL PROPERTIES OF
FRICTION STIR WELDING ON ALUMINUM 6092/SIC/25P/T6 WELDED
PLATES

by

UMAR BIN PATTHI

A Thesis

Submitted to the Postgraduate Studies Programme

as a Requirement for the Degree of

MASTER OF SCIENCE

MECHANICAL ENGINEERING

UNIVERSITI TEKNOLOGI PETRONAS

BANDAR SERI ISKANDAR,

PERAK

APRIL 2013

DECLARATION OF THESIS

Title of thesis

Investigation of Physical and Mechanical Properties of Friction Stir
Welding on Aluminum 6092/SiC/25p/T6 Welded Plates

UMAR BIN PATTHI

I

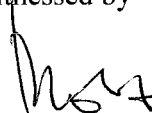
hereby declare that the thesis is based on my original work except for quotations and citations which have been duly acknowledged. I also declare that it has not been previously or concurrently submitted for any other degree at UTP or other institutions.



Signature of Author

Permanent address:PT 2413, Desa Seri
Iskandar, Bandar Seri Iskandar, 32610
Seri Iskandar, Perak

Date : 6/5/13

Witnessed by **Dr Mokhtar Awang**
Associate Professor
Mechanical Engineering Department
Universiti Teknologi PETRONAS
31750 Tronoh, Perak.


Signature of Supervisor

Assoc. Prof. Dr. Mokhtar Bin Awang

Date : 6/5/13

ACKNOWLEDGEMENT

First of all I would like extend my outmost and sincere gratitude to my supervisor Associate Professor Dr Mokhtar Awang for his guidance and support during the whole duration of my study period. Without his enthusiasm in helping me it would be impossible for me to finish or completing my research work. Next I would also like to extend my outmost appreciation to my Co-supervisors Associate Professor Dr Faiz Ahmad and Associate Professor Dr Ahmad Majdi Abdul Rani for their advice, support and useful suggestion in completing my research work.

I am also thankful to all materials laboratories technicians for their help and guidance in using the equipment. Lastly but not the least, I would like to extend my gratitude to my beloved family for their sincere support and encouragement in driving me to finish this research work.

I appreciate UTP management for providing me financial support through Graduate Assistantship (GA) scheme and also for funding the research work under STIRF code number 43/09.

ABSTRACT

Friction Stir Welding (FSW) is a relatively new welding technique and its physics is still not widely known. Compared to fusion welding, this technique reduces problem associated with metal re-solidification as the technique involves no melting stages suitable for joining high strength aerospace material such as aluminum metal matrix composite (AMMC). Initially FSW had been developed and successfully applied for welding softer material such as aluminum alloy. Scarce research had been conducted on FSW of AMMC where the material have a higher stiffness, strength and wear resistance compared to monolithic aluminum alloy. Research of FSW on aluminum 6092 series reinforce with 25% discontinuous SiC particles volume with T6 ageing (aluminum 6092/SiC_{25p}/T6) has not been reported. The objectives of this research were to compare Friction Stir Welding of aluminum 6092/SiC_{25p}/T6 plates using CNC (computer numerical control) milling Bridgeport and MTS (Material Testing System) FSW machine and also to examine the effect of different welding parameters on microstructure and mechanical properties of the welded plates. Welded samples microstructure was examined using Scanning Electron Microscopy (SEM), Energy Dispersive X-ray Spectroscopy (EDX) and X-Ray Diffraction (XRD) technique. Mechanical properties were tested using Vickers hardness test and tensile test. Tensile test was conducted according to ISO/TTA 2 (1997) standard. Microstructure observation showed re-distribution of fine and coarse SiC particle across the weld area. XRD results depicted insignificant difference of post weld stresses as well as maintained material phases. The weld center showed increase in hardness and an adequate retained material strength. In conclusion FSW caused changes in the material microstructure due to the onset of plastic deformation, no changes in weld phase were detected, increased weld hardness as well as retained weld strength were obtained.

ABSTRAK

Kimpalan kacau geseran (FSW) dikenali sebagai teknik yang agak baru dan penggunaan teknik ini masih di peringkat awal. Antara kelebihan kaedah ini berbanding teknik konvensional yang lain, adalah ia mengurangkan masalah yang berkaitan dengan pemejalanan semula kerana ia adalah teknik yang tidak melibatkan peringkat lebur. Kelebihan ini menyebabkan ia berpotensi tinggi dalam teknik kimpalan bahan aeroangkasa seperti AMMC. Pada mulanya FSW telah berjaya dibangunkan dan digunakan untuk kimpalan bahan lembut seperti aloi aluminium. Namun penyelidikan yang terhad telah dijalankan dengan menggunakan AMMC yang mempunyai kekakuan, kekuatan dan rintangan haus yang lebih tinggi berbanding dengan aloi aluminium monolitik. Penyelidikan FSW pada siri aluminium 6092 dengan pengukuhan 25% jumlah zarah selanjara SiC (aluminium 6092/SiC25p/T6) belum pernah dilaporkan. Objektif kajian ini adalah untuk membandingkan FSW aluminium 6092/SiC25p/T6 menggunakan CNC (Computer Numerical Control) milling Bridgeport dan MTS (Material Testing System) FSW machine, dan juga menyiasat pengaruh parameter terhadap mikrostruktur dan sifat mekanik bahan kimpalan. Mikrostruktur telah dianalisis dengan menggunakan Mikroskop Imbasan Elektron (SEM), Sebaran tenaga sinar-X Spektroskopi (EDX) dan Pembelauan Sinar-X (XRD). Ujian kekerasan telah dilakukan dengan menggunakan teknik ujian kekerasan Vickers. Ujian tegangan telah dijalankan mengikut ISO/TTA 2 (1997). Pemerhatian mikrostruktur menunjukkan taburan zarah halus dan kasar silika karbida (SiC) di seluruh kawasan kimpalan. Analisis mikrostruktur mendedahkan perbezaan dalam pengagihan semula zarah SiC antara zon di kawasan kimpalan yang terdiri daripada pusat kimpalan, kawasan maju kimpalan dan kawasan undur kimpalan. Keputusan XRD menggambarkan perbezaan yang tidak ketara dalam komposisi kimia kimpalan. Pusat kimpalan menunjukkan peningkatan dalam kekerasan dan pengekalanan kekuatan material yang mencukupi. Kesimpulannya FSW menyebabkan perubahan mikrostruktur bahan melalui perubahan plastic dan hasil kimpalan menunjukkan ia bukan sahaja mengekalkan sifat-sifat bahan asal kimpalan bahkan memperbaiki kualiti bahan tersebut.

In compliance with the terms of the Copyright Act 1987 and the IP Policy of the university, the copyright of this thesis has been reassigned by the author to the legal entity of the university,

Institute of Technology PETRONAS Sdn Bhd.

Due acknowledgement shall always be made of the use of any material contained in, or derived from, this thesis.

© UMAR BIN PATTHI, 2013

Institute of Technology PETRONAS Sdn Bhd

All rights reserved.

TABLE OF CONTENT

| | |
|--|------|
| DECLARATION OF THESIS | iv |
| ACKNOWLEDGEMENT | v |
| ABSTRACT | vi |
| ABSTRAK..... | vii |
| COPY RIGHT | viii |
| LIST OF TABLES..... | xii |
| LIST OF FIGURES | xiii |
| | |
| CHAPTER 1 INTRODUCTION..... | 1 |
| 1.1 Chapter Overview | 1 |
| 1.2 Background Study..... | 1 |
| 1.3 Problem Statement | 4 |
| 1.4 Research Objectives..... | 5 |
| 1.5 Scope of Work | 5 |
| 1.6 Organization of the Thesis..... | 5 |
| 1.7 Chapter Summary | 6 |
| | |
| CHAPTER 2 LITERATURE REVIEW | 7 |
| 2.1 Chapter overview | 7 |
| 2.2 Aluminum metal matrix composite | 7 |
| 2.3 Friction Stir Welding | 8 |
| 2.3.1 Tool Design..... | 8 |
| 2.3.2 Friction stir welding process..... | 9 |
| 2.3.3 Weld zones in friction stir welded sample..... | 10 |
| 2.4 Challenges in Friction stir welding on aluminum metal matrix composite | 12 |
| 2.5 Microstructure study of Friction Stir Welded material..... | 13 |
| 2.6 Mechanical study of Friction Stir Welded material..... | 17 |
| 2.7 Effect of welding parameters on friction stir welded sample | 21 |
| 2.8 Temperature distributions in Friction stir welding process | 26 |
| 2.9 XRD Analysis | 27 |

| | |
|--|-----------|
| 2.10 FSW material flow | 28 |
| 2.11 FSW comparison to conventional welding technique | 29 |
| 2.12 Chapter Summary | 31 |
| CHAPTER 3 METHODOLOGY | 33 |
| 3.1 Chapter Overview | 33 |
| 3.2 Work piece Material | 34 |
| 3.3 Design and Fabrication of tool and Clamp Assembly | 36 |
| 3.3.1 Tool Design..... | 36 |
| 3.3.2 Clamping Assembly..... | 39 |
| 3.4 Experimental Details..... | 40 |
| 3.4.1 Friction Stir Welding performed using CNC Milling Bridgeport | 41 |
| 3.4.2 Friction Stir Welding performed using MTS FSW machine..... | 42 |
| 3.5 Characterization Technique | 44 |
| 3.5.1 Scanning Electron Microscope of Welded Samples..... | 44 |
| 3.5.2 X-ray Diffraction of Welded Samples | 44 |
| 3.5.3 Tensile Test of Welded Samples | 45 |
| 3.5.4 Vickers Hardness Test | 45 |
| 3.6 Chapter summary | 46 |
| CHAPTER 4 RESULT AND DISCUSSION..... | 47 |
| 4.1 Chapter Overview | 47 |
| 4.2 CNC milling Bridgeport samples | 47 |
| 4.2.1 Weld microstructure | 48 |
| 4.2.2 Effect of welding parameter on weld mechanical properties | 49 |
| 4.3 MTS FSW machine Analysis | 52 |
| 4.3.1 Analysis of welding parameter on weld quality | 54 |
| 4.3.2 Effect of welding parameter on weld nugget microstructure | 57 |
| 4.3.2.1 <i>Tool rotation</i> | 60 |
| 4.3.2.2 <i>Tool traverse speed</i> | 65 |
| 4.3.2.3 <i>Tool tilting</i> | 69 |
| 4.3.2.4 <i>Comparison on weld zones microstructure</i> | 72 |
| 4.3.3 Effect of welding parameter on mechanical properties | 83 |

| | |
|---|-----|
| 4.3.3.1 <i>Tool rotation</i> | 85 |
| 4.3.3.2 <i>Tool traverse speed</i> | 86 |
| 4.3.3.3 <i>Tool tilting</i> | 89 |
| 4.4 Analysis of weld hardness | 89 |
| 4.5 Microstructure and mechanical comparison between CNC milling Bridgeport and MTS FSW machine | 93 |
| 4.5.1 Weld Microstructure analyses | 93 |
| 4.5.2 Weld mechanical results | 95 |
| 4.5.3 FESEM Energy Dispersive X-ray Spectroscopy Results | 96 |
| 4.5.4 XRD analyses of weld | 97 |
| 4.6 Chapter Summary | 101 |
| CHAPTER 5 CONCLUSION AND RECOMMENDATIONS..... | 103 |
| 5.1 Chapter overview..... | 103 |
| 5.2 Conclusion | 103 |
| 5.3 Recommendations..... | 105 |
| APPENDIX A..... | 105 |
| REFERENCE | 105 |

LIST OF TABLES

| | |
|--|-----|
| Table 2.1 Mechanical properties of the friction stir welded Al–TiB ₂ MMC [48] | 27 |
| Table 3. 1 Work piece Specification | 35 |
| Table 3.2 XRF analysis on Aluminum 6092/SiC _{25p} /T6 | 36 |
| Table 3.3 Equivalent standard for tool steel requirement as A681 | 37 |
| Table 3.4 Tool steel chemical composition (weight %) | 37 |
| Table 3.5 Independent parameter variables for CNC milling Bridgeport | 42 |
| Table 3.6 Independent parameter variables for MTS FSW machine | 43 |
| Table 4. 1 Tensile test of CNC milling Bridgeport samples | 50 |
| Table 4. 2 Quantitative analysis of coarse particle in the aluminum alloy matrix | 58 |
| Table 4. 3 Quantitative analysis of aluminum alloy matrix..... | 58 |
| Table 4. 4 Full spectrum EDX analysis on (a) base metal and (b) welded sample | 59 |
| Table 4. 5 Tensile test results for MTS FSW machine..... | 84 |
| Table 4. 6 Average hardness reading for MTS FSW machine welded samples | 90 |
| Table 4. 7 Tensile Test comparison between MTS FSW machine welded sample and CNC milling Bridgeport Sample..... | 95 |
| Table 4. 8 Hardness test comparison between MTS FSW machine welded sample and CNC milling Bridgeport sample | 95 |
| Table 4. 9 Lattice spacing analysis for CNC milling Bridgeport weld sample..... | 101 |
| Table 4. 10 Lattice spacing analysis for MTS FSW machine welded sample | 101 |

LIST OF FIGURES

| | |
|---|----|
| Figure 1. 1: Joining methods for MMC [8] | 3 |
| Figure 2. 1: FSW technique on a normal plates [2]..... | 10 |
| Figure 2. 2: Top view of FSW feature for butt joint [29] | 10 |
| Figure 2. 3: Location of weld nugget, TMAZ and HAZ [32] | 12 |
| Figure 2. 4: Parameter for Δ Defective welds, O defect free welds and \square limit for the friction stir welding on aluminum 6061/Al ₂ O ₃ /20 _p [33]..... | 13 |
| Figure 2. 5: Precipitate evolution between the (a) base metal, (b) fusion welded aluminum alloy and (c) Friction stir welded aluminum alloy [40]..... | 14 |
| Figure 2. 6: Transition line between the TMAZ (left side) to the advancing side of the weld nugget for (a) aluminum reinforce with 20% alumina and (b) aluminum reinforce with 10% alumina [44]..... | 16 |
| Figure 2. 7: Typical scanning electron (SE) (a) image of the retreating edge of the weld region, (b) approximate center of the weld region, (c) advancing edge of the weld region and (d) base material [47]..... | 17 |
| Figure 2. 8: Tensile tests on AMMC with Al ₂ O ₃ particulate conducted parallel (transverse) to the welding line [48]..... | 18 |
| Figure 2. 9 Tensile tests on AMMC with SiC particulate conducted (a) parallel (transverse) and (b) perpendicular (longitudinal) to the welding line [51] .. | 19 |
| Figure 2. 10: Hardness reading for welded aluminum MMC with SiC particulate [40]...20 | 20 |
| Figure 2. 11: Hardness reading for as welded and T4 heat treated aluminum composite welded sample [51]..... | 21 |
| Figure 2. 12: Variation of the hardness at the center of WZ with the welding speed at several tool speeds [30] | 24 |
| Figure 2. 13: Temperature history on temperature vs displacement TC1 and TC3 indicate reading on the advancing side while TC2 and TC4 indicate reading on the retreating side [68]..... | 27 |
| Figure 2. 14: Phase and peak intensity of (a) base metal and (b) weld nugget [60]..... | 28 |

| | |
|---|----|
| Figure 2. 15: Comparison of (a) base metal and (b) post weld structure for fusion welded AMMC reinforce with silicon carbide particulate [74] | 30 |
| Figure 2. 16: Comparison of (a) base metal and (b) post weld structure for fusion welded AMMC reinforce with alumina particulate [74]..... | 31 |
| Figure 3. 1 Experimental Flow Chart | 34 |
| Figure 3.2 Image of extruded work piece of AMMC used in this work (dimension of 12.7 mm X 127 mm X 203 mm) | 35 |
| Figure 3.3: Solid Model of the tool designed in the study | 37 |
| Figure 3.4: Isometric and right views of the FSW tool (dimension in mm)..... | 37 |
| Figure 3.5 Heat treatment processes for H13 tool steel..... | 38 |
| Figure 3. 6 Continuous cooling transformation (CCT) diagram for H13 tool steel [75] .. | 39 |
| Figure 3.7: Isometric view of clamping assembly for CNC milling Bridgeport (dimension in millimeter) | 40 |
| Figure 3.8: CNC milling Bridgeport..... | 42 |
| Figure 3.9: State of the art MTS FSW machine | 43 |
| Figure 3.10: Weld cross section | 44 |
| Figure 3.11: Geometry for tensile sample according to ISO/TTA 2 (1997) standard..... | 45 |
| Figure 3. 12: Hardness indentation made across the weld zones | 46 |
| Figure 4. 1: Onion flow of the FSW cross sectioned sample | 48 |
| Figure 4. 2: Interface between the weld nugget and the TMAZ, magnification at 500X.. | 49 |
| Figure 4. 3: Interface between the weld nugget and the TMAZ, magnification at 1000X | 49 |
| Figure 4. 4: Comparison between weld strength of welded samples and base metal (BM) using CNC milling Bridgeport | 50 |
| Figure 4. 5: Comparison between elongation to failure percentages of welded samples and base metal (BM) using CNC milling Bridgeport..... | 51 |
| Figure 4. 6: Vickers Hardness Test | 52 |
| Figure 4. 7: FSW welded sample surface shows formation of side flash..... | 53 |
| Figure 4. 8: Cross section of FSW welded sample..... | 53 |
| Figure 4. 9: Weld nugget observation in AMMC welded test sample | 55 |
| Figure 4. 10: (a) Sample with high tool rotation (1200 rpm) and (b) Sample with lower tool rotation (900 rpm) which showed formation of flash on sample with the higher tool rotation | 56 |

| | |
|--|----|
| Figure 4. 11: Formation of flashes at the edge of the crowned surface for (a) tilted sample compared to (b) un-tilted sample..... | 56 |
| Figure 4. 12: Location of (a) spot EDX for spectrum1 and (b) EDX graph indicating the SiC particulate on the indicated spot, spectrum1..... | 57 |
| Figure 4. 13: (a) Location of the spot EDX Spectrum2 (b) EDX graph indicating the grayish background as the aluminum alloy matrix, spectrum 2 | 58 |
| Figure 4. 14: Full spectrum analyses and EDX graph for (a) weld nugget (b) Base metal | 59 |
| Figure 4. 15: FESEM images of (a) Backscattered image of the welded samples and EDX mapping of (b) silicon and (c) aluminum elements..... | 60 |
| Figure 4. 16: (a) Advancing side and (b) Retreating side of weld sample with traversal speed of 125mm/min and tool rotation of 700 rpm | 62 |
| Figure 4. 17: (a) Advancing side and (b) Retreating side of weld sample with tool traverse speed of 125 mm/min and tool rotation of 900 rpm | 63 |
| Figure 4. 18: (a) Advancing side and (b) Retreating side of weld sample with traverse speed of 125 mm/min and tool rotation of 1200 rpm | 64 |
| Figure 4. 19: (a) Advancing side and (b) Retreating side of weld sample with tool traverse speed of 100 mm/min and tool rotation of 900 rpm | 66 |
| Figure 4. 20: (a) Advancing side and (b) Retreating side of weld sample with tool traverse speed of 125 mm/min and tool rotation of 900 rpm | 67 |
| Figure 4. 21: (a) Advancing side and (b) Retreating side of weld sample with tool traverse speed of 150 mm/min and tool rotation of 900 rpm | 68 |
| Figure 4. 22 (a) advancing side and (b) retreating side of the un-tilted welded sample.... | 70 |
| Figure 4. 23: (a) advancing side and (b) retreating side of the tilted welded sample..... | 71 |
| Figure 4. 24: Distribution of SiC particles in the weld regions for sample welded at tool rotation of 1200 rpm and tool traverse speed of 10 mm/min | 72 |
| Figure 4. 25: Distribution of SiC particles in the weld regions for sample welded at tool rotation of 1200 rpm and tool traverse speed of 125 mm/min | 73 |
| Figure 4. 26: Microstructure evaluations for friction stir welded sample in the Base metal | 74 |
| Figure 4. 27: Microstructure evaluations for friction stir welded sample in TMAZ region | 74 |

| | |
|--|----|
| Figure 4. 28: Microstructure evaluations for friction stir welded sample in the weld nugget | 75 |
| Figure 4. 29: Transition line between the weld nugget and TMAZ | 75 |
| Figure 4. 30: Formation of fine cracks on the coarse SiC particulate | 76 |
| Figure 4. 31: Formation of pores at the interface between the aluminum matrix and the coarse SiC particulate | 77 |
| Figure 4. 32: Distribution of reinforcement particle in the advancing side..... | 78 |
| Figure 4. 33: Distribution of reinforcement particle near the center of the weld nugget .. | 78 |
| Figure 4. 34: Distribution of reinforcement particle in the retreating side..... | 79 |
| Figure 4. 35: Mapping of aluminum distribution within the advancing side of the weld nugget | 80 |
| Figure 4. 36: Mapping of aluminum distribution within the weld center of the weld nugget | 80 |
| Figure 4. 37: Mapping of aluminum distribution within the retreating side of the weld nugget | 81 |
| Figure 4. 38: Onion like rings within the weld zone | 82 |
| Figure 4. 39: Microstructure band of segregated fine SiC particle within the weld zone, magnification at 300X | 82 |
| Figure 4. 40: Microstructure band of segregated fine SiC particle within the weld zone, magnification at 500X | 83 |
| Figure 4. 41: Elongation to failure percentage from FSW using MTS FSW machine..... | 84 |
| Figure 4. 42: Tensile test results from FSW using MTS FSW machine | 85 |
| Figure 4. 43: Influence of tool rotation on tensile strength | 87 |
| Figure 4. 44: Influence of tool rotation on elongation to failure percentage..... | 87 |
| Figure 4. 45: Influence of tool traverse speed on tensile strength..... | 88 |
| Figure 4. 46: Influence of tool traverse speed on elongation to failure percentage | 88 |
| Figure 4. 47: Tensile Test Sample..... | 89 |
| Figure 4.48: Three different locations of hardness..... | 91 |
| Figure 4. 49: Upper Section vickers hardness reading | 92 |
| Figure 4. 50: Middle section vickers hardness reading | 92 |
| Figure 4. 51: Root section vickers hardness reading | 93 |
| Figure 4. 52: (a) CNC milling Bridgeport and (b) MTS FSW welded sample | 94 |

| | |
|---|-----|
| Figure 4. 53: EDX comparison between (a) CNC milling Bridgeport and (b) MTS FSW machine welded sample | 96 |
| Figure 4. 54: XRD Peaks for CNC milling Bridgeport weld nugget sample | 97 |
| Figure 4. 55: XRD Peaks for MTS FSW machine weld nugget sample | 98 |
| Figure 4. 56: Phase analysis on weld nugget, thermo-mechanical affected zone (TMAZ) and heat affected zone (HAZ) and base metal for CNC milling Bridgeport sample | 99 |
| Figure 4. 57: Phase analysis on weld nugget, thermo-mechanical affected zone (TMAZ) and heat affected zone (HAZ) and base metal for MTS FSW machine | 100 |

LIST OF ABBREVIATIONS AND NOMENCLATURES

| | |
|----------|--------------------------------------|
| E | Young's Modulus |
| E_t | Total Elongation to Failure |
| σ | Yield stress |
| RA | Reduction of Area |
| UTS | Ultimate Tensile Strength |
| SEM | Scanning Electron Microscope |
| EDX | Energy Dispersive X-ray Spectroscopy |
| XRD | X-ray Diffraction |
| XRF | X-ray Fluorescence |
| MMC | Metal Matrix Composite |
| FSW | Friction Stir Welding |
| DRZ | Dynamic Re-crystallization |
| TMAZ | Thermal Mechanical Affected Zone |
| HAZ | Heat Affected Zone |
| MTS | Material Testing Systems |
| CCT | Continuous Cooling Transformation |
| AMMC | Aluminum Metal Matrix Composite |
| TEM | Transmission Electron Microscope |

CHAPTER 1

INTRODUCTION

1.1 Chapter Overview

This chapter presents an introduction to the research work and entails the background study, problem statement, research objectives, scope of work and thesis organization.

1.2 Background Study

Metal matrix composite (MMC) consists of a monolithic material which acts as a medium for embedded particles. The particles are usually known as reinforcement. The reinforced particles are evenly spread throughout the metal matrix resulting in a homogenous material which acts as reinforcement to the material structural properties. The resultant properties depend on the type of reinforcement embedded within the metal matrix. As an example, the introduction of ceramic particles cause the material to have a higher strength and wear resistance, better thermal resistance, making it lighter in weight, and improving friction coefficient and thermal conductivity [1].

There are two types of reinforcements that can be used in MMC. The reinforcements can either be continuous reinforcement or discontinuous reinforcement [2]. Continuous reinforced MMC are made from long strand of fibers and the unified orientation of the fibers is responsible for an anisotropy material property. On the other hand, discontinuous reinforced MMC are made from short strand of fibers or particles and the reinforcement orientations are distributed randomly resulting in isotropic

properties [2]. Both reinforcement types possess distinctive strength properties and have their own potential in different applications.

Although the introduction and development of MMC revealed its potential application, there are still remain several challenges. One of these challenges lies in its welding process. Therefore, it is important to know the fundamentals of welding process and its types that are readily available in the industry.

In welding process, materials of the same type or class are brought together and caused to joined (and become one) through the formation of primary (and occasionally secondary) chemical bonds under the combined action of heat and pressure. Welding also establishes continuity between two adjacent materials [3]. To establish continuity in joints, discontinuity at the atomic scale must be avoided which is different to mechanical joining methods [4]. Different welding technique will cause different effect on weld quality (Figure 1.1). So it is imperative to know the type of joining process that shows best result in terms of promoting continuous joining especially on aluminum metal matrix composite (AMMC). There are several welding techniques that can be readily used in joining AMMC such as solid state welding, fusion welding and others. Among the most common types of welding on AMMC material is fusion welding [5]. Although fusion welding processes show adequate retained material properties, deleterious deterioration in the material's post weld properties draws some question to its reliability.

Fusion welding on AMMC shows the effect of high heat and melting in deteriorating the materials' physical and mechanical properties. High heat and melting of AMMC cause the reinforced particle migration as well as formation of new phases within the material. To curb such defects, solid state welding technique was introduced. Potential solid state welding methods for MMC are diffusion welding, magnetically impelled arc welding and friction stir welding [6, 7].

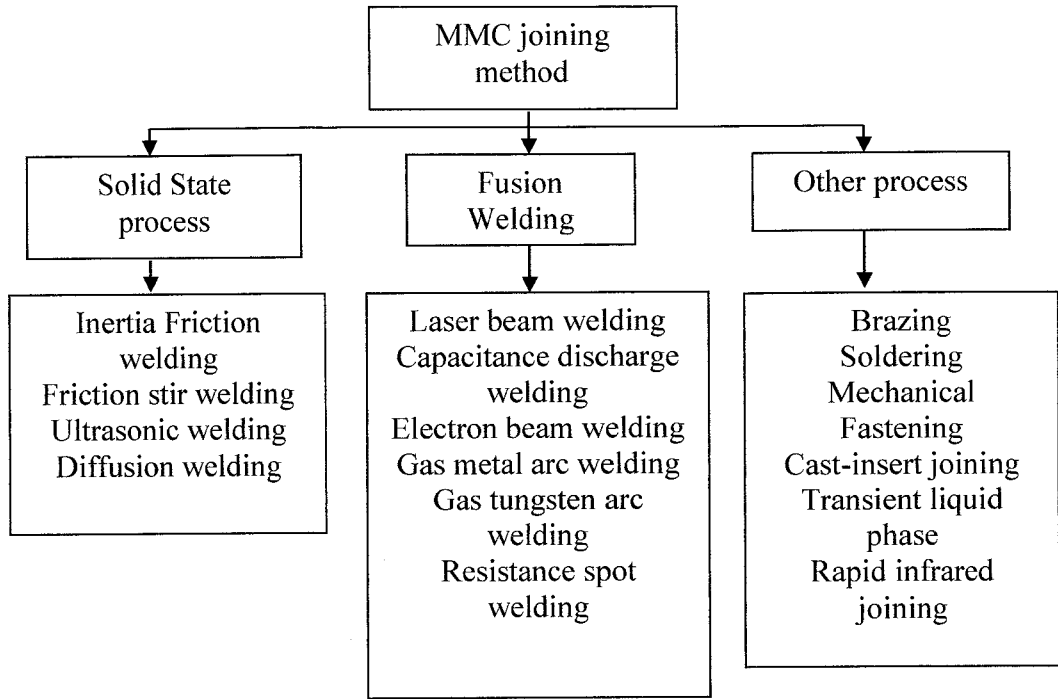


Figure 1. 1: Joining methods for MMC [8]

Friction stir welding (FSW) is a relatively new welding process invented by The Welding Institute (TWI) UK, in 1991 [8]. The joining is done in solid phase plastic transformation, without melting. Moreover, there is and no filler material is used during the entire welding process. The welding is performed by plastically joining the material through the rotation and the movement of the tool across the welding line [9]. In this technique, the joining process occurs below the melting temperature of the material which might reduce problems associated with high heat. Due to high demand for lightweight materials, FSW processes have already been implemented in the industrial fields such in the joining of aluminum in the air craft and automobile sectors [11]. Commonly, FSW is implemented on soft or ductile material such as aluminum and is rarely used for high strength or even brittle materials such as composite, high carbon steel and ceramic [2].

Several researchers have published several works on FSW of AMMC [12, 13]. However, a limited data is published on AMMC with a high reinforcement volume fraction [14]. A low volume fraction of reinforced AMMC is relatively easier to weld and

produces better weld quality compared to a high volume fraction of reinforcement. It is also known that higher reinforcement volume might lead to severe tool wear.

In 1999, NASA conducted a FSW experiment on aluminum 6092/SiC/17.5p-T6 [15]. The work concluded that FSW was only feasible to weld AMMC with SiC reinforcement lesser than 25% by volume. It is known that as reinforcement volume increases, the material tends to be stiffer and its ductility decreases. The work done by NASA however did not provide parameters that effect on the resultant welded samples in terms of their microstructure and mechanical properties. Currently, no published research work has been conducted on Aluminum 6092 reinforced with 25% SiC particulate [14].

1.3 Problem Statement

One of the concerning issues in MMC application is its joining process. Fusion welding is a common technique that is used to join such material. Although the joining process can be done adequately through conventional fusion welding processes, it was discovered that the process causes defects such as material decomposition and reinforcement particle migration and reduction in strength due to the liquidation of the welding joint. FSW provides a solution for this by introducing solid state welding where material can be joined without melting which could retain the material strength and its original properties. Initially FSW had been developed and successfully applied for welding softer materials such as aluminum and magnesium alloy. Scarce research had been conducted on FSW of AMMC where the material have a higher stiffness, strength and wear resistance compared to monolithic aluminum alloy. Research of FSW on aluminum 6092 series reinforce with 25% discontinuous SiC particles volume with T6 ageing is yet to be explored.

1.4 Research Objectives

The main objectives of this project are:

- a) To compare microstructure and mechanical properties of welded aluminum 6092/SiC/25p-T6 sample using CNC milling Bridgeport and FSW-plant by MTS.
- b) To examine the effects of welding parameter on microstructure and mechanical properties of aluminum 6092/SiC/25p-T6 welded plates.

1.5 Scope of Work

This work is focused on analyzing the effect of FSW on AMMC in terms of its microstructure and mechanical properties using CNC milling Bridgeport and FSW-plant by MTS. Aluminum 6092/SiC/25p-T6 plates with the dimensions of 12.7mm X 127mm X 203 mm were used for the experimental samples. Analysis on the effect of FSW welding parameter was conducted on the material microstructure and mechanical properties. Microstructure analysis was performed across the different weld zones which are the base metal, heat affected zone (HAZ), thermo mechanical affected zone (TMAZ) and the weld nugget. Chemical composition and lattice space analysis on the welded samples were also performed. Comparison between the samples welded by CNC milling Bridgeport and FSW-plant samples were also included in the analysis.

1.6 Organization of the Thesis

Chapter 1 presents an introduction to the joining of AMMC, the problems associated and the process involved in the joining of AMMC through FSW. The objectives and scope of work for the project are also discussed. Additionally, this chapter summarizes the objectives and provides a brief overview of the thesis.

In chapter 2, theory and comprehensive literature review about friction stir welding on AMMC is presented. The chapter reviews the critical theory behind the welding techniques and their influence on the welded material emphasizing their post

weld microstructure and mechanical effects. The chapter discusses prior work done related to this subject and also highlights the welding application.

Chapter 3 discusses the material properties and methodology used in executing the research work. Procedures applied during the friction stir welding process and also the technique used to analyze the welded material was deliberated thoroughly.

Chapter 4 presents the result and discussion obtained from the analyses. Here the resultant weld was cross sectioned and then was analyzed using different techniques. Analysis for this work was conducted using scanning electron microscope (SEM), energy dispersive X-ray spectroscopy (EDX), X-ray fluorescence (XRF), X-ray diffraction (XRD), tensile test and Vickers hardness test.

Chapter 5 discusses the conclusion of the entire research work. The discussion on the findings is summarized and resulting conclusions made from the study of FSW on AMMC are listed. A few recommendations are also presented in this chapter which includes the machine upgrades and also future experimental analysis.

1.7 Chapter Summary

This chapter presents the introduction of this project. Among the brief overview on FSW on AMMC, their application in the industry and factors that influences the welding quality were also emphasized.

The main problem to be tackled was clearly addressed in the problem statement. The problems and the need for it to be evaluated was also discussed. The chapter then presents with the research objectives, scope of work and ends with thesis organization.

CHAPTER 2

LITERATURE REVIEW

2.1 Chapter overview

This chapter provides an overview of past researches related to FSW on AMMC. The literature review includes fundamental study on the FSW mechanics such as weld parameter and tool geometry. Study on the welding effects on AMMC in terms of its microstructure and mechanical properties comprise the main component for this literature review. Effect of weld parameter was also included in the microstructure and mechanical study of FSW welded sample. Comparison studies to assess the feasibility of FSW to other welding processes were presented. Material plastic flow during welding process was also studied in terms of the flow rate and flow distribution within the weld nugget.

2.2 Aluminum metal matrix composite

As mentioned earlier, AMMC has a great potential in industrial applications. The introduction of discontinuous reinforced aluminum (DRA) AMMC to replace continuous AMMC has steadily sparked interest in the various industries. Maruyama *et al.* [16] reported that this material is being thoroughly reevaluated from basic research laboratories to materials suppliers and original equipment manufacturers across the globe.

According to a research by Maruyama *et al.* [16], the material covers variety of industries from the aerospace industry into transport, electronic and as well as in the recreational industry. This wide application is mainly due to the unique property which AMMC possesses such as good wear resistance, low thermal expansion, thermal conductivity and other properties. A review conducted by Suraj [1] further support the

reason of MMC being a potential for space application. The review also reveals that the properties of AMMC in terms of high temperature capabilities, high thermal conductivity, low coefficient of thermal expansion (CTE) and high specific stiffness and strength that makes it highly valuable for aero-space developments [17,1]. These properties are vital for adding value when used in space craft structure. [18, 19].

Improvement of MMC manufacturing in terms of cost effectiveness further increases its potential usage [1]. For example, an introduction of discontinuous reinforced MMC to replace continuous reinforce MMC, makes the fabrication of such material easier and has lower production cost [20]. The high pursuit in light weight and car engine efficiency has also paved the way to continual effort in this material's application in the automotive industry. The ongoing interest in replacing car parts that are readily made from steel and aluminum plates with superior material such as MMC is also one of the motivational drives in the material application [21,22].

2.3 Friction Stir Welding

Friction stir welding is one of the potential joining techniques for AMMC. The process involves no melting stages which is deem crucial in joining heat sensitive materials such as AMMC. In this section further detail review in-terms of tool design and welding methodology was conducted. The methodology includes welding steps and the parameters involve in the welding process. Details on the weld zones were also included in this section.

2.3.1 Tool Design

It is imperative to know the function of tool geometry as it will influence weld quality [23]. There are two main components for a FSW tool design; the pin (probe) and the tool shoulders.

The main function of the tool shoulder is to supply heat that is needed during the welding process. The shoulder is also evidently important in controlling the coupling of the plasticized material during the welding process. Material coupling is vital to ensure

that the plasticized material remains localized during the welding process. A number of shoulder designs had been developed to further enhance coupling effects. For example, slots made underneath the shoulder had significantly increased coupling of the plasticized material by entrapping the material within it [14]. Another way to localize the welded material during the welding process is by tilting or angling the welding tool. Tool tilt will help to entrap and ensure an effective flow of the welded material from the front to the back of the tool [14].

Tool pin (probe) is also an important part to stir the welding material during the welding process. Various pin designs have been developed by TWI to increase welding efficiency and weld quality. Among such designs are the newly featured screwed pin head developed by TWI known as flare-triffluteTM and A-skew^{TM b}. These tool pins showed double increment of welding speed, reduction of axial force by 20 percent, increased weld area and reduction of upper plate thinning [14]. The design of the tool pin was also found critical in welding thick plates, for example, the implementation of tapered tool pin design to weld hull of ships [24]. Several types of materials had been used for the tool used for the welding. Amongst common material used for the fabrication of the tool is H13 tool steel [25, 26].

2.3.2 Friction Stir Welding Process

The joining process occurs by plunging a rotating tool between two adjacent plates that is fixed in a position. The tool is then left to dwell in a specific position for a few second before it begins its movement along the weld line. The joining of the work piece is carried out by mixing the joint material through the rotation of the tool and supplement of heat via friction between the rotating tool and the surface of the welded plates [9]. The stirring action would allow the material within the welding line to be mixed plastically and thus producing a welded joint [3]. Melting of the material will not occur during the welding process where the welded plates only experience dynamic or static re-crystallization [27,28]. Schematic diagram of FSW process is shown in Figure 2.1. The weld top section is also displayed in Figure 2.2 which shows several common features of FSW butt welding. The parameters involved in the weld process are the tool rotation

(rpm) and tool speed (mm/min). The effects of parameters changes were discussed in several papers [14, 29, 30, 31].

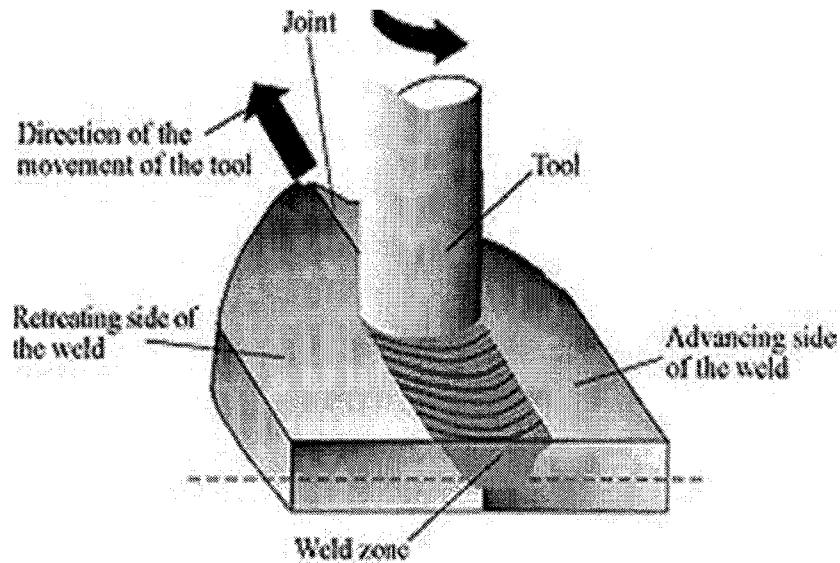


Figure 2. 1: FSW technique on a normal plates [2].

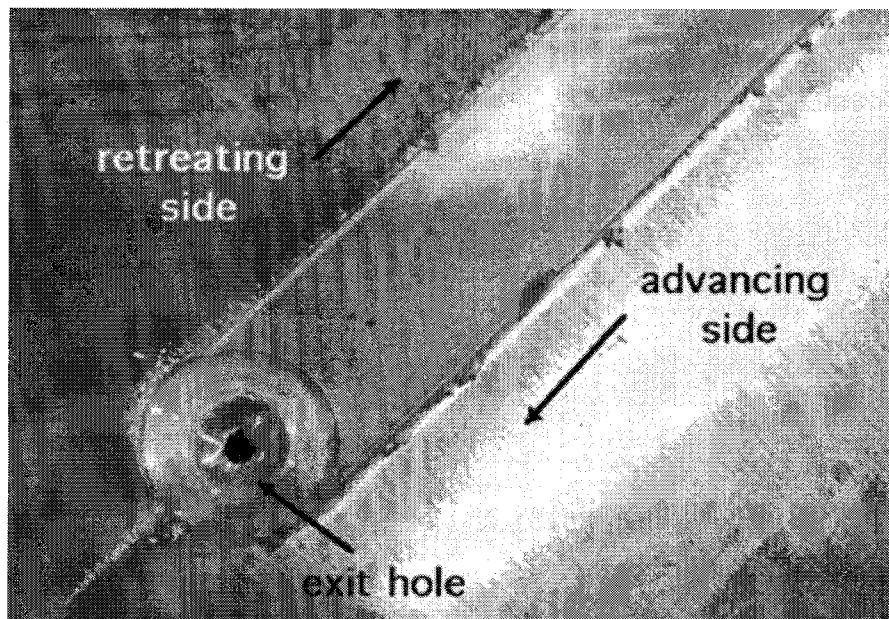


Figure 2. 2: Top view of FSW feature for butt joint [29].

2.3.3 Weld zones in friction stir welded sample

There are four specific zones that could be analyzed in a cross sectioned piece of FSW welded sample. The four zones are the weld nugget, thermo mechanical affected zone

(TMAZ), heat affected zone (HAZ) and the base material [32]. Figure 2.3 shows the location of the weld zones. Detailed explanations of the different zones are as follows:

(a) Weld Nugget

This is the main area where the welding takes place. Usually in FSW cross section piece, formation of onion like ring shape is observed in the weld nugget. This is usually caused by the intense plastic deformation process during the welding caused by the stirring action. Such deformation would result in obtaining fine and uniform grain microstructure caused by dynamic recrystallization (DRZ) [32].

The shape of the nugget zone is basically determined by the geometry of the tool being used during the stirring process. Basically, a basin shape nugget is formed by the welding process. This occurs due to an extreme deformation experience at the upper surface of the welded plate caused by contact with the tool shoulder [32].

(b) TMAZ

This region is the zone between the weld nugget and HAZ. The zone experience changes both from the temperature and plastic deformation [32]. Although the zone experience deformation caused by the stirring action, dynamic recrystallization will not occur as there is an inadequate stirring action within this zone. TMAZ can normally be recognized with its highly deform grain structure.

(c) HAZ

Heat affected zone (HAZ) is the area of the weld zones that experiences heat generated from the welding. Compared to the weld nugget and TMAZ, plastic deformation does not occur in this region [32]. The zone maintains the material's original properties. Precipitate coarsening might occur within this region due to the exposure of heat from the weld nugget. Formation of eutectic melting was not observed in this region.

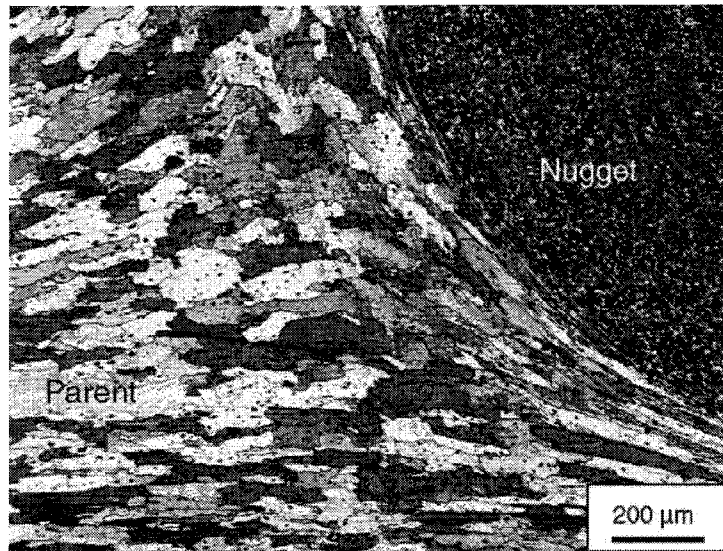


Figure 2. 3: Location of weld nugget, TMAZ and HAZ [32]

2.4 Challenges in Friction stir welding on AMMC

A research done by Marzoli *et al.* [33] showed challenges in welding AMMC compared to monolithic aluminum alloy. The type of AMMC used in this research was AA6061 reinforced with Al_2O_3 (alumina) particle. In the welding process, it was understood that in comparison to welding monolithic aluminum 6061, the energy needed to plasticize the reinforced aluminum alloy was significantly higher. Energy is supplied to the welded material in terms of heat and the stirring force from the rotating tool. Therefore, a higher tool rotation was needed to weld the reinforced aluminum alloy (AMMC). The research also showed that lower tool traversal speed was applicable to weld the reinforced aluminum alloy. Low tool traversal speed was due to the inability of the welding machine to hold a higher welding force exhibited from the reinforced aluminum alloy.

This phenomenon occurs partly due to the presence of reinforced particle. [34,35]. Figure 2.4 shows the limit in conducting the welding using FSW on AMMC.

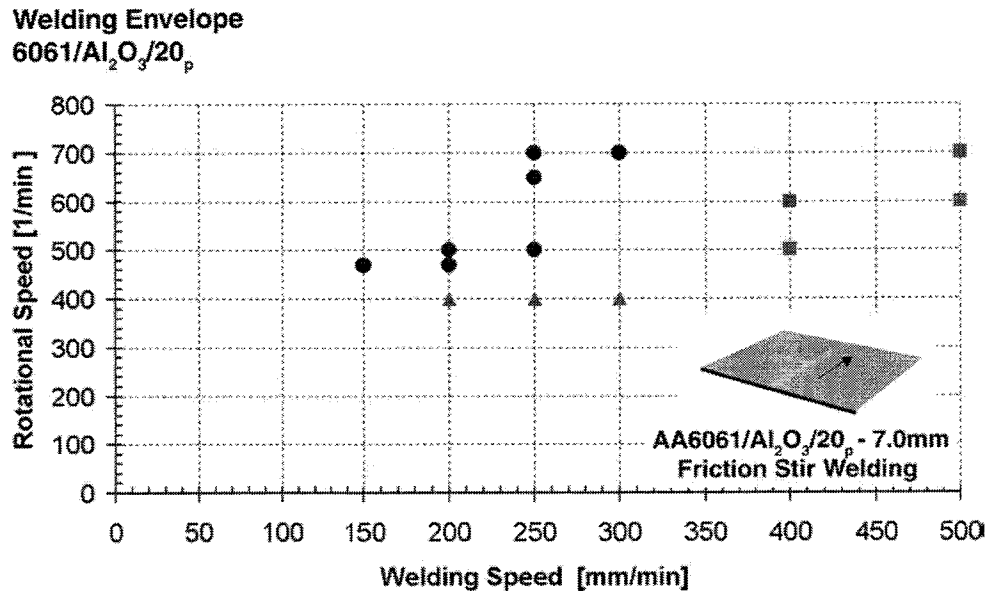


Figure 2. 4: Parameter for Δ Defective welds, O defect free welds and \square limit for the friction stir welding on aluminum 6061/Al₂O₃/20_p [33]

Adverse wear effects on the rotating tool during the welding process are also one of the main challenges in welding AMMC by FSW process. Such conditions reduce the welding efficiency where the tool has to be constantly changed after a few runs. Wear of the tool also causes the deposition of the tool particle into the welded material which changes the material properties and reduces the weld quality [32].

2.5 Microstructure study of Friction Stir Welded material

Research works on AMMC using FSW process showed improved material properties compared to fusion welding process [3]. Understanding of FSW processes on post weld properties such as its microstructure and mechanical properties still remains vague and open for discussion [36].

One of the most critical problems related to AMMC is its deleterious reaction to increase heat which changes the material's original microstructure. Previous study done by Yang *et al.* [37] showed sound and retained post weld microstructure properties of FSW welded AMMC plates. There was no evidence of liquation or eutectic structure in the post weld microstructure. Liquation is basically element separation of an alloy due to the liquid formation in the material [38, 39]. Liquation will cause the formation of

eutectic element which will deteriorate the welding properties. The study stated that there is a danger of cracking in the weld if liquidation occurred seriously.

Cao *et al.* [40] further clarified that there were no occurrence of liquation or eutectic melting by using FSW on aluminum alloy. The study showed a retained material microstructure in the post welded sample where predominant Al_2Cu precipitate in base metal maintains its original structure in the weld nugget. The study continued by comparing FSW micrograph to fusion welded aluminum alloy. SEM micrograph on fusion welded aluminum 2219 shows formation of lamellar like structure which conforms eutectic melting of Al_2Cu . Figure 2.5 shows the comparison between FSW and fusion welding on aluminum 2219 alloy. Results on fusion welding were further clarified by research conducted by Chen *et al.* [41] and Wang *et al.* [42] on laser beam welding.

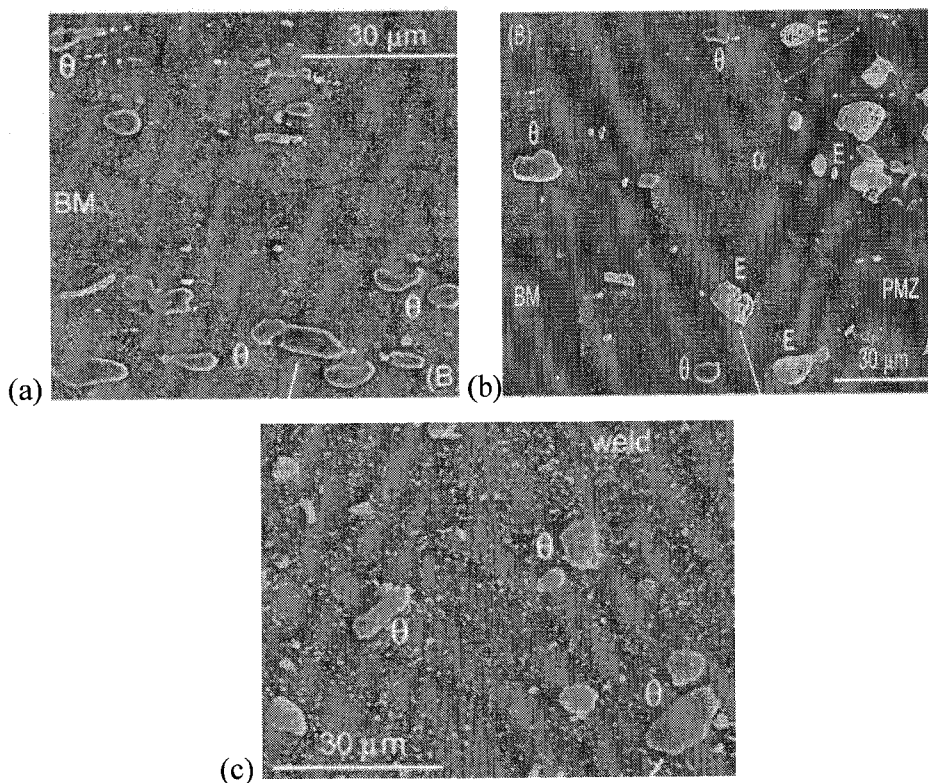


Figure 2. 5: Precipitate evolution between the (a) base metal, (b) fusion welded aluminum alloy and (c) Friction stir welded aluminum alloy [40]

A research done by Storjohann *et al.* [43] concluded that FSW gives better results when compared to fusion welding. The type of material used in this investigation was aluminum 6061 reinforced with alumina particulate and aluminum alloy 2124 reinforced

with SiC whiskers. Investigations on aluminum alloy 6061 reinforced with alumina particulate showed minimal changes in the coarse particles (alumina) distribution but a significant particulate breakage in the weld nugget. TMAZ regions showed formation of alumina clustering leading to a higher hardness in the region compared to the base metal. In comparison, observation on aluminum alloy 2124 reinforced with SiC whiskers reported a low tendency of the reinforcement particle breakage, which was partly due to the smaller particle size and a higher dynamic fluidity of the reinforcement particles. Despite that, there was a slight particle reorientation after the FSW was conducted. It was reported that most of the SiC whiskers were aligned along the welding direction.

Course particulate breakages were also reported in a similar study done by Iuri Boromel *et al.* [44]. The study showed an increase in particulate breakage within the weld nugget particularly in the advancing side (AS). Such increment in fine SiC particulate had led to an increase in the reinforcement particulate concentration in the weld nugget which is shown in Figure 2.6. Usually in unreinforced aluminum alloy, the stirring process causes a formation of a uniform grain structure but not for reinforced aluminum alloy. The study showed a distribution of unequal grain sizes in the welded zone where small and large grains were detected in the grain structure.

A research by Marzoli *et al.* [33] also shows that the welding process causes fragmentation of the reinforced material, resulting in numerous small and round particles being observed in the weld nugget. The research also stated that there was a slight decrease of hardness in HAZ but there was a little loss of hardness in the weld zone which was the result of the fragmentation of the reinforcement particle.

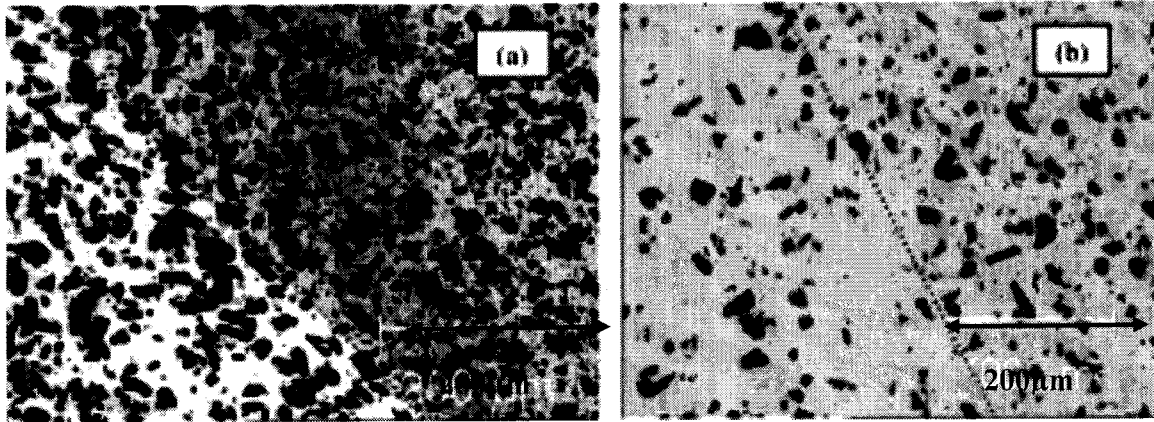


Figure 2. 6: Transition line between the TMAZ (left side) to the advancing side of the weld nugget for (a) aluminum reinforce with 20% alumina and (b) aluminum reinforce with 10% alumina [44]

Further study by Uzun [45] highlights the influence of rapid tool rotation on the reinforcement particle distribution within the weld nugget. It was known that the tool rotation causes breakage of the reinforcement particle and also the formation of pores around the reinforcement particles. The rapid rotation of the tool not only creates cracks in the particle but also causes refinement of the coarse particle within the welding zone. A thorough observation can be made on the distribution of fine and coarse particles within the weld nugget. Mapping of the weld cross section conducted in the study further proved such distribution. The rotation also caused variation in reinforcement particle density within the welding zone. One of the causes of the variation of density was the banding of the refine particle causing an onion like ring to be observed in the weld cross section [46].

Crystallographic texture study conducted by Root *et al.* [47] further adds new insight on the microstructure behavior. The type of material used was Al 6061 with 10% of Al_2O_3 (alumina). The focus of this study was the investigation of the crystallographic texture of the weld and the interfaces between the reinforcement particle and the metal matrix. The study also focused on particle redistribution and the nucleation behavior of grain after the welding process. It was observed that the stirring process causes the reinforcement particle to break and the smaller particle relocated to the advancing side and center of the tool which is shown in Figure 2.7. There were almost none of smaller alumina particle observed in the retreating side of the stirring tool. Grain structure

observation shows that smaller grain structures nucleated around the alumina particle which acted as a heterogeneous site where particle stimulated nucleation usually occurs.

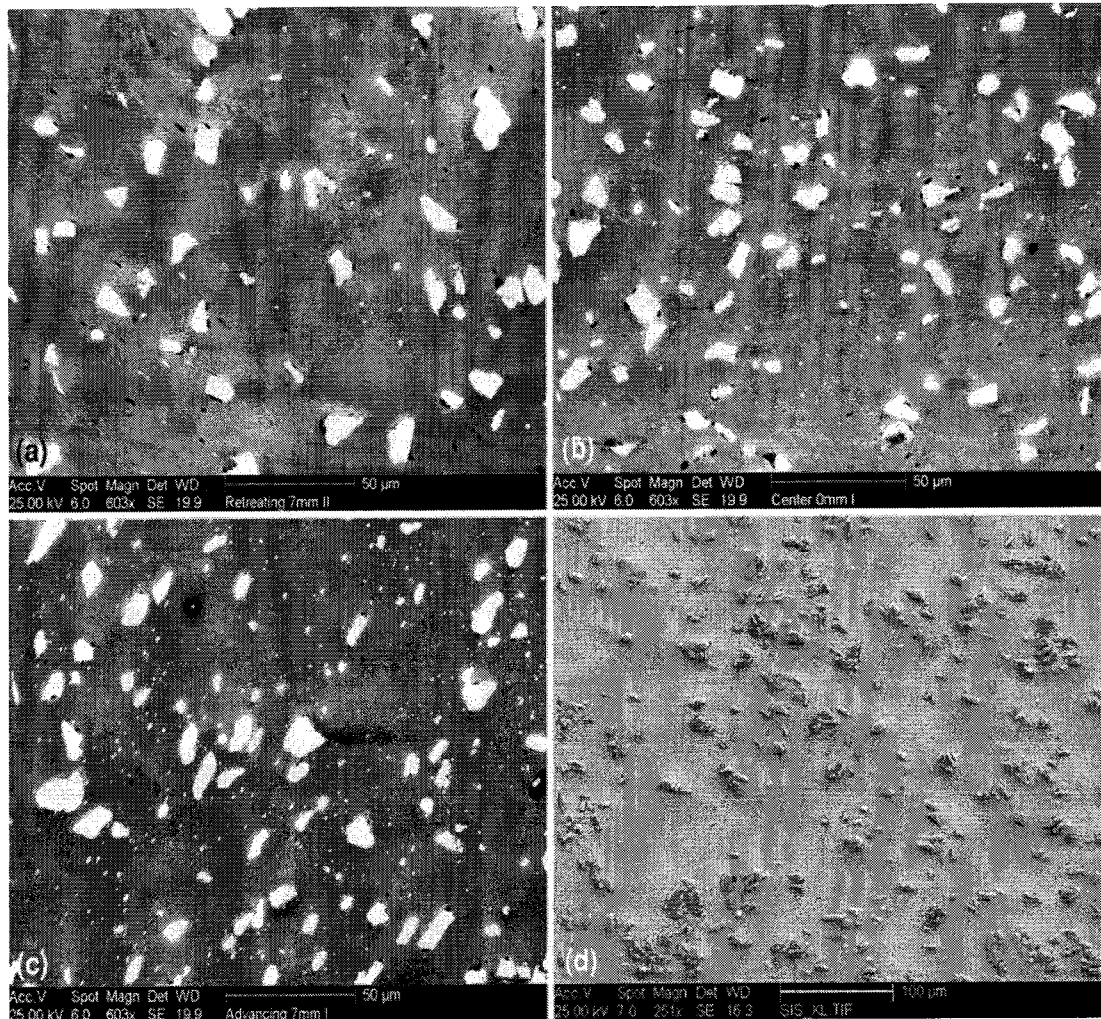


Figure 2. 7: Typical scanning electron (SE) (a) image of the retreating edge of the weld region, (b) approximate center of the weld region, (c) advancing edge of the weld region and (d) base material [47].

2.6 Mechanical study of Friction Stir Welded material

Besides changes in the welded sample microstructure, FSW also showed significant changes in the material mechanical properties. A research conducted by Cavalierea *et al.* [48] was performed to evaluate the fatigue behavior of AMMC joined by FSW. The type of material used in this study was aluminum alloy 7005 reinforced with alumina (Al_2O_3) particle. The parameters set for the welding were tool rotation of 600 rpm with welding speed of 250 mm/min. According to the study, the welding resulted in a very fine and

equiaxed grain microstructure. The weld strength was studied by performing tensile test perpendicular and parallel to the welding line. Interestingly, the result showed that there were small reductions in the yield strength and the ultimate tensile strength (UTS), and a decrease in the ductility in transversal tensile properties, shown in Figure 2.8. Similar research findings in this subject were confirmed by Su *et al.* [49] and another study done by Cavalierea *et al.* [50] using aluminum alloy workpiece. It showed that the cracks only occur in the TMAZ/HAZ region upon cracking. It also showed that the failure occurs due to the interface failure of the alumina particle with the aluminum metal matrix. Therefore, the bonding interface between the reinforcement material and the aluminum metal matrix will be an issue compromising the tensile strength of the material.

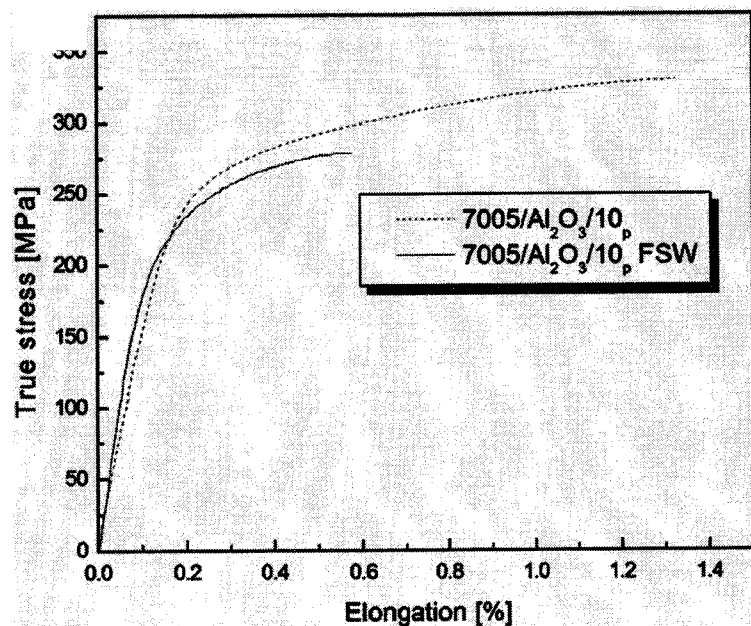


Figure 2. 8:Tensile tests on AMMC with Al₂O₃ particulate conducted parallel (transverse) to the welding line [48]

FSW study by Feng *et al.* [51] conducted on AMMC reinforced with SiC particulate also showed an increase material strength when compared to the parent material as shown in Figure 2.9. This was mainly attributed to the onset of SiC particulate refining and the dynamic recrystallization (DRZ) of the aluminum grain during the welding process [52, 54]. The material strength was also contributed by homogenous distribution of the SiC particle during the welding process itself.

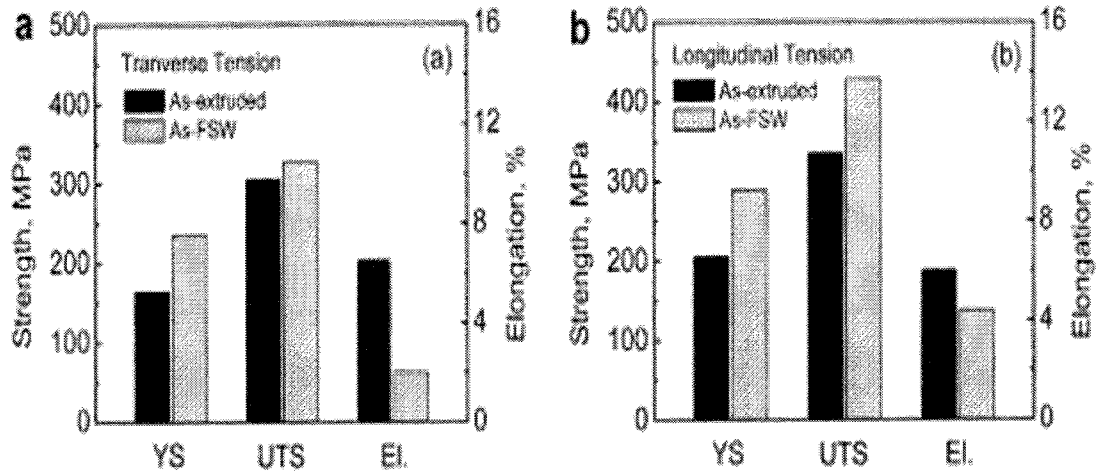


Figure 2. 9 Tensile tests on AMMC with SiC particulate conducted (a) parallel (transverse) and (b) perpendicular (longitudinal) to the welding line [51]

It was also known that through FSW, the hardness of weld was retained or slightly softer compared to the base metal [55-58]. A micro hardness test which can be seen in Figure 2.10 shows hardness distribution across the welded zone in FSW post weld sample [57]. The reading showed a slight decrease in hardness when compared to the parent metal.

According to a study by Gopalakrishnan and Murugan [59], such decrease in the weld nugget hardness was attributed to the disruption caused by the reinforcement particulate on to the dynamic re-crystallization process. Such disruption caused a decrease in fine grain distribution within the weld nugget which slightly affects the weld hardness.

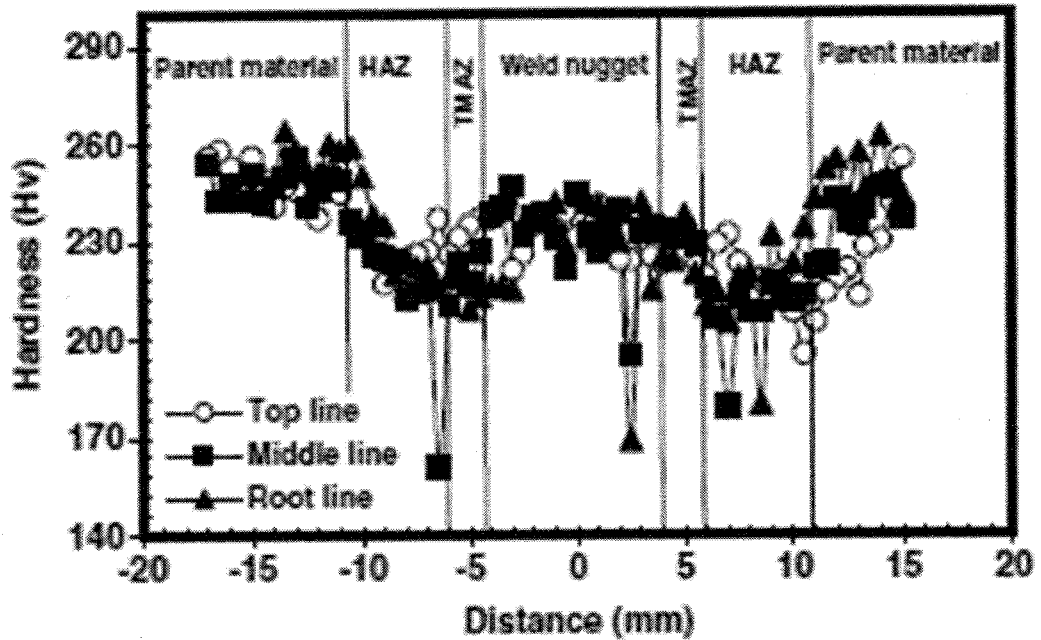


Figure 2. 10: Hardness reading for welded aluminum MMC with SiC particulate [40]

Other similar study by Feng *et al.* [51] and Thangarasu *et al.* [60] showed contradictory reports of weld hardness increment in the weld nugget. This occurred due to the knocking and chipping effect of the coarse reinforcement particle during the stirring process causing an increase density. The study also showed that the weld hardness across the welding zones, that is, TMAZ, HAZ and the weld nugget were similar after the weld T4 heat treatment. Similar hardness distributions were caused by the dissolving of prior weld precipitate and then reappeared again after the weld cooled. Such development caused precipitation-strengthening effect across the weld zones. Figure 2.11 shows the resultant micro hardness across the weld zones.

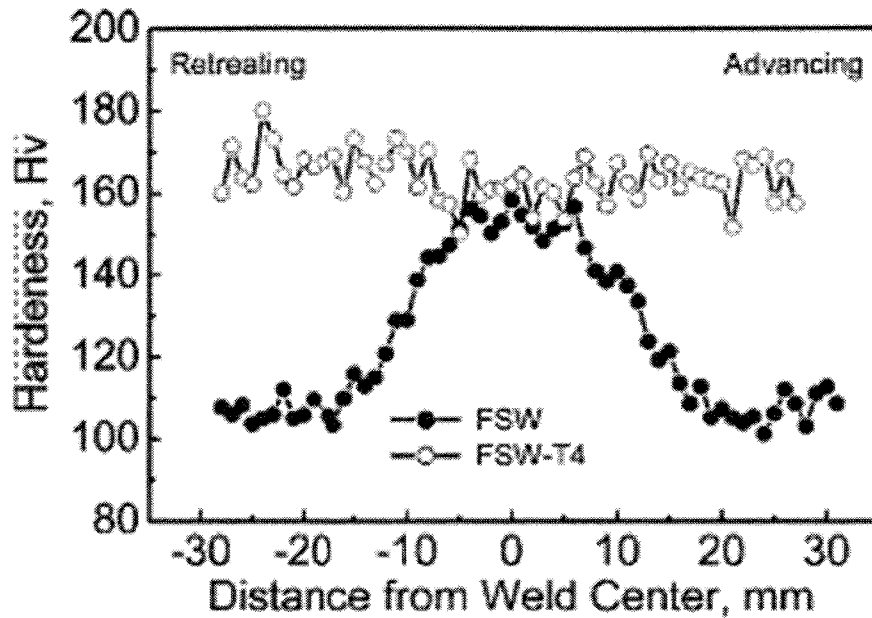


Figure 2. 11: Hardness reading for as welded and T4 heat treated aluminum composite welded sample [51]

A study conducted by Storjohann *et al.* [43] FSW also showed a slightly softer and scattered hardness distribution in the DRZ (weld nugget) region when compared to the base metal. The material hardness was not well distributed in the DRZ region, which was partly due to the irregularity of the metal flow at different places. Suitable parameter for smooth metal flow that ensures even distribution must be noted. It was also reported that a high density of dislocation occurs in the DRZ region which leads to a higher hardness compared to the HAZ region that has fewer dislocations. The density of the dislocation depended on the extent of heating and cooling in the welding region.

2.7 Effect of welding parameters on friction stir welded sample

It is important to understand the effect of tool geometry and welding parameters on the weld line. There is scarce work related to this subject using AMMC. An example is a pilot research work by NASA [15] which did not provide parameter effect on the welded samples in terms of its microstructure and mechanical properties. However, various works on welding parameters analysis have been conducted using monolithic aluminum

alloy. Those works can give an overall idea of the effect of welding parameter changes on AMMC.

A research conducted by Gaafer *et al.* [30] showed the influence of the tool rotation and welding speeds on the welding quality. The type of material used in this study was AA7020-O aluminum alloy plates. Results showed that an optimal welding condition was reached at 1400 rpm with the welding speed of 20-40 mm/min. The research observation showed that at low tool rotational speed and high traverse speed, the heat generated was insufficient. This contributes to the formation of cavities or tunneling defect which was observed in the weld nugget. However, at a higher tool rotational and lower traverse speeds, an excess of heat was generated from the rotating tool. Heat excess causes excessive material fluidity which also causes similar formation of cavities or tunneling defect in the weld nugget. The study also included the influence of weld parameters on the weld microstructure. It was known at the primary phase that due to the re-crystallization of the aluminum grains, uniform structure is formed. As the tool rotational speed increased, it was seen that the aluminum grain also increase in size. An increase in the tool rotational speed caused a higher heat input and slower cooling rate in the weld zone which contributed to the grain size increment. Formation of Al_2O_3 was observed in the center of the welding zone at 1800 rpm and 20 mm/min. This layer also caused changes in the mechanical and corrosion resistant properties of the joint product.

Han *et al.* [61] also tried to relate the influence of welding parameters on weld defects. The result shows that as welding speed increases from 124mm/min to 267 mm/min, the onset of tunnel type voids was significantly visible on the weld nugget. An early detection of defects was observed at an excessive tool rotational speed of 1800 mm/min and weld speed of 124 mm/min. The research also correlates such phenomenon to the inadequate heat input and high cooling rate due to high weld speed. The second reason for formation of defects is an excessive tool rotational speed and inadequate pressure from the tool shoulder which causes chipping or flash formation [62].

Hao *et al.* [63] validated the influences of tool rotational speed on the material grain sizes. Their work showed a significant increase in grain size as tool rotation was increased from 400 to 1200 rpm and tool speed decreased from 400 mm/min to 100

mm/min. The increase size of the grain was attributed to the increase heat input which caused grain coarsening and led to increase in grain sizes causes softening of the weld area.

FSW parameters investigation conducted by Sharma *et al.* [64] further explained the influence of parameter changes on the material microstructure. Parameter manipulation was basically performed on the weld speed and tool rotation. The study showed that as welding speed increased and tool rotation decreased the average grain sizes also tend to decrease. Results also showed an improvement in the weld mechanical properties. This parameter changed results in an increased heat input within the stirring zone. Such increase in heat input would improve material fluidity which will result in a homogenous weld nugget microstructure. However, by increasing welding speed, the results showed an increase in grain sizes. Increase in grain sizes was attributed to limited time available for the stirring due to the rapid movement of the tool.

A study that was carried by Kim *et al.* [62] showed the influence of welding parameters on the particle distribution within the stirring zone. The study was performed on cast aluminum plates which show the distribution of Si particles within the stirring zones. The result showed that as welding speed increased from 250mm/min to 750 mm/min; the size of the particles decreased. The research explained that such observation was due to the limited heat input caused by the rapid movement of the tool. Limited heat supplies cause a decrease in material fluidity and stiffen the aluminum matrix. A decreasing supply of heat caused the Si particles to grind with the stiffer aluminum matrix resulting in increased of fine Si particles.

Gaafer *et al.* [30] also investigated the influences of weld parameters on the hardness profile. No changes in the material hardness were witnessed at the increase of rotational speed of 1120 rpm to 1400 rpm. However, the hardness in the center of the welding nugget increased as the tool traverse speed was increased to 1800 rpm. Figure 2.12 shows the influence of welding speed to the weld hardness. Escalation of the weld hardness is due to the increasing effect of the dynamic recrystallization caused by the rapid tool rotation.

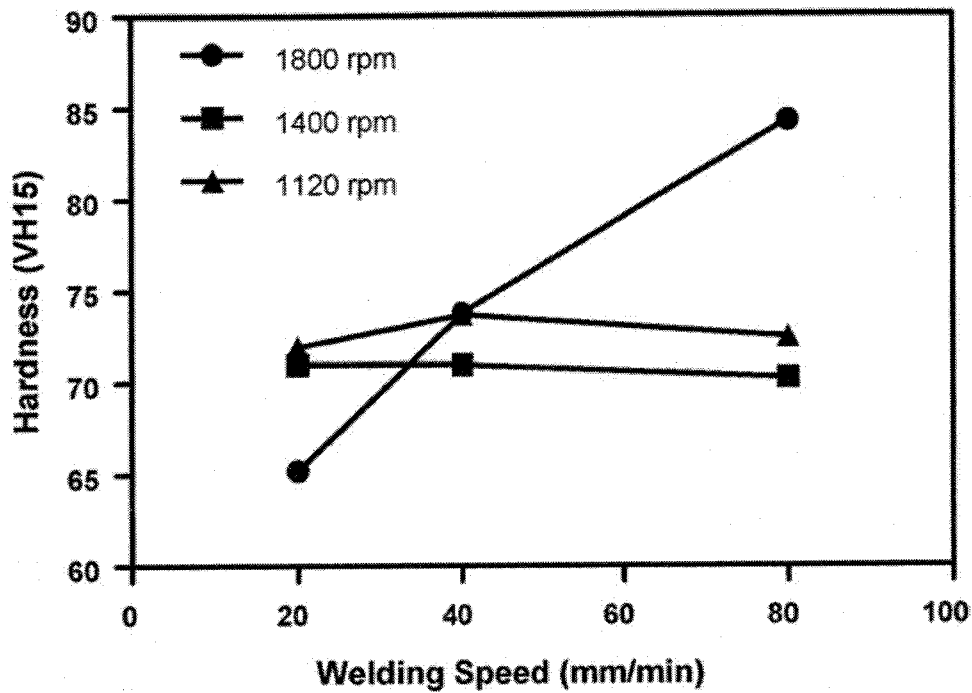


Figure 2. 12: Variation of the hardness at the center of WZ with the welding speed at several tool speeds [30]

Another correlated FSW study on aluminum alloy attempted to relate different probe geometry with the welding microstructure and mechanical properties. The study was carried out by Vijay *et al.* [65] on the relationship of dynamic flow versus the static flow during FSW plastic deformation. Squared tool pin head shows more desirable result when compared with other probe geometry because of its larger pulse rate (pulse/s). Pulse was generated from the sweeping of the tool edges into the welded material. The result showed better material fluidity around the tool pin when compared to other pin geometry. Such conditions caused better grain refinement to the onset of dynamic re-crystallization within the weld nugget and thus yielding better material strength [3]. The result is displayed in Table 2.1.

Table 2.1 Mechanical properties of the friction stir welded Al–TiB2 MMC [65]

| Types of tool pin profile | Average tensile strength (MPa) | Average (%)elongation | Joint efficiency (%) |
|---------------------------|--------------------------------|-----------------------|----------------------|
| Tapered square | 223.33 | 5.32 | 78.92 |
| Tapered hexagon | 247.89 | 6.67 | 87.59 |
| Tapered octagon | 245.27 | 6.22 | 86.67 |
| Square | 281.51 | 6.37 | 99.47 |
| Hexagon | 262.29 | 5.83 | 92.68 |
| Octagon | 240.00 | 3.39 | 84.81 |

Lorrain *et al.* [66] studied the effect of using unthreaded pin to weld AMMC plate. The research acknowledges the fact that using flat or threaded pin will prevent defects and improve weld quality. The study also explained that by using such design the tool would also be exposed to high wear where the threaded pins will be unthreaded and flat design will be rounded off. Study shows similar material flow between in the unthreaded tool pin when compared to common threaded tool pin. Unthreaded tool pin showed low flow motion observed at the bottom edge of the weld zone due to unthreaded pin design. This effect was reduced by using a cylindrical tapered pin with a three flat design.

Ramulu *et al.* [67] studied the effect of tool shoulder diameter on aluminum alloy. Three diameter values were chosen for the welding process that is 18mm, 15mm and 12mm. All shoulder diameters showed a defect free weld. Although good weld quality was achieved but as the tool shoulder diameter increased, a higher torque and axial force were required for the welding process. These factors will reduce welding efficiency

2.8 Temperature distributions in Friction stir welding process

Temperature is an important factor in determining the quality of weld in FSW process. Temperature influences the residual stresses, grain sizes and the overall strength of the welded joint [3]. So it is imperative that the welding temperature is kept within the optimum value to ensure weld quality.

A research by Yuh *et al.* [68] attempted to measure heat distribution across the welding line during the stirring process. The research was conducted by measuring the temperature distribution across the welding from both advancing side and retreating side using thermocouple sensors on an aluminum alloy plate. The samples were then tested using tensile strength to determine weld quality. Based on their results the optimum temperature values were at 365 °C and 390 °C. The result also showed that the advancing side of the weld showed a higher temperature reading when compared to the retreating side as shown in Figure 2.13. Such low temperature would not cause material melting for most Al-Cu-Mg-Si alloy where the melting temperature will be at 660 °C [69]. Low heat dispersion during the welding process was also evident by heat flux modeling conducted by Hamilton *et al.* [70]. Despite that there is certain difficulty associated to temperature analysis. The problem was the difficulty to analyze heat variation directly in welding area as the rotating tool could damage the thermocouple sensor. Infra-red heat sensors can be applied to detect temperature changes within the welding region, but it would only identify changes within the welding surface.

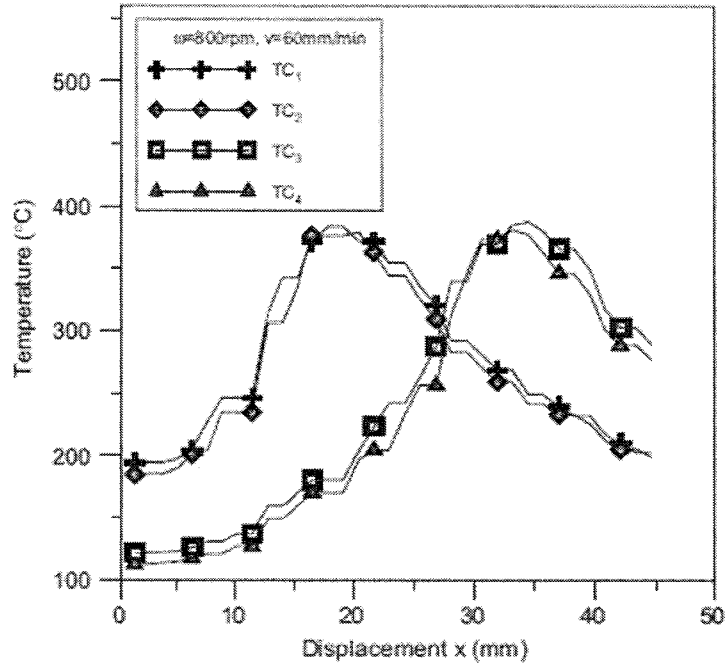


Figure 2. 13: Temperature history on temperature vs displacement TC1 and TC3 indicate reading on the advancing side while TC2 and TC4 indicate reading on the retreating side [68]

2.9 XRD Analysis

XRD analysis reveals interesting information regarding weld composition in the post weld sample. A study conducted by Bozkurt *et al.* [64] on phase analysis showed similar material phases in the post weld XRD analysis. However, there was decrease in peak intensity due to partial phase dissolution. Formation of SiO_2 phase due to the entrapment of O_2 gasses during the stirring action was also reported. Formation on Al_4C_3 phase was also not detected in the post weld analysis which commonly develops in fusion welded samples. XRD analysis is shown in Figure 2.14.

Feng *et al.* [60] also showed similar result in terms of decrease peak intensity in his XRD analysis on the welded joint. The study concluded that decrease in peak intensity was related to partial phase dissolution during the welding process. Most of the partial dissolution of the peak intensity would take place within the weld nugget. The

result from the study showed similar peak intensity in the HAZ when compared to the base metal. Significant increase in phase dissolution was obtained by T4-treatment.

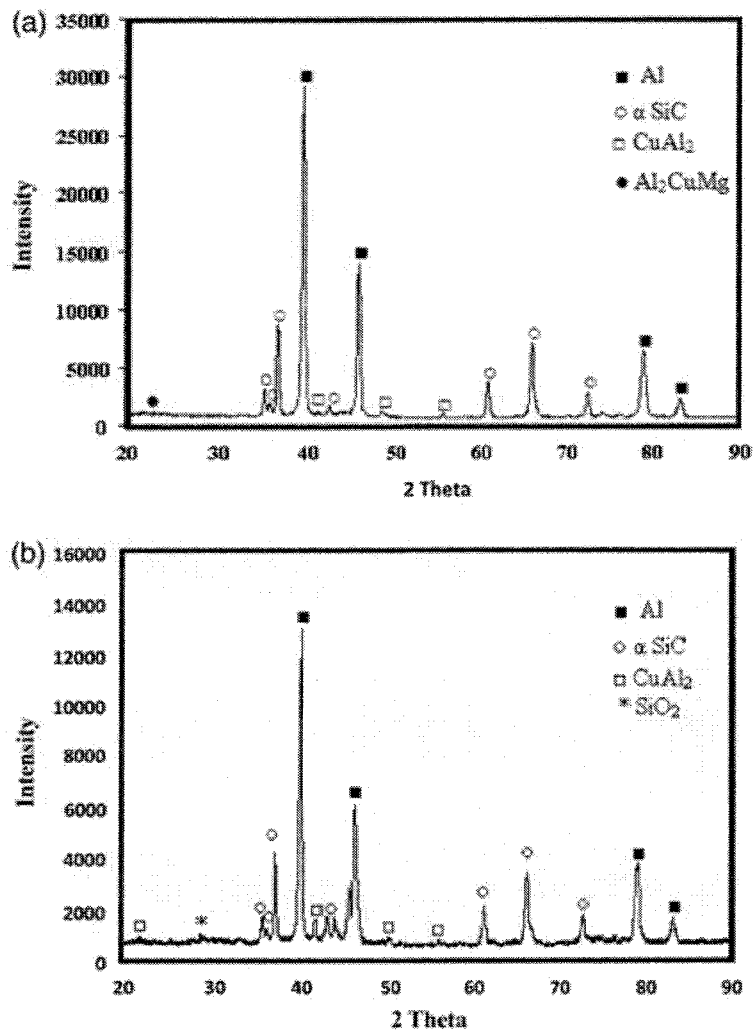


Figure 2. 14: Phase and peak intensity of (a) base metal and (b) weld nugget [60]

2.10 FSW material flow

Study on the material flow both from the advancing side and the retreating side of the tool is important in this area. Therefore, Plastic flow characteristics will influence post-weld microstructure and mechanical properties.

Past research performed by Root *et al.* [47] showed that the material flows from both retreating side and advancing side of the tool were not symmetry. The study showed

that the velocity of the advancing side is much higher when compared to the retreating side. This phenomenon resulted in a better welding quality in the advancing side of the weld due to higher plastic deformation. A number of studies on material flow also showed similar result in terms of the flow velocity between the advancing side and the retreating side [18,20,71-73].

Through computer modeling, an anticipation of the flow modeling could be mapped. A study by Reynolds [71] was conducted to model the material flow movement around the tool during the welding process. The study showed that material flow around the welding zone can be classified into three different zones that are near the top of the weld, mid-section of the weld and lastly the bottom of the weld. The zones were described by the variations in the material flow. Near the top of the weld the material was rotated along the welding axis and deposited in the advancing side of the tool. While in the mid-section of the weld, the material was deposited on the back side of the tool. The research also showed that the material in the mid-section was deposited behind the tool by no more than one pin diameter. It could be seen that the material in the mid-section traveled around the welding line through the retreating side and deposited behind the tool approximately by a diameter of the welding tool. Lastly, near the bottom side of the weld, the material experienced similar but smaller flow movement compared to the top side of the weld. The material flow movement was limited due to the presence of the backing plate.

2.11 FSW comparison to conventional welding technique

FSW has a potential to replace conventional welding techniques used for joining MMC. FSW reduces defects caused by liquidation that result in particle depletion and changes in the material microstructure. The refinement of the reinforcement particle through FSW further enhances the reliability of the material's physical properties.

Fusion welding is one of the common methods used in AMMC joining. Among successful fusion welding methods to join AMMC are electron beam and laser beam welding. Although such welding technique was successful used, deleterious chemical reactions were not successfully avoided.

Storjohann *et al.* [74] studied AMMC joining using laser beam welding process. They used AMMC reinforced with alumina particles and AMMC reinforced with SiC whiskers. Their study found difficulties in joining AMMC through fusion welding processes. The results showed that the weld penetration for the welding process is relatively small and a decrease in density of the reinforcement particle in the weld nugget. The decrease in reinforcement density was due to the migration phenomenon that is usually associated with fusion welding processes. The research observation found clumping of Al_2O_3 particles and porosity in the weld zone. AMMC reinforced with SiC whiskers also showed several problems related to high heat intensity through the usage of laser beam welding. The result showed occurrence of porosity and the formation of Al_4C_3 dendritic particles within the weld zone. Al_4C_3 was formed by the deterioration of the SiC whiskers caused by high heat intensity and reaction of the separated carbon with the aluminum matrix. Al_4C_3 formation and the onset of reinforcement particle migration would definitely cause detrimental deterioration to material strength. Figures 2.15 and Figure 2.16 show that weld defects were found on AMMC welded joint by laser beam welding.

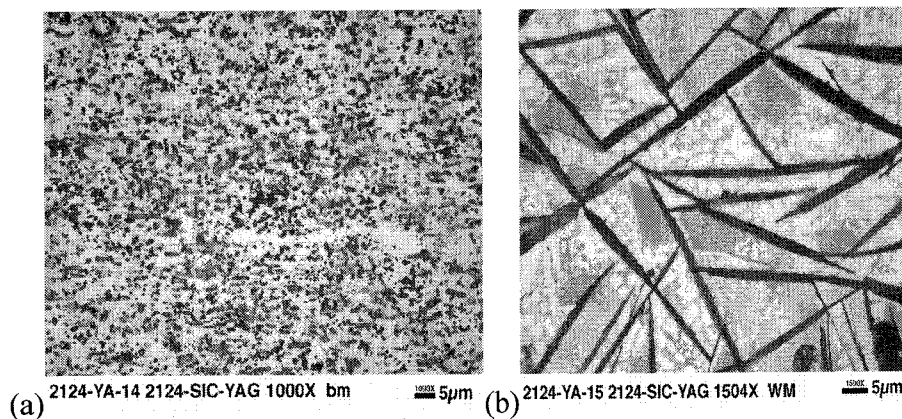


Figure 2. 15: Comparison of (a) base metal and (b) post weld structure for fusion welded AMMC reinforce with silicon carbide particulate [74]

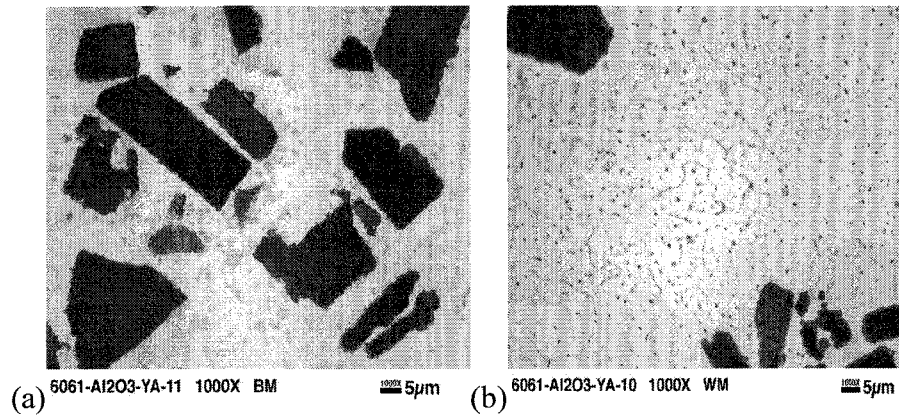


Figure 2. 16: Comparison of (a) base metal and (b) post weld structure for fusion welded AMMC reinforce with alumina particulate [74]

2.12 Chapter Summary

This chapter has presented the theoretical knowledge and literature review on the friction stir welding of AMMC. The discussion in the chapter begins with an introduction to FSW processes and continued with discussion on FSW mechanism, welding parameters and types of tool design.

Furthermore, key studies related to post weld microstructure and mechanical properties were thoroughly discussed here. A comparison study on the difference of weld microstructure and mechanical properties between fusion welding and FSW were also incorporated. Next the effect of welding parameters on the post weld microstructure and mechanical properties were reviewed. Besides that, material flow visualization was also studied in order to understand the mechanism that influences weld properties. Temperature studies on FSW were also discussed in the literature review. Material and FSW application were incorporated in the literature review as well.

From literature review, it is understood that various researches have been conducted systematically on aluminum metal matrix composite. It was found that previous studies limited the type of aluminum composite used with most of them using aluminum 2xxx series. Limited research was also found using a high reinforcement volume percentage because of various challenges associated with it. Therefore, it is necessary to expand research on FSW using different aluminum alloy series with a high

reinforcement volume percentage such as aluminum 6092/SiC/25_p/T6. This material, with its unique properties, is highly valued especially in the aerospace industry. There is also limited study that had been performed to relate welding parameters to on AMMC welded sample in terms of its post weld microstructure and mechanical properties.

CHAPTER 3

METHODOLOGY

3.1 Chapter Overview

This chapter embodies the material used in the welding process, tools and clamping assembly design, experimental setup, welding procedures and weld analysis techniques. Welded samples were analyzed using a Scanning Electron Microscope (SEM), Energy Dispersive X-ray Spectroscopy (EDX), X-ray diffraction (XRF), Universal Testing machine and Vicker's hardness test. Two types of machines were used in the experiment which were CNC milling Bridgeport and MTS FSW machine.

The research work begins with workpiece characterization to conclude elemental properties of the material. Next, tool and clamping design and fabrication were discussed as well as an evaluation on the tool material selection was also discussed. Later, welding tests were conducted on two separate machines, they are, CNC milling Bridgeport and MTS FSW machine. Three tests were conducted on the CNC milling Bridgeport while eight tests were conducted on the MTS FSW machine. Finally, methodology of finding weld microstructure and conducting mechanical test are discussed in this chapter. SEM, EDX and XRD were used for the material characterization. Weld hardness was tested using Vickers hardness test while weld strength was tested using tensile test. The experimental flow chart is presented in Figure 3.1.

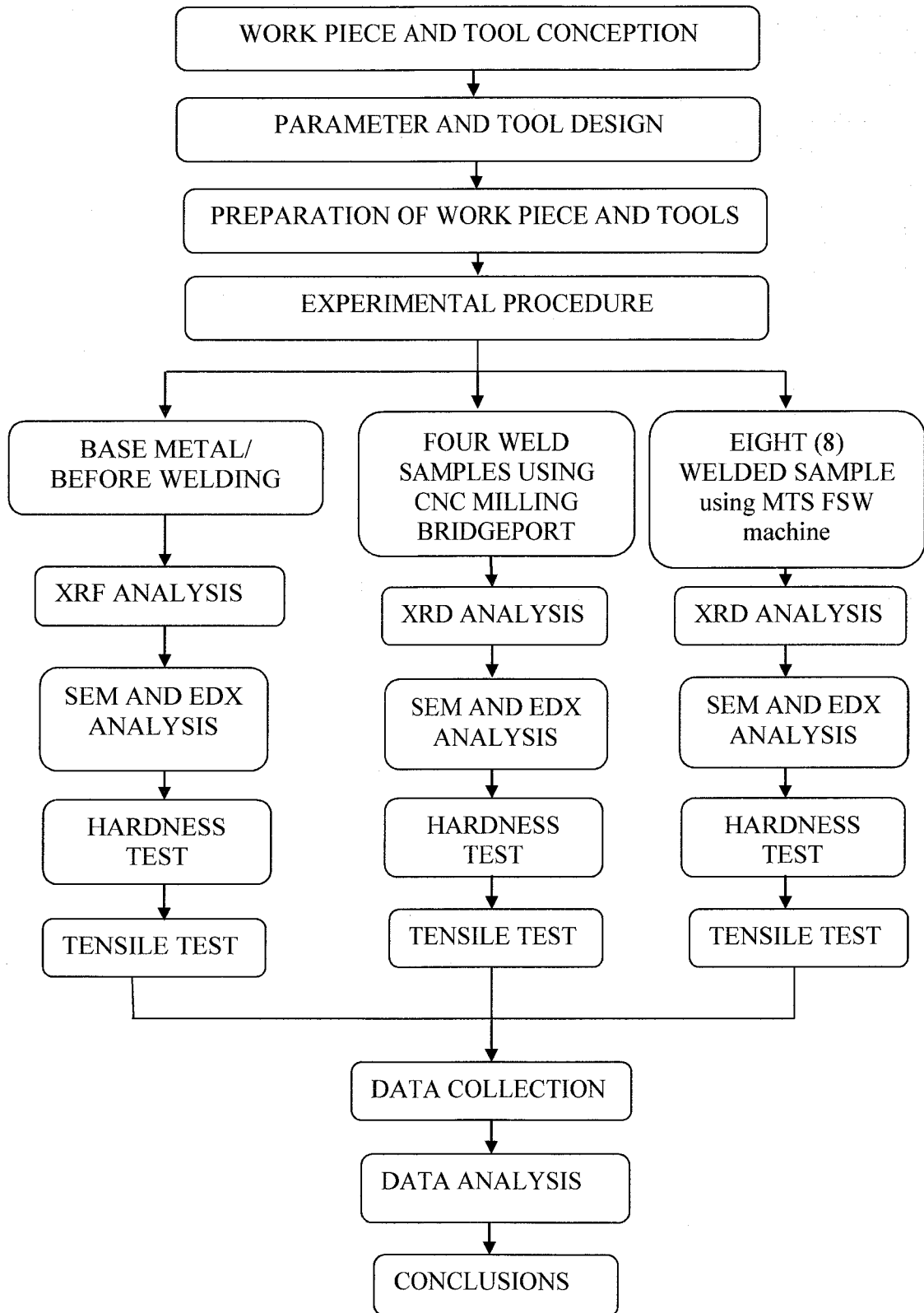


Figure 3. 1 Experimental Flow Chart

3.2 Work piece Material

In this research, an extruded aluminum 6092 reinforced with 25 volume percentage SiC particles and T6 heat treated as shown in Figure 3.2. Table 3.1 and Table 3.2 show the specifications and chemical composition of the aluminum composite used in the study. The material is known for its good electrical conductivity, corrosion resistance, is light in weight and possesses great strength [2].

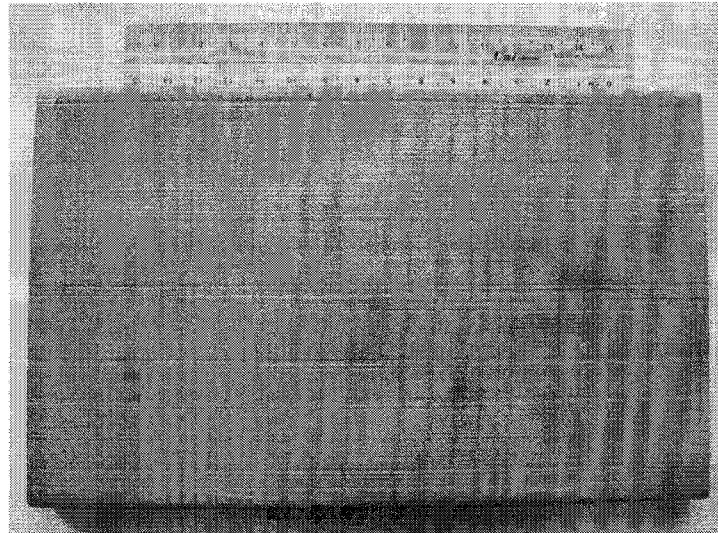


Figure 3.2 Image of extruded work piece of AMMC used in this work (dimension of 12.7mm X 127mm X 203mm)

Table 3. 1 Work piece Specification

| | |
|------------------------------|---------------------------|
| Matrix alloy | 6092 -T6 |
| Reinforcement | SiC particulate |
| Reinforcement Volume loading | 25% |
| Dimensions | 12.7 mm X 127 mm X 203 mm |
| Type of extrusion | Sheet plate |

Table 3.2 XRF analysis on Aluminum 6092/SiC_{25p}/T6

| Element | Wt% |
|---------------|-------|
| Si | 0.72 |
| Fe | 0.13 |
| Cu | 0.77 |
| Mg | 0.98 |
| Mn | 0.01 |
| Ti | 0.01 |
| Cr | 0.01 |
| Zn | 0.02 |
| O2 | 0.31 |
| Other element | 0.15 |
| Al | 96.89 |

3.3 Design and Fabrication of tool and Clamp Assembly

3.3.1 Tool Design

The material used for the welding tool is 2344/RDC 2V which is shown in Table 3.3. The material is specifically chosen for its properties in-terms of its hardness and high melting point. The material's chemical composition is shown in Table 3.4. Upon purchasing, the material is machined using CNC lathe Bridgeport to the required shape. A tapered probe concept is chosen because of its reliability to weld thick plates [26]. Screw like features on the tool probe was not incorporated in the design because of the high wear rate during the welding process. Modification on to the tool shoulders such as scroll features was also avoided in order to compare coupling effects by tilting the tool by 3 degrees. The material shape and dimensions are shown in Figure 3.3 and Figure 3.4, respectively.

After the material was machined to the required shape (Figure 3.4), heat treatment was conducted on the material for 7 hours which is shown in Figure 3.5. The detail of the heat treatment steps are as follows, first the welding tool was inserted in the tube furnace and preheated initially for two hours to increase temperature from 24 – 732°C. Next, the welding tool was constantly preheated; slowly from 732 - 760°C for another two hours. Then the temperature was raised to 1000°C for one hour. After the material reached to the maximum temperature of 1000°C air quench was conducted to room temperature (24°C) for two hours. Air quenching was conducted for this type of material as rapid quenching by water or oil would cause cracking. Heat treatment was conducted according to the continuous cooling transformation (CCT) diagram as shown in Figure 3.6 [75]. The intended hardness from 597 HV to 603 HV was reached from the heat treatment process. Original material hardness as obtained from the vendor is 241 HV in annealed state.

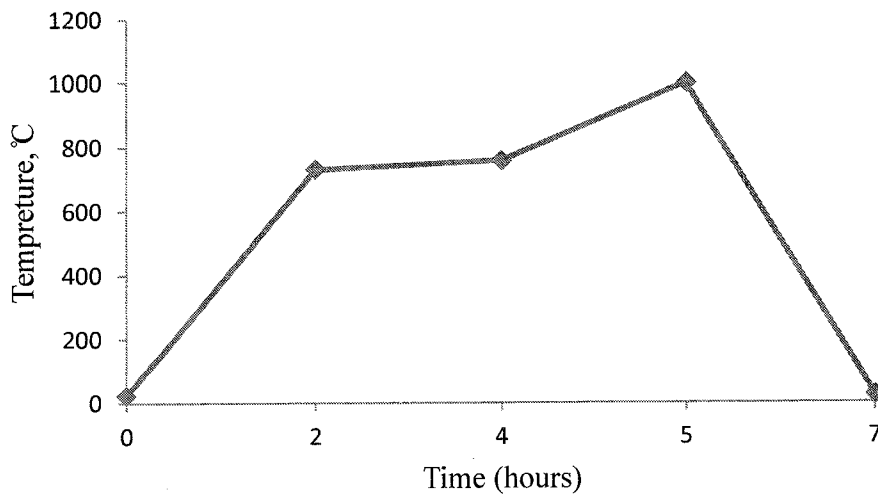


Figure 3.5 Heat treatment processes for H13 tool steel

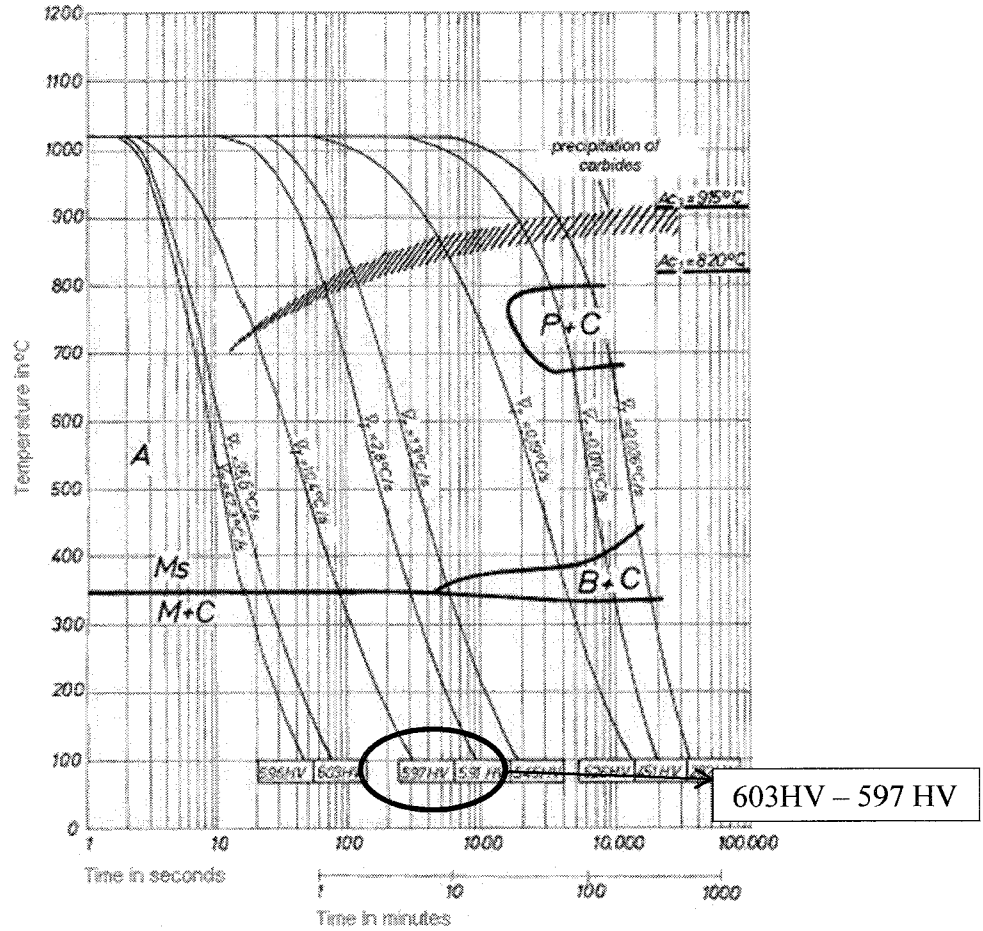


Figure 3. 6 Continuous cooling transformation (CCT) diagram for H13 tool steel [75]

3.3.2 Clamping Assembly

A clamping assembly was also designed to support the work piece during the welding process. The clamping system is shown in Figure 3.7.

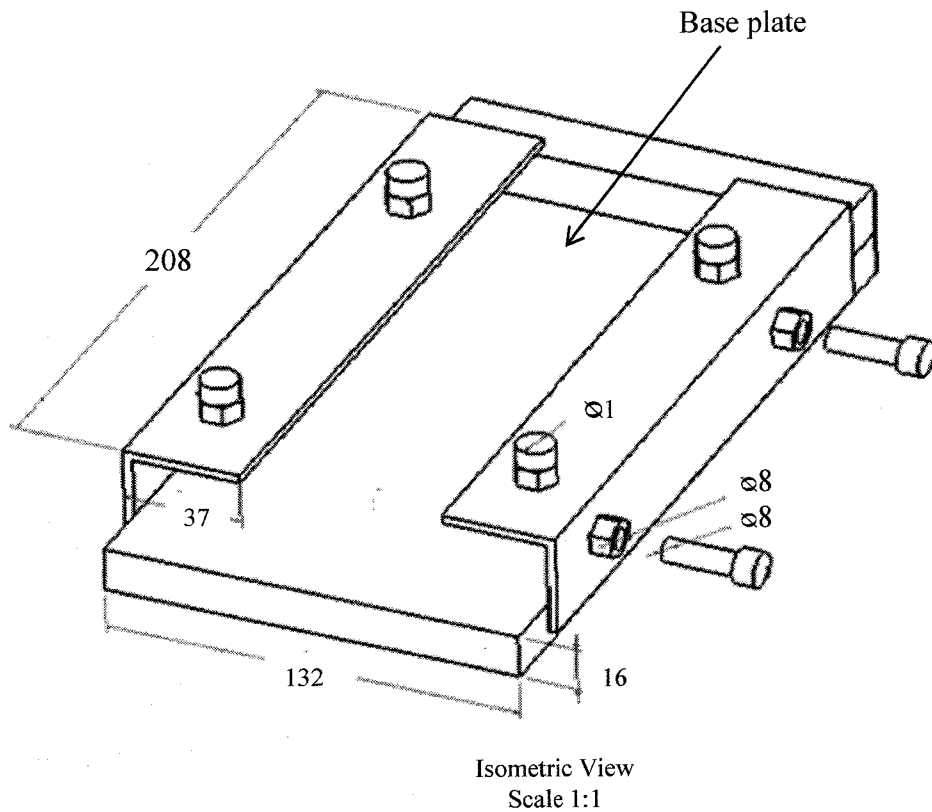


Figure 3.7: Isometric view of clamping assembly for CNC milling Bridgeport (dimension in millimeter)

3.4 Experimental Details

The experiment was conducted by considering controlled and independent variables. The controlled variable during the test run is the tool geometry while the independent variables are the tool traverse speed, tool rotational speed (RPM) and the tool tilting angle.

To begin the welding process, work piece was clamped onto the clamping assembly by using bolts and nuts. The clamping assembly will prevent work piece movement and vibration during the welding process. The clamping assembly was then placed on to the CNC milling Bridgeport machine bed and clamped tightly to it. The machines were then programed according to the desired tool movement. Three weld parameters were set for the CNC milling Bridgeport while eight parameters were set for

the MTS FSW machine. The purpose for the parameter variation is to analyze the effect of different welding parameters on the weld properties. Similar parameter was set for both of the machines to analyze the difference in terms of the weld quality.

A standard welding procedure was set for both machines:

- 1) The tool was rotated at to the desired rpm.
- 2) The tool was then plunged into the edge and center of the work piece until it reached the depth of approximately 80% of the plates' thickness.
- 3) The tool remains at a constant dwelling in a stationary position for about 10 seconds.
- 4) After 10 seconds, the tool moved in transverse direction along the plate joint until it reached the other edge of the plate. A constant speed and tool rotation was maintained during the movement.
- 5) Finally, the tool was ejected out of the welding line leaving a shallow boring hole at the edge of the welded AMMC piece.

3.4.1 Friction Stir Welding performed using CNC Milling Bridgeport

FSW process was first performed using CNC milling Bridgeport as shown in Figure 3.8. The machine has a bearing surface of 1120mm x 540 mm, downward force of 7.8 kN, motor maximum speed of 10,000 rpm, welding velocity of 36 m/min and torque of 114 Nm. Four different tests were conducted using CNC milling Bridgeport. Two independent variables were used to conduct the tests namely the tool traverse speed and tool rotational speed. Tool tilting angle was not varied due to the incapability of the machine to tilt the tool during the welding process. The parameters used are given in Table 3.5.

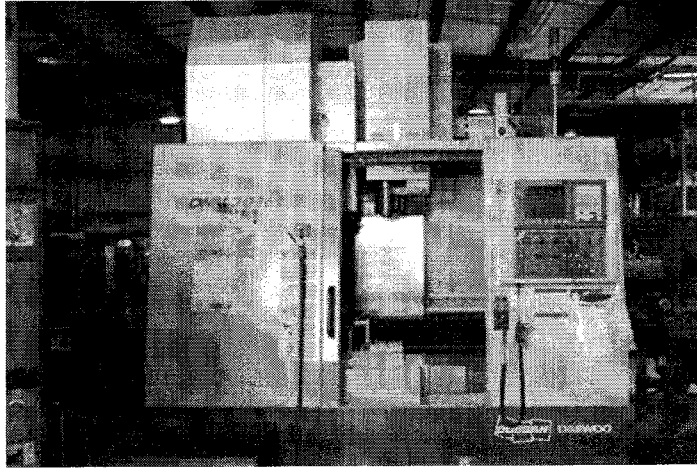


Figure 3.8: CNC milling Bridgeport

Table 3.5 Independent parameter variables for CNC milling Bridgeport

| Sample number | Tool speed (mm/min) | RPM | Tilt angle Degree (°) | Tool type |
|---------------|---------------------|------|-----------------------|-----------|
| 01 | 8 | 1200 | 0 | tapered |
| 02 | 10 | 1200 | 0 | tapered |
| 03 | 12 | 1200 | 0 | tapered |
| 04 | 14 | 1200 | 0 | tapered |

3.4.2 Friction Stir Welding performed using MTS FSW machine

Welding was performed using MTS FSW machine which can be viewed in Figure 3.9. The machine has a bearing surface of 2450x1250mm, maximum welding velocity of 6 m/min, motor maximum speed of 3200 rpm, maximum downward force of 35 kN and maximum torque of 180 Nm. Eight different parameter variations were used for the weld test. Due to the adaptation of the machine to high loading, lower tool rotation and higher tool traverse speed were used for the weld test. Tool tilting angle was varied using the FSW plant which could increase the weld quality because of the coupling effects. The parameters are shown in Table 3.6.

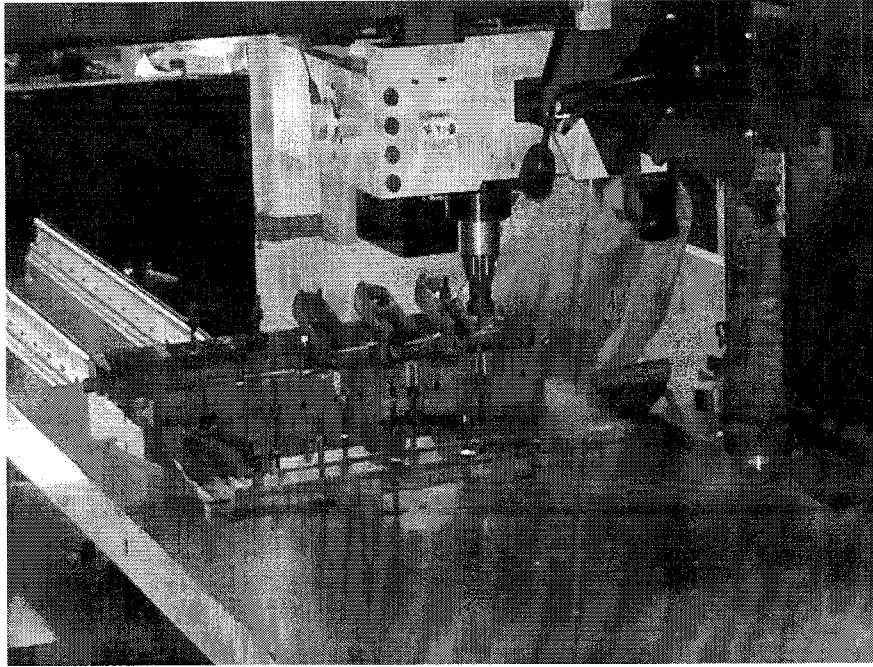


Figure 3.9: State of the art MTS FSW machine

Table 3.6 Independent parameter variables for MTS FSW machine

| Sample number | Tool speed mm/min | RPM | Tilt angle Degree (°) | Tool type |
|---------------|-------------------|------|-----------------------|-----------|
| 01 | 10 | 1200 | 0 | tapered |
| 02 | 100 | 1200 | 0 | tapered |
| 03 | 100 | 1200 | 3 | tapered |
| 04 | 100 | 900 | 3 | tapered |
| 05 | 150 | 900 | 3 | tapered |
| 06 | 125 | 900 | 3 | tapered |
| 07 | 125 | 1200 | 3 | tapered |
| 08 | 125 | 700 | 3 | tapered |

3.5 Characterization Technique

3.5.1 Scanning Electron Microscope of Welded Samples

The samples' preparation was carried out by cross sectioning the welded plates which is shown in Figure 3.10. The samples were then ground using paper grit size from 180 to 1200 then followed by polishing. The polished samples were then etched using Keller's reagent.

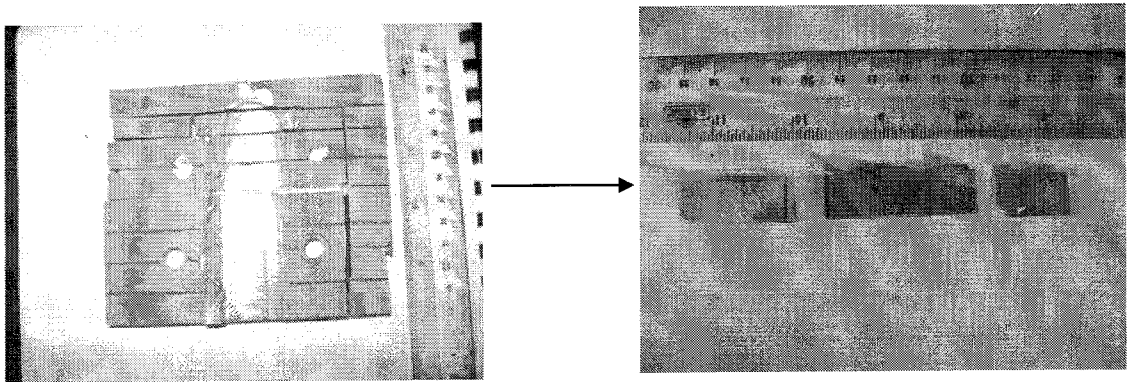


Figure 3.10: Weld cross section

The effect of machining parameters on weld zone microstructure was investigated using SEM. Microstructure observation was mainly conducted on the base metal, HAZ, TMAZ and the weld nugget. Thorough observation within the weld nugget was performed on the advancing side (AS) and the retreating side (RS). The effect of parameter variations on the weld zones microstructure was also analyzed.

The elements on the cross sectioned pieces were examined using EDX embedded with the SEM machine. EDX analysis was conducted to determine different elements on the material microstructure.

3.5.2 X-ray Diffraction of Welded Samples

XRD analysis was carried out on the welded samples to determine phase changes between the weld zones. The technique was also used to determine stresses within the material by comparing changes in the material space lattice. The examined zones were

the weld nugget, thermo mechanical affected zone (TMAZ), heat affected zone (HAZ) and the base metal. The weld zones are shown in Figure 3.12.

3.5.3 Tensile Test of Welded Samples

Tensile test was performed to determine the maximum load of the welded material before break as well as to determine the percent elongation of the specimen. Tensile test was conducted according to ISO/TTA 2 (1997) standard [76]. An average pin head velocity of 0.001 mm/s was used for the test. The schematic drawing for the tensile test specimen is shown in Figure 3.11.

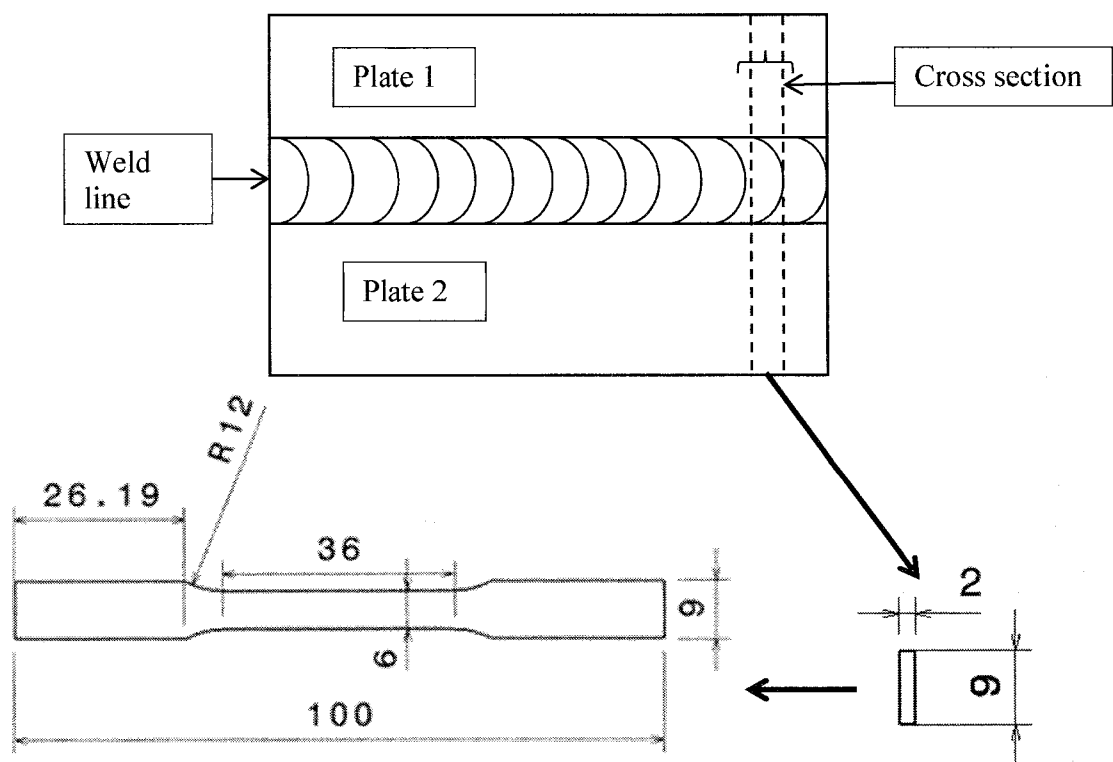


Figure 3.11: Geometry for tensile sample according to ISO/TTA 2 (1997) standard (dimensions in mm)

3.5.4 Vickers Hardness Test

Vickers hardness test was conducted to determine the hardness distribution across the weld zones of HAZ, TMAZ, weld nugget and the base metal. Three line of indentation were marked across the weld zones which are shown in in Figure 3.12. An average load of 200g was applied for the indentation.

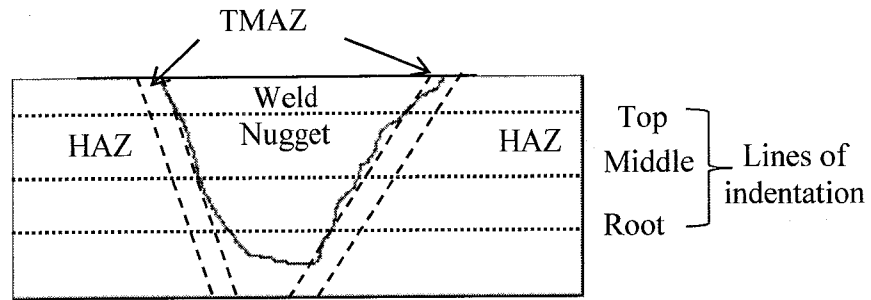


Figure 3. 12: Hardness indentation made across the weld zones

3.6 Chapter summary

This chapter has presented the materials and methodology involved in this research work. The chapter begins with a simple review of the research procedure and goes on to evaluate the properties of the materials employed in the analyses. Description on the tool and clamping assembly was presented in this chapter. Moreover, welding procedures were also discussed.

Thorough description of operating SEM, EDX, XRF and XRD techniques were discussed in this chapter. Techniques and design for the tensile test were also described with detailed geometry of the tensile test sample and the standard used to conduct the tensile test. Vickers hardness test procedure was also described in this chapter.

CHAPTER 4

RESULT AND DISCUSSION

4.1 Chapter Overview

This chapter discuss physical and microstructure analysis of on aluminum 6092/SiC/25p-T6 metal matrix composite friction stir welded plates. This composite is known for its greater strength and stiffness compared to monolithic aluminum alloys. The cross sections of the welded samples were analyzed in terms of its post weld microstructure and mechanical properties. SEM micrograph was used to analyze SiC particulate distribution and to detect formation of defects within the welding zones. SEM analysis was conducted using different magnifications to analyze the weld microstructure. Chemical composition was determined using EDX and XRD techniques which were used to detect elements and compound changes in the post welded samples. Mechanical testing was also performed to compare material strength and hardness for various samples. The influence of weld parameters were also analyzed using techniques mentioned above. Welded samples were prepared using CNC milling Bridgeport and MTS FSW machine.

4.2 CNC milling Bridgeport samples

Preliminary FSW tests were conducted using CNC milling Bridgeport. The welded samples that were prepared using CNC milling Bridgeport revealed several challenges in production of the welded samples. It was found that the machine was not able to hold high machining loading during the weld process. Therefore, the welding was conducted using slower traversal speed and a higher tool rotation which causes an excess of heat during the welding process. Besides that, CNC milling Bridgeport was not able to tilt the tool during the welding process which was essential for coupling effect. Coupling effect is considered important to contain the plasticized material within the weld line during the welding process. This limitation causes fewer parameter variations allowed during the

welding process. Despite that, initial microstructure and mechanical analysis on the weld nugget was conducted on the welded samples obtained from the CNC milling Bridgeport. Typically in FSW cross sectioned, the sample is divided into 4 separate zones, which are the parent metal (base metal), heat affected zone (HAZ), thermo mechanically affected zone (TMAZ) and the weld nugget. The location of these zones can be viewed in Figure 4.1. Typical onion flow was observed on these kinds of welds, which was caused by the material flow during the joining process.

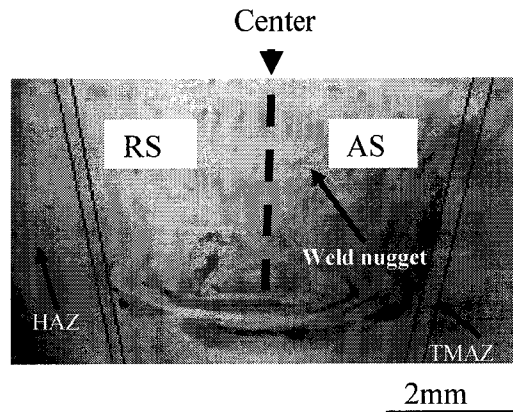


Figure 4. 1: Onion flow of the FSW cross sectioned sample

4.2.1 Weld microstructure

SEM analysis was conducted to analyze the microstructure difference between the weld zones inside the weld cross sections. Microstructure observation shows a more homogenous and broader spread of coarse and fine SiC particles distribution within the weld nugget compared to the other zones shown in Figure 4.2 and Figure 4.3. Electron micrograph shows an increase of fine particles density inside the weld nugget. This increment was due to the rounding and chipping effects during the welding process. The effect causes sharp edges of coarse SiC particles to be chipped thus producing finer SiC particles.

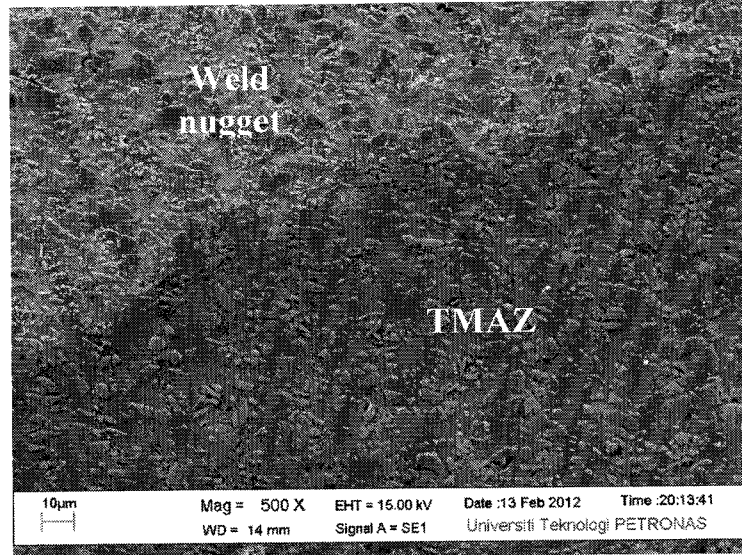


Figure 4. 2: Interface between the weld nugget and the TMAZ, magnification at 500X

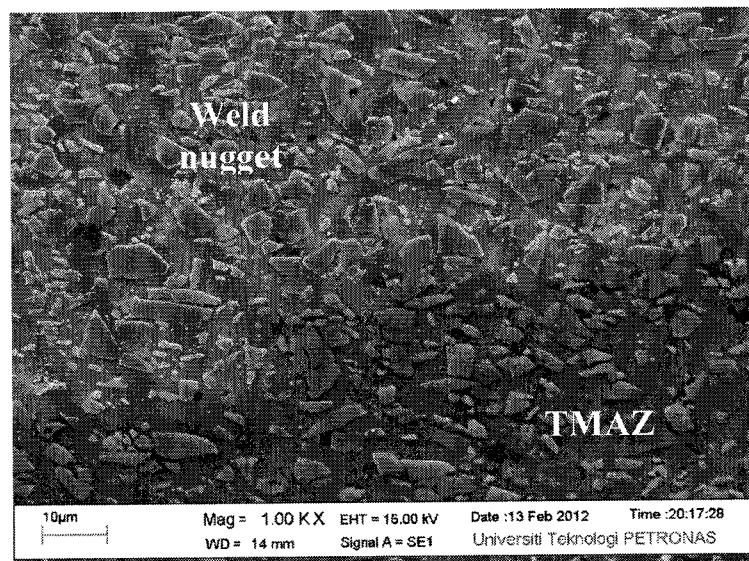


Figure 4. 3: Interface between the weld nugget and the TMAZ, magnification at 1000X

4.2.2 Effect of welding parameter on weld mechanical properties

It is noticed that most of the welded samples that were prepared using CNC milling Bridgeport showed extensive defect within the welding line. These were due to the limitation on the machine itself such as incapability to provide tool tilting angle and to maintain a high machine torque during the welding process. These limitations of the machine prevented coupling effects which resulted in formation of extensive tunneling

defects especially in the upper part of the weld nugget [14]. Only two test samples were considered suitable for the tensile test that were conducted using low traversal speed and high tool rotation shown in Table 4.1. The samples depict an adequate retainment tensile strength when compared to the base metal but a steep reduction of material elongation to failure percentage was observed. The results are shown in Figure 4.4 and Figure 4.5.

Table 4. 1 Tensile test of CNC milling Bridgeport samples

| Sample | Speed (mm/min) | RPM | Tensile Strength (MPa) | Elongation % |
|------------|----------------|------|------------------------|--------------|
| 01 | 8 | 1200 | 121.15 | 1.288 |
| 02 | 10 | 1200 | 207.33 | 1.562 |
| Base metal | n/a | n/a | 266.54 | 2.884 |

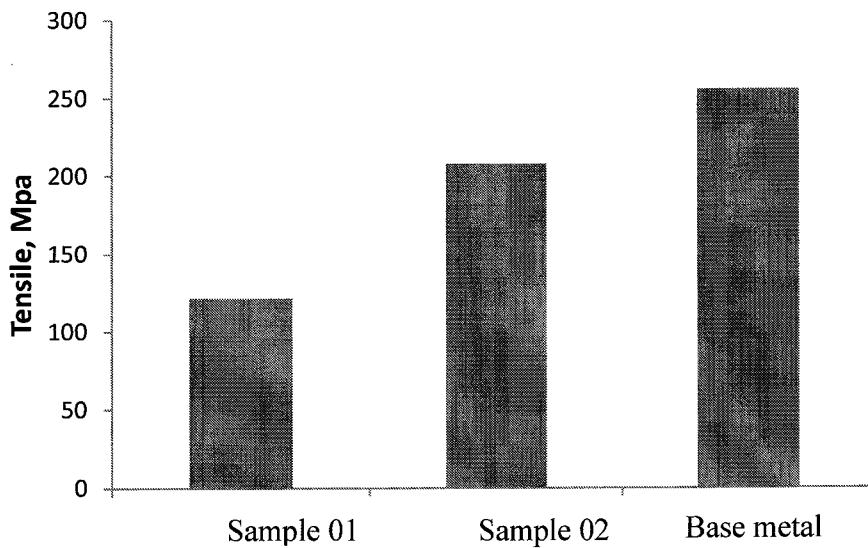


Figure 4. 4: Comparison between weld strength of welded samples and base metal (BM) using CNC milling Bridgeport

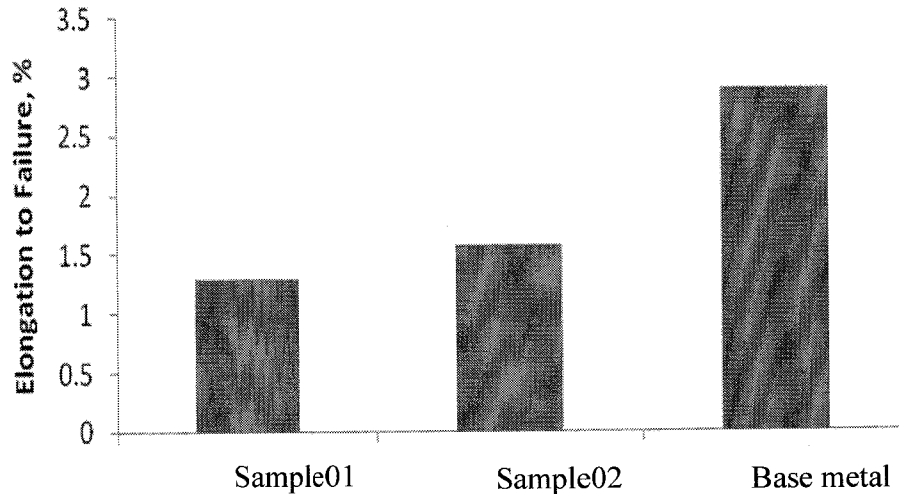


Figure 4. 5: Comparison between elongation to failure percentages of welded samples and base metal (BM) using CNC milling Bridgeport

Preliminary hardness reading was also performed on the CNC milling Bridgeport welded samples. Hardness results are displayed in Figure 4.6. Vickers hardness test showed minor increase in the weld nugget which is of about 1.54 % compared to the base metal. The slight increment of weld hardness was due to the effects of dynamic recrystallization (DRZ) caused by hot plastic deformation during the welding process. DRZ increases weld hardness by reducing grain size which will then decreases dislocation throughout the weld nugget. Another cause of increasing weld nugget hardness is the increase in fine SiC particulate concentration which causes an increase in dislocation pinning. Besides that, increase in fine SiC particulate would also causes increment of SiC particulate concentration which contributed to the hardness rise. Vicker's test also showed an uneven scatter of hardness reading across the weld nugget. Discrepancy in hardness reading within the weld nugget is caused by random or ununiform material flow within the zone.

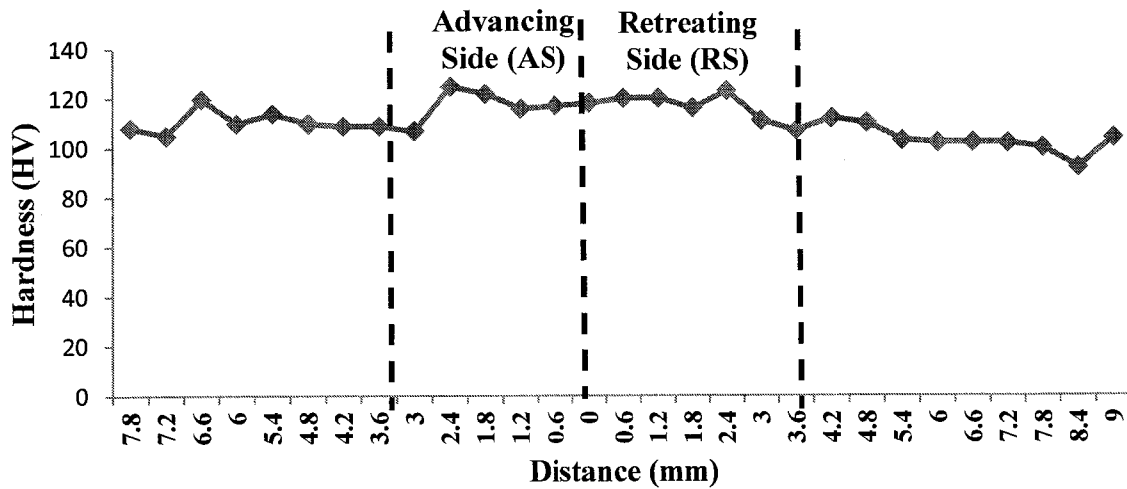


Figure 4. 6: Vickers Hardness Test

4.3 MTS FSW machine Analysis

Welded samples using MTS FSW machine showed improvement in weld proficiency compared to samples using CNC milling Bridgeport. The capability of the machine to hold high loading during the welding process increases parameter variation in terms of tool traverse speed and tool rotational speed. Successful test run using higher tool traverse speed also decreases production time which further increases welding efficiency. MTS FSW machine also provide tool tilting angle which increases weld quality through its coupling effects. Eight samples were produced using MTS FSW machine as shown in Table 3.6.

Figure 4.7 and Figure 4.8 show photograph of welded samples by MTS FSW machine. Photograph images shows formation of crowning like structure on top of the welded plates that were caused by the stirring effect. Another typical observation in the welded sample was the formation of flashes at the edge of the weld. An increase in flashes is detrimental in the welded samples as it reduces the volume of the plasticized material within the weld zone. This would then causes defects such as holes or tunnels particularly in the top section of the weld nugget.

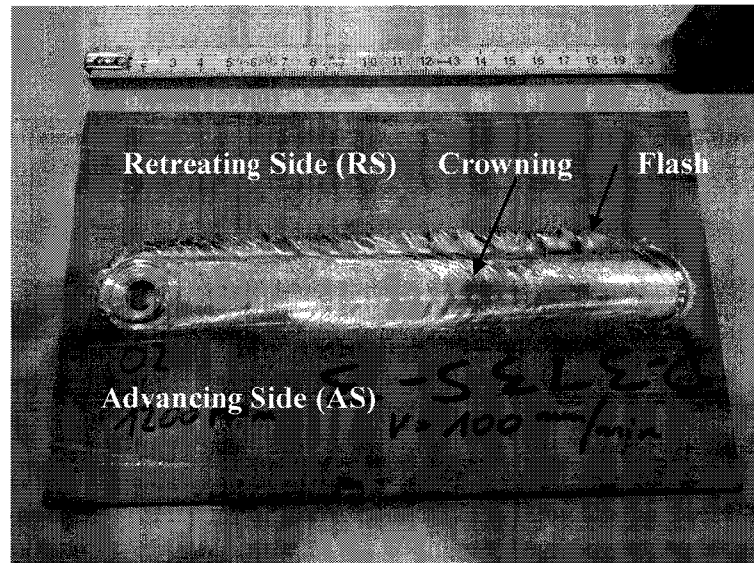


Figure 4. 7: FSW welded sample surface shows formation of side flash

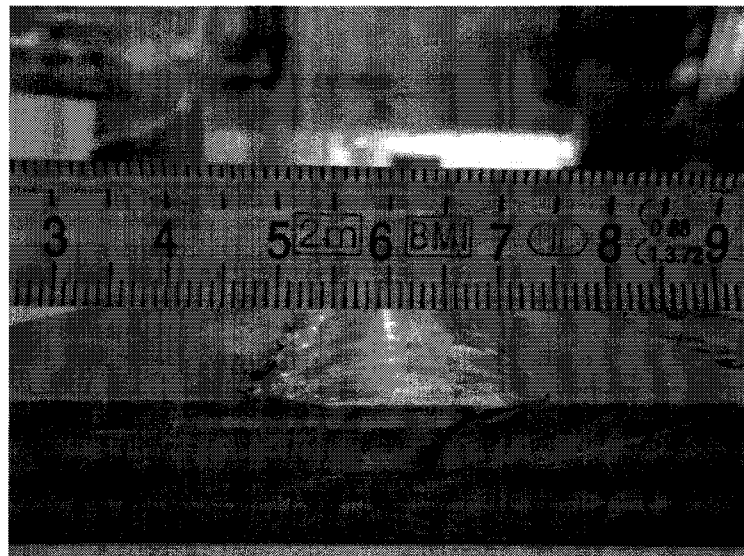


Figure 4. 8: Cross section of FSW welded sample

Next parametric analysis was conducted on the welded samples in terms of the weld quality, microstructure and mechanical properties within the weld nugget. Welding parameters were arranged in terms of the tool traverse speed, tool rotational speed and tool tilting. Microstructure, chemical composition, tensile and hardness test were used to analyze the parameter effects on the welded samples.

4.3.1 Analysis of welding parameter on weld quality

Weld quality was analyzed by comparing FSW welded samples in terms of defects formation within the weld nugget such as tunneling or smaller wormhole defects. Three different welding parameters that influenced the weld quality were used, i.e tool rotational speed (rpm), tool traverse speed (mm/min) and tilting angle of the tool. The parameters used for FSW weld samples are given Table 3.6.

Welded sample at lower tool rotation, sample 04, 06 and 08 (Figure 4.9(d), (f) and (h)) shows improve welding quality compared to samples welded at higher tool rotation. Welded sample at higher tool rotation (1200 rpm) showed defects such as tunnel and wormhole, which is shown in sample 02, 03 and 07 (Figure 4.9(b), (c) and (g)). Increase in tool rotational speed resulted in raised heat supply into the weld nugget causing a significant surge in material fluidity. This further facilitates the rapid stirring action causing some of the material to spill away from the weld nugget which contributed to the observed weld defects. Material spilt caused formation of flashes near the edge of the crowning surface shown in Figure 4.10.

Moreover, sample with high tool traverse speed also resulted in the formation of tunnel like defects within the weld nugget. Weld sample 05 (Figure 4.9 (e)), with a high tool traversal speed of 150 mm/min showed formation of large sized tunnels near the top corner of weld nugget. Compared to samples with less tool traversal speed, visible defect on the weld nugget was not detected such as sample 04 and 06 in Figure 4.9 (d) and (f). Rapid movement of the tool had caused inadequate stirring of the material where most of the material in the advancing side was not deposited back into the zone.

Finally, welded sample using tilted and non-tilted tool angle were also compared. The advantage in tilting the tool angle to 3° was to ensure proper material flow around the tool pin and also to ensure that the material did not spill at the edge of the tool shoulder. Most of the samples tilted at 3° showed a significant increase in weld quality. The effect of tool tilt angle can be significantly seen when comparing sample 02 and 03, in Figure 4.9 (b) and (c) which showed a decreased tunneling defect in the tilted sample. Tunneling defects were basically due to displacement of the plasticized material away from the weld nugget. Movement of the plasticized material away from the weld formed into flash at the

edge of the upper section of the weld nugget which was observed on un-tilted samples shown in Figure 4.11. Flashes were decreased by tilting the tool during the welding process.

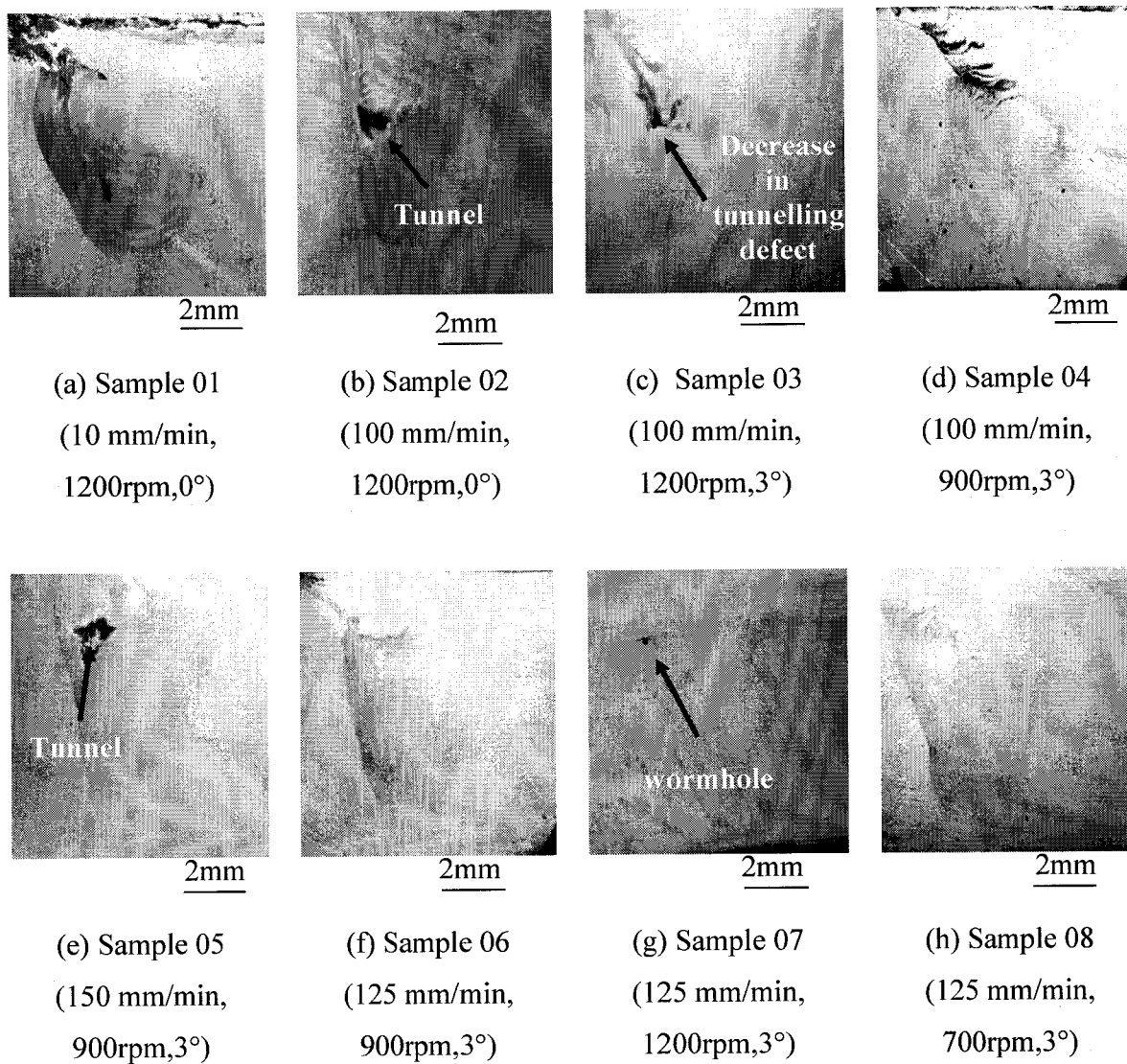


Figure 4. 9: Weld nugget observation in AMMC welded test sample

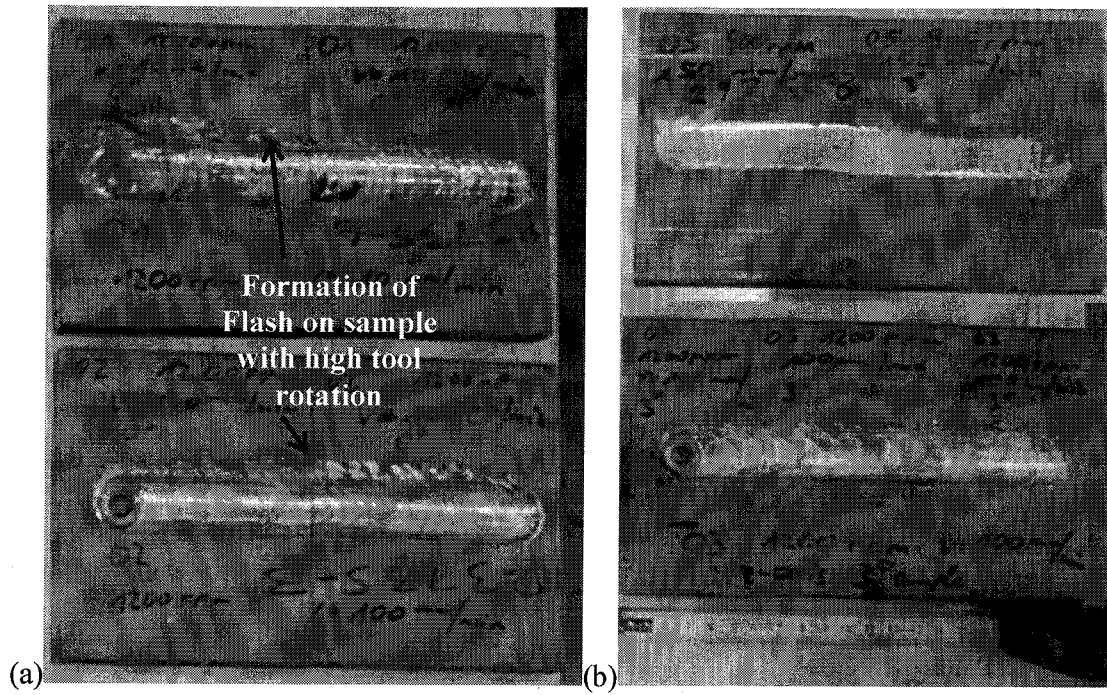


Figure 4. 10: (a) Sample with high tool rotation (1200 rpm) and (b) Sample with lower tool rotation (900 rpm) which showed formation of flash on sample with the higher tool rotation

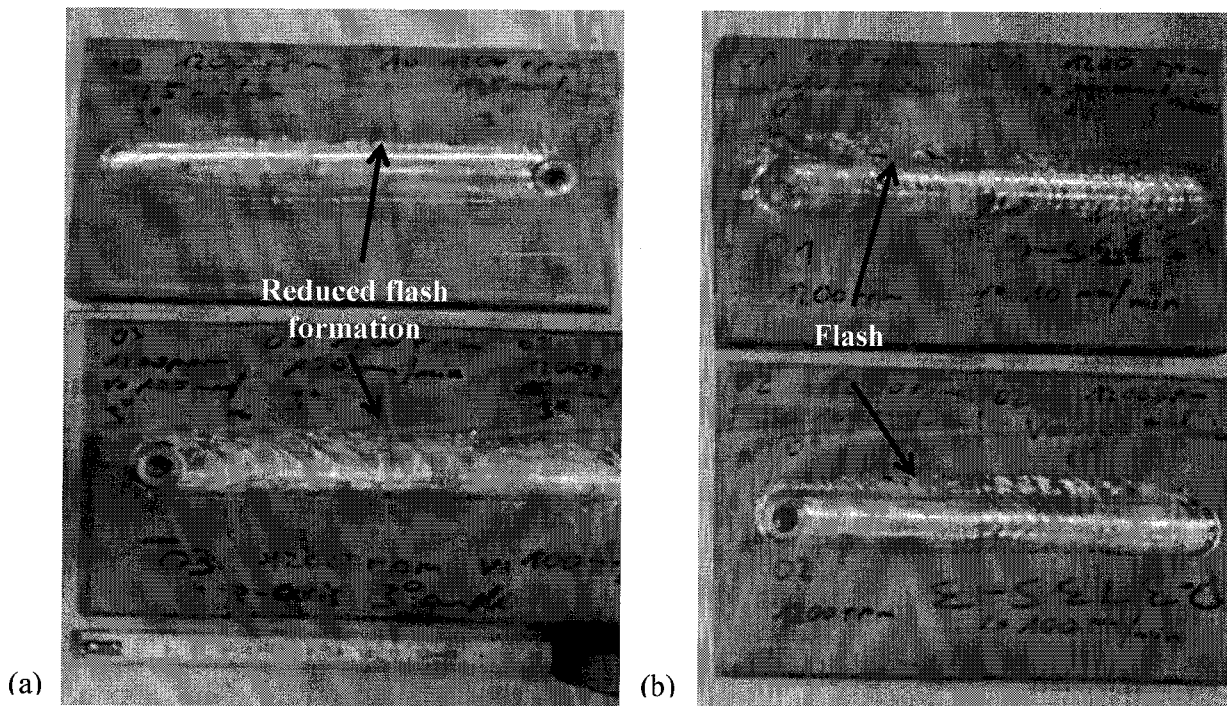


Figure 4. 11: Formation of flashes at the edge of the crowned surface for (a) tilted sample compared to (b) un-tilted sample

4.3.2 Effect of welding parameter on weld nugget microstructure

Before conducting microstructure analysis, EDX was used to identify and confirm different elements on the weld micrograph. Spot analysis on Figure 4.12 (spectrum 1) which was done on the bright coarse particulate indicates the location of SiC particles where a high intensity of silicon (Si) and carbon (C) elements were found. The quantitative analysis for spectrum 1 in Table 4.2 further support the suggestion of SiC particles by indicating a high weight percentage of both Silicon and carbon elements. Next spot analysis for spectrum 2 in Figure 4.13 and Table 4.3, showed that the grayish background behind the bright SiC particulate as the aluminum matrix where the readings showed a high weight percentage of Aluminum (Al).

Full spectrum analysis (Figure 4.14) on the welded microstructure showed that elements within the welded samples were relatively similar to the base metal. Elements of aluminum (Al), magnesium (Mg), Silicon (Si), Carbon (C) and Oxygen (O) were detected for both the base metal and the welded region. Table 4.4 shows almost similar atomic weight percentages of elements between the base metal and the weld nugget.

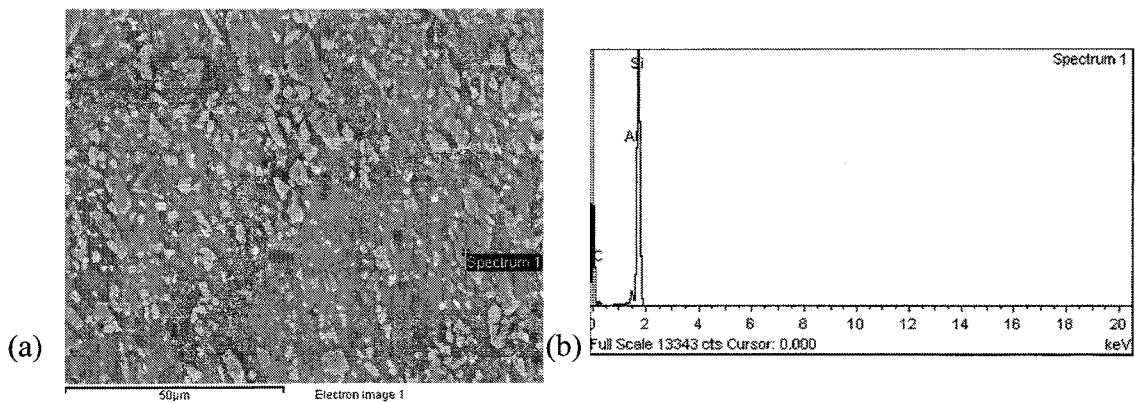


Figure 4. 12: Location of (a) spot EDX for spectrum 1 and (b) EDX graph indicating the SiC particulate on the indicated spot, spectrum 1.

Table 4. 2 Quantitative analysis of coarse particle in the aluminum alloy matrix

| Element | Weight% | Atomic% |
|---------|---------|---------|
| CK | 35.76 | 56.51 |
| AlK | 2.24 | 1.57 |
| SiK | 62.01 | 41.91 |
| Totals | 100.0 | |

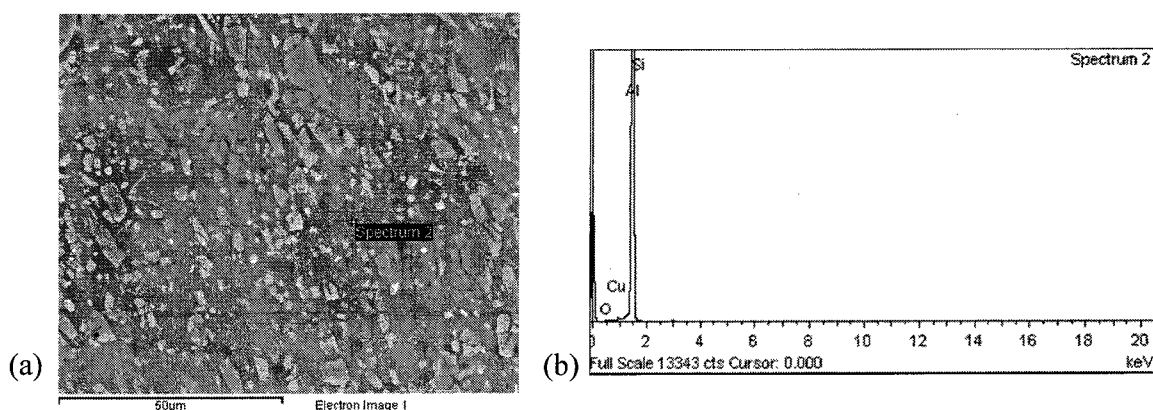


Figure 4. 13: (a) Location of the spot EDX Spectrum2 (b) EDX graph indicating the grayish background as the aluminum alloy matrix, spectrum 2

Table 4. 3 Quantitative analysis of aluminum alloy matrix

| Element | Weight% | Atomic% |
|---------|---------|---------|
| CuK | 0.74 | 0.31 |
| OK | 3.28 | 5.43 |
| AlK | 94.80 | 93.14 |
| SiK | 1.19 | 1.12 |
| Total | 100.00 | |

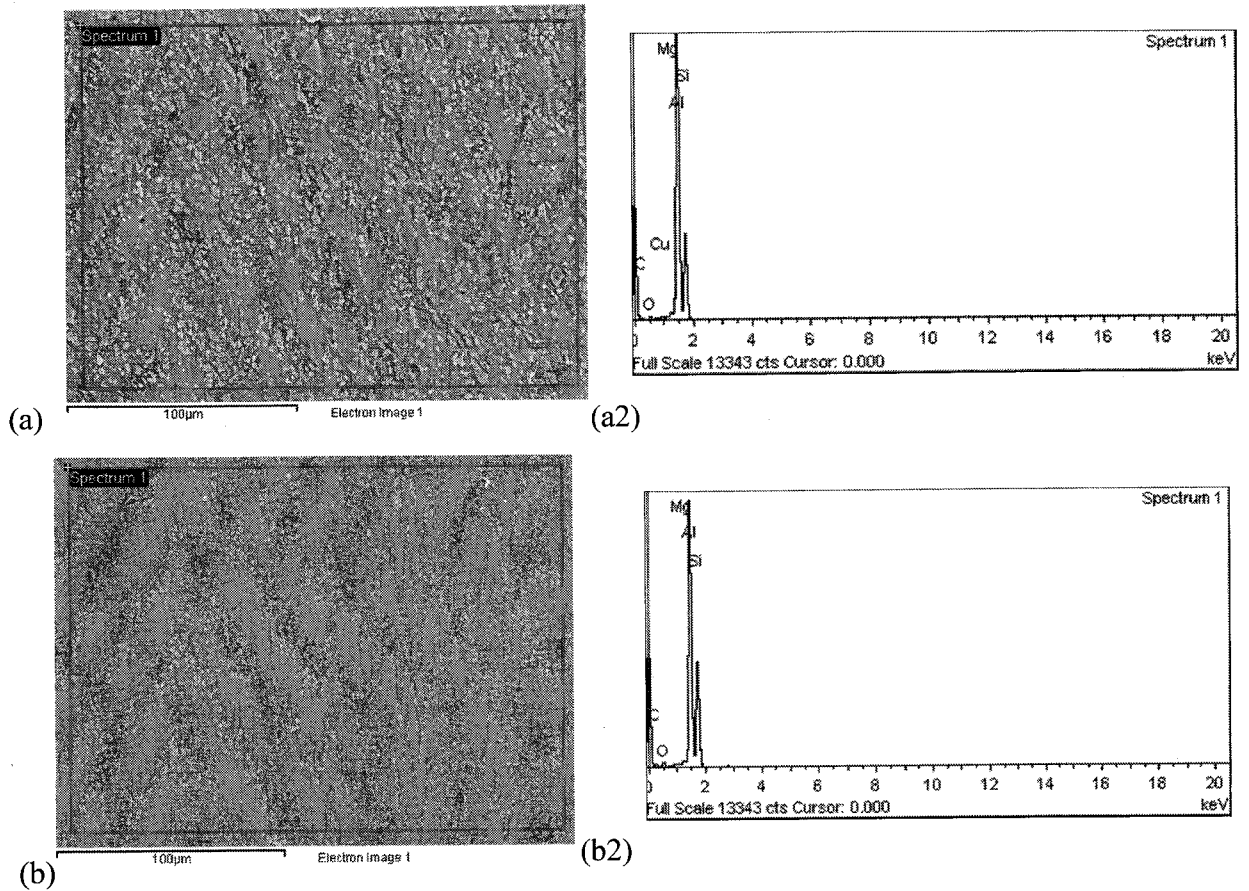


Figure 4. 14: Full spectrum analyses and EDX graph for (a) weld nugget (b) base metal

Table 4. 4 Full spectrum EDX analysis on (a) base metal and (b) weld nugget

| Element | Weight% | Atomic% |
|---------|---------|---------|
| C K | 24.39 | 40.68 |
| O K | 7.83 | 9.80 |
| Mg K | 0.39 | 0.32 |
| Al K | 39.27 | 29.15 |
| Si K | 28.13 | 20.06 |
| Totals | 100.00 | |

| Element | Weight% | Atomic% |
|---------|---------|---------|
| C K | 22.03 | 38.70 |
| O K | 2.63 | 3.47 |
| Mg K | 0.30 | 0.26 |
| Al K | 39.29 | 30.72 |
| Si K | 35.74 | 26.85 |
| Totals | 100.00 | |

EDX mapping in Figure 4.15 further reveals the types of element's distribution and microstructure that is expected on a welded sample cross section. EDX mapping of silicon in Figure 4.15 (b) indicated the distribution of SiC particulate while mapping of aluminum in Figure 4.15 (c) shows aluminum matrix distribution. The result from mapping shows dense distribution of SiC particles within the weld nugget. An analysis on the EDX mapping also showed formation of coarse and fine SiC particles within the weld nugget.

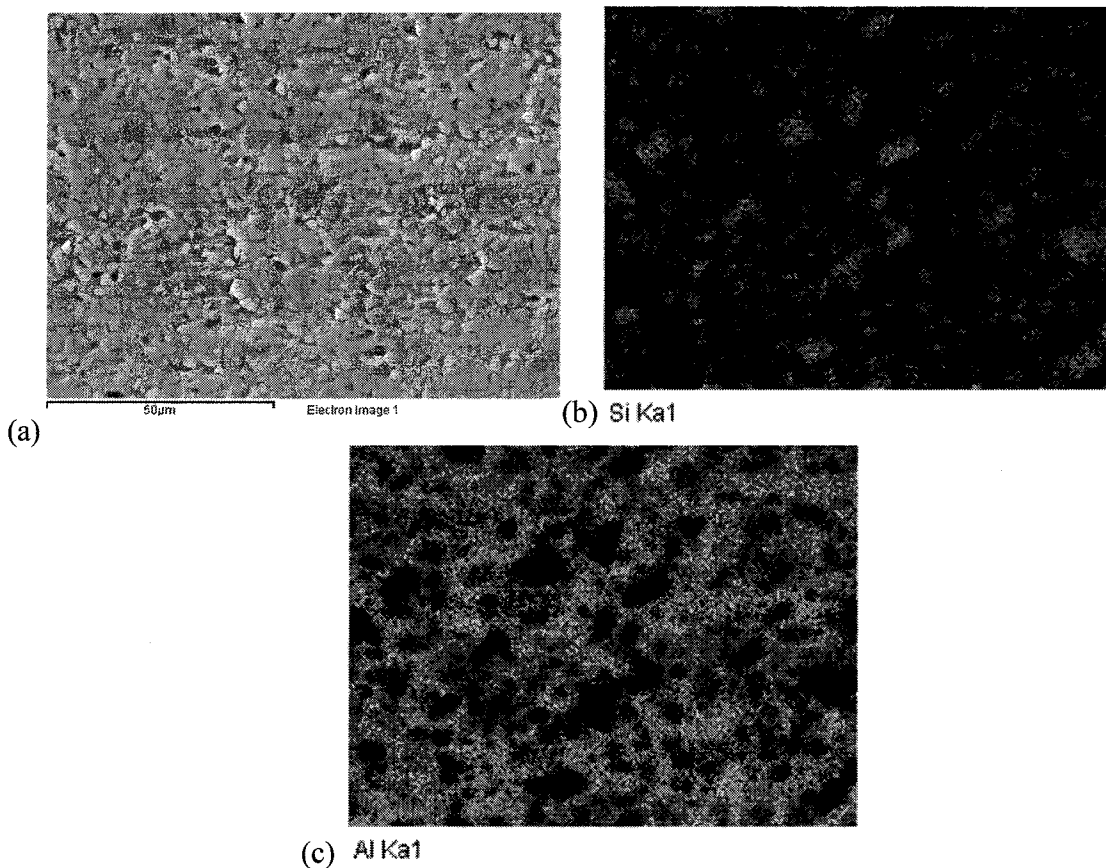


Figure 4. 15: FESEM images of (a) Backscattered image of the welded samples and EDX mapping of (b) silicon and (c) aluminum elements

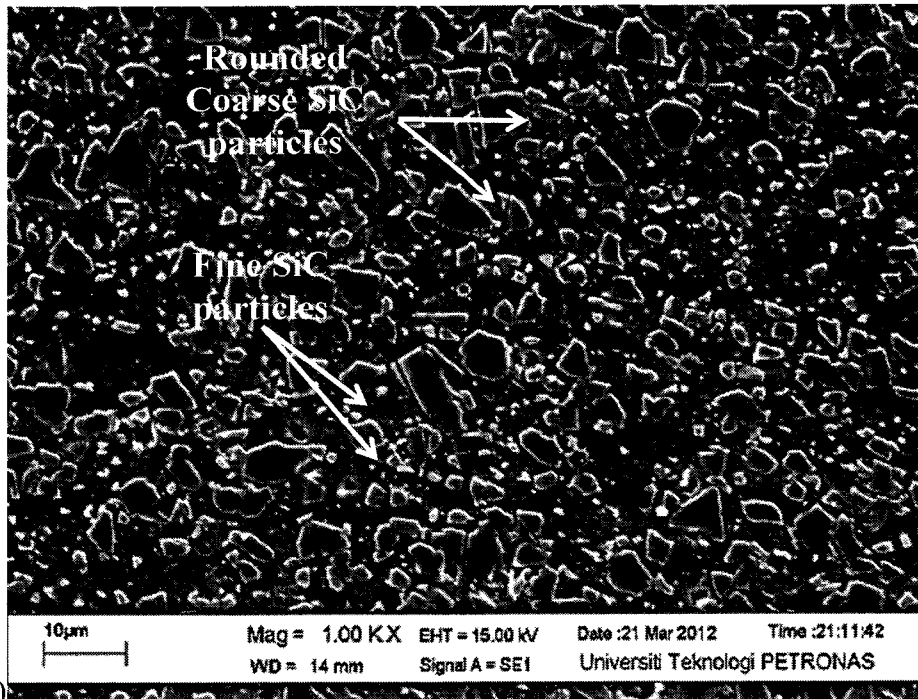
4.3.2.1 Tool rotation

Tool rotation showed significant effect on the weld microstructure. The tests were conducted using constant tool traverse speed of 125 mm/min and varied tool rotation of 700 rpm, 900 rpm and 1200 rpm. First of all, weld sample that was joined by tool rotation of 700 rpm (Figure 4.16) shows unsymmetrical SEM micrograph between the advancing

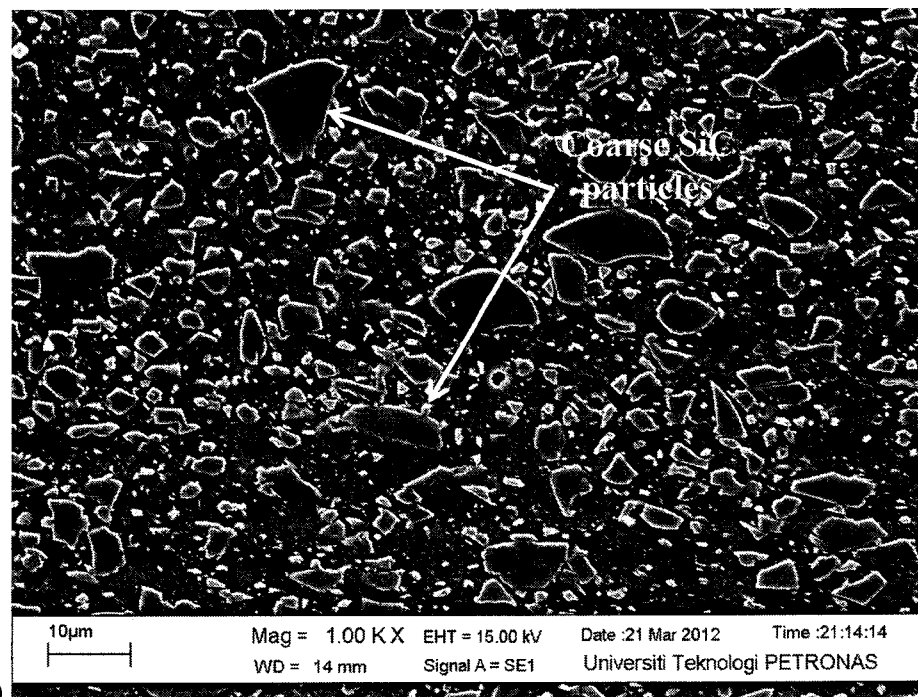
side and the retreating side of the weld nugget. Microstructure observation showed higher amount of coarse SiC particles in the retreating side when compared to the advancing side. This shows that the retreating side experienced lower stirring effects when compared to the advancing side.

An increase of tool rotation from 700 rpm to 900 rpm (Figure 4.16 and Figure 4.17 respectively) showed almost similar SiC particles distribution between the advancing side and retreating side of the weld nugget. Similar microstructure observations between the two zones were caused by increasing rounding and chipping effect due to the rise in tool rotation. Rounding and chipping effects is a solid collision between the SiC particles and the rotating tool which causes chipping of sharp edges from the coarse SiC particles. Besides that, increasing the tool rotation to 900 rpm also causes a more compacted SiC particles distribution within the weld nugget. This distribution may be due to increasing compression exerted by rising centrifugal forces from the increased stirring action.

As the tool rotation increases to 1200 rpm (Figure 4.18) higher concentration of fine SiC particles were observed in the advancing side of the weld nugget. This development causes an unsymmetrical distribution of SiC particles between the advancing side and the retreating side of the weld nugget. The advancing side of the weld will experience more welding velocity causing more SiC particles fragmentations within the zone [71]. Besides that, because of the higher welding velocity in the advancing side most of the stirred material will be deposited back to the zone causing a slight increase in SiC particles concentration. Although increases in fine particle density do improve the weld properties, the inhomogeneous distribution between the advancing side and the retreating side might cause drawbacks for the mentioned sample. In addition, microstructure band was also identified in the mentioned welded sample which might cause setbacks in the weld properties. Formation of band microstructure might cause irregularities especially in the advancing side, which may potentially causes flaws in the material strength. The cause of microstructure band will be discussed later in this chapter.

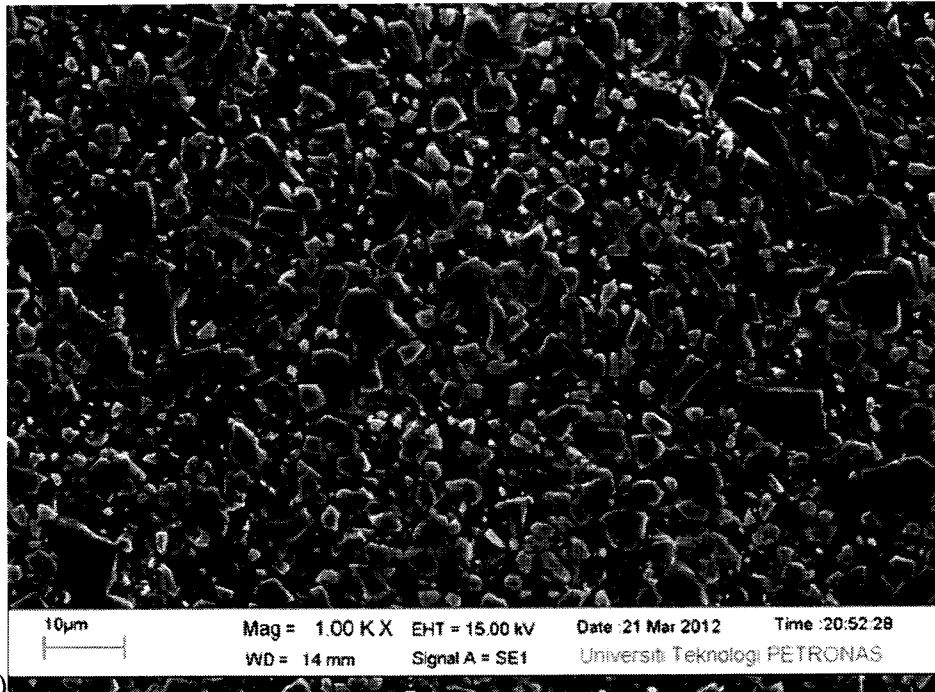


(a)

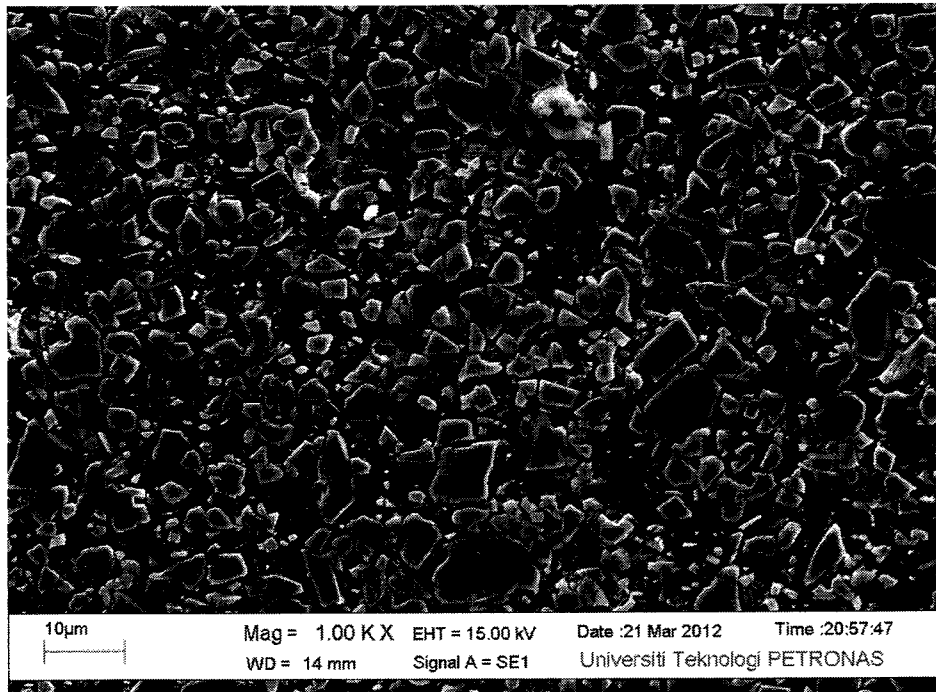


(b)

Figure 4. 16: (a) Advancing side and (b) Retreating side of weld sample with traversal speed of 125mm/min and tool rotation of 700 rpm



(a)



(b)

Figure 4. 17: (a) Advancing side and (b) Retreating side of weld sample with tool traverse speed of 125 mm/min and tool rotation of 900 rpm

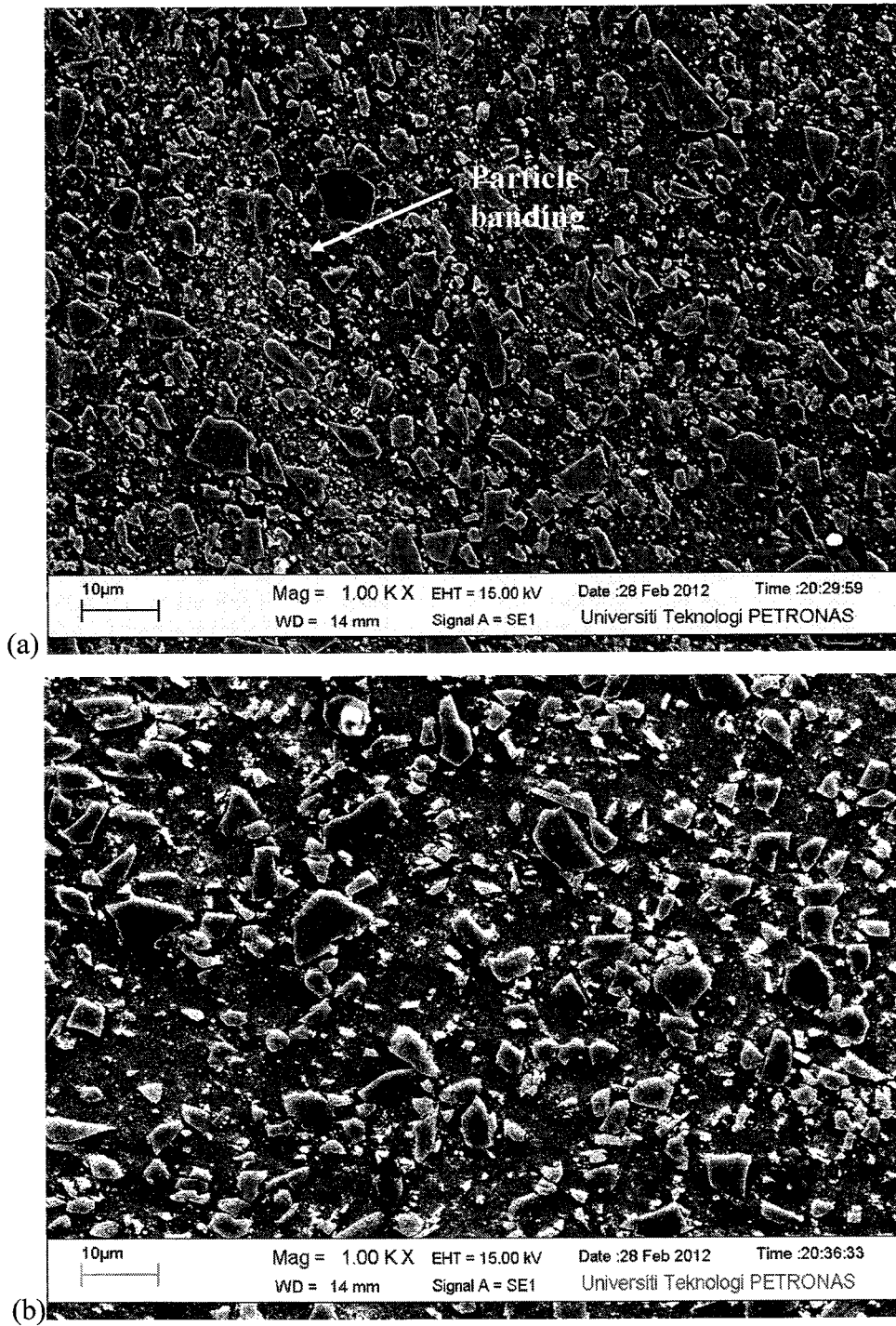


Figure 4. 18: (a) Advancing side and (b) Retreating side of weld sample with traverse speed of 125 mm/min and tool rotation of 1200 rpm

4.3.2.2 Tool traverse speed

The effect of tool traverse speed on the weld microstructure was also studied. In this research work, the tool rotational speed was fixed at 900 rpm while the tool traverse speed was varied by 100 mm/min, 125 mm/min and 150 mm/min. SEM micrograph for the three welded samples is shown in Figure 4.19, Figure 4.20 and Figure 4.21. Observation on sample welded at tool traverse speed of 100 mm/min showed homogenous and oriented spread of SiC particles in the advancing side of the weld nugget as shown in Figure 4.19. While in the retreating side, similar concentration but a more random orientation of the SiC particles were observed.

As the tool traverse speed increased from 100 mm/min (Figure 4.19) to 125 mm/min (Figure 4.20), a more similar spread of SiC particles were observed between the advancing side and the retreating side of the weld nugget. Besides that, random orientations of SiC particles were observed at both from the advancing side and retreating side of the weld nugget. Such phenomenon may be due to the lower stirring of the plasticized material caused by the escalation of tool traverse speed. Compared to low tool traverse speed, higher tool traverse speed reduces heat supply which decreases mixing and deposition of the stirred material especially in the advancing side of the weld nugget [61].

Finally as the speed increased to the highest speed of 150 mm/min (Figure 4.21), lower concentration and larger spread of SiC particles was observed within the weld nugget. An increase of tool traverse also showed a decrease of fine SiC particles concentration within the weld nugget. It was also observed that as the tool traverse speed increases from 125 mm/min to 150 mm/min a symmetrical SiC particle orientation between the advancing side and the retreating side was also observed. This may be due to decreasing movement of the plasticized material that causes minimal changes to the material original microstructure.

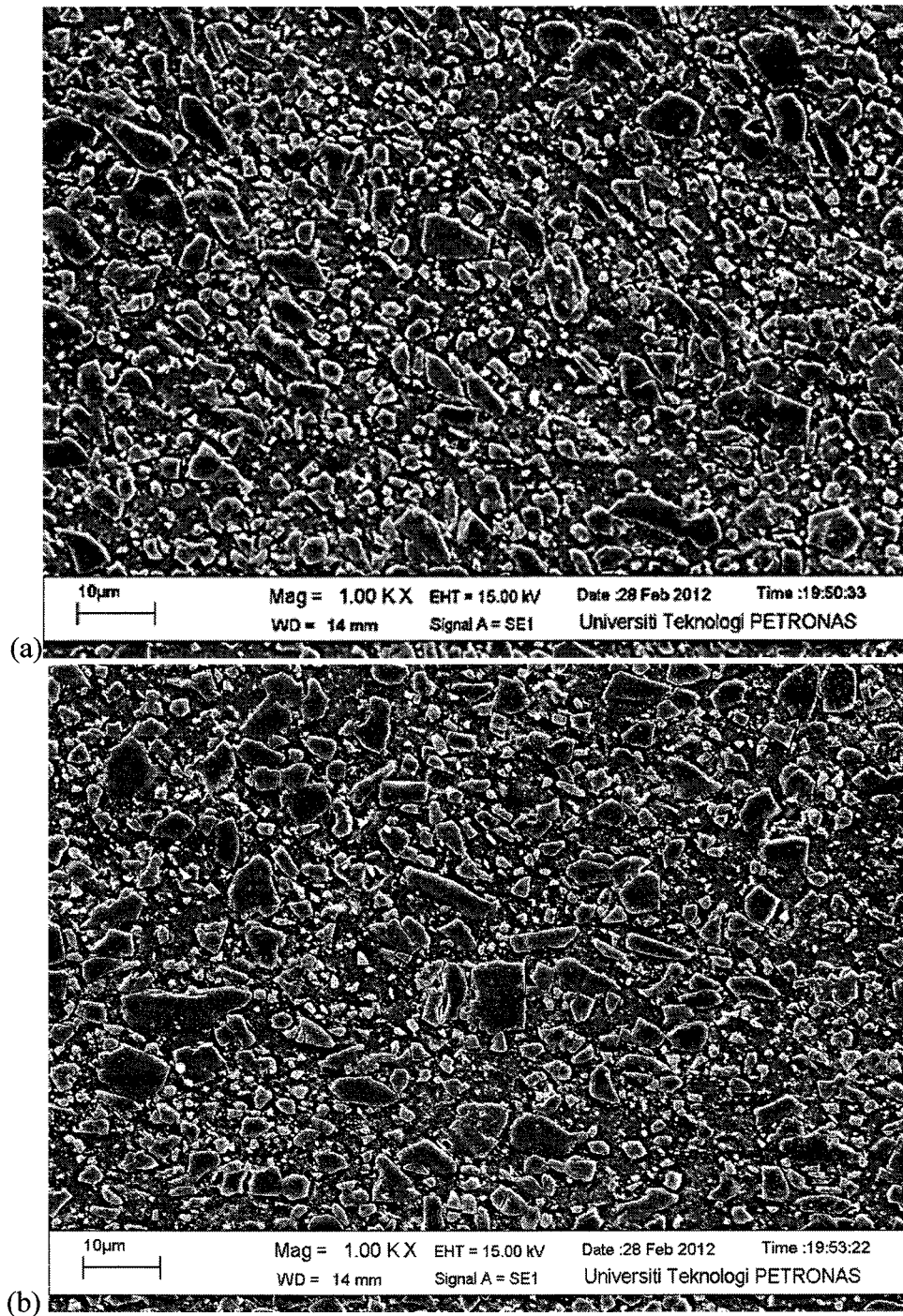


Figure 4. 19: (a) Advancing side and (b) Retreating side of weld sample with tool traverse speed of 100 mm/min and tool rotation of 900 rpm

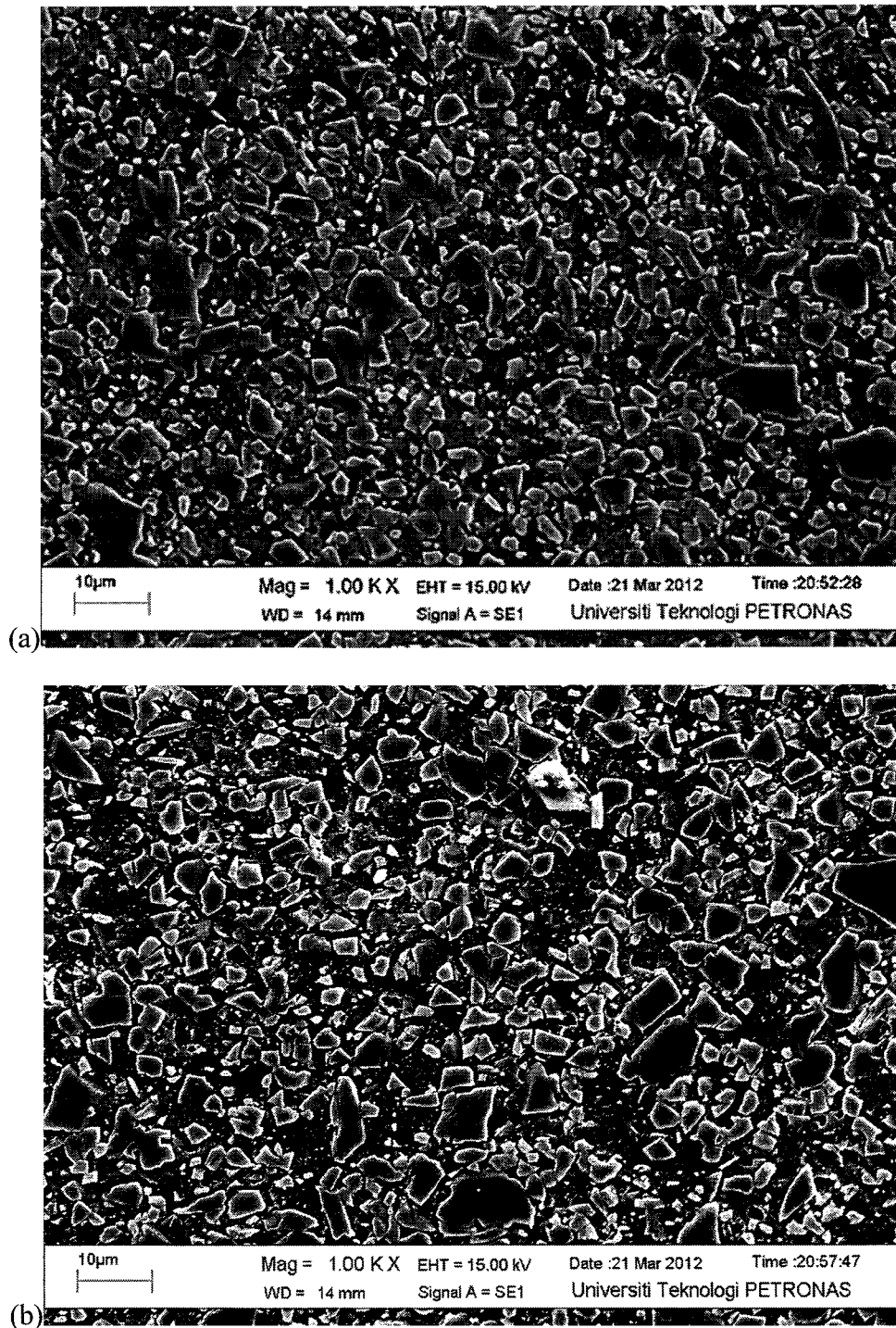


Figure 4. 20: (a) Advancing side and (b) Retreating side of weld sample with tool traverse speed of 125 mm/min and tool rotation of 900 rpm

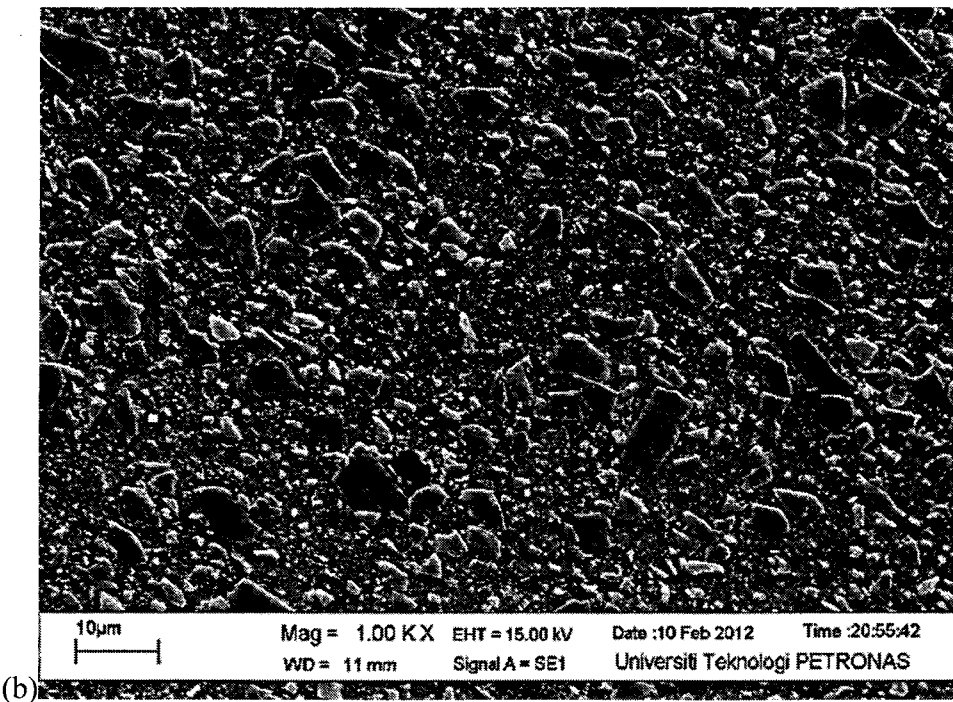
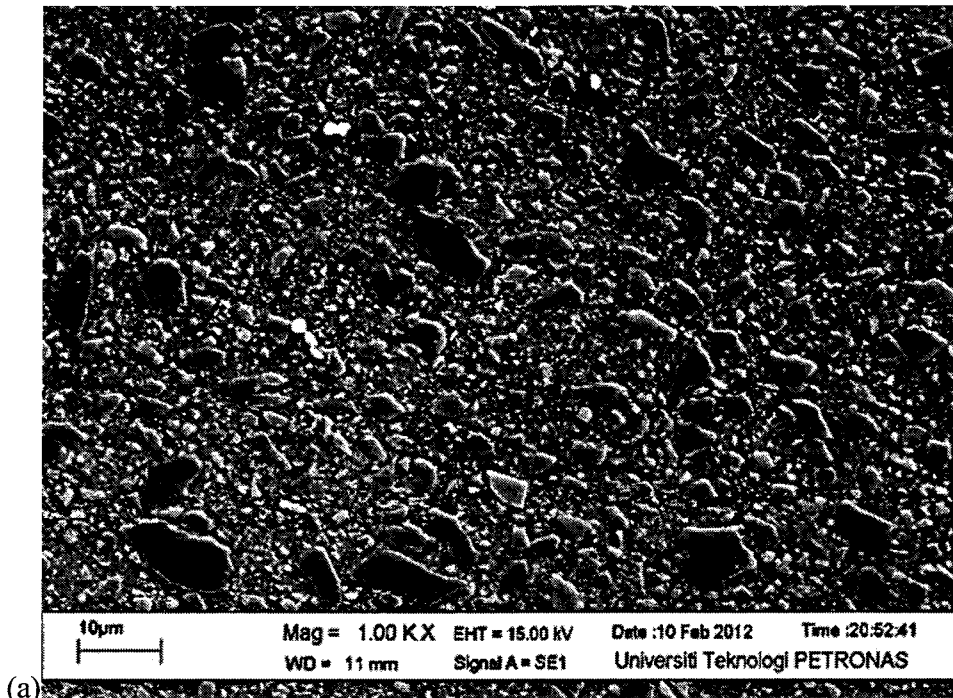


Figure 4. 21: (a) Advancing side and (b) Retreating side of weld sample with tool traverse speed of 150 mm/min and tool rotation of 900 rpm

4.3.2.3 Tool tilting

Comparison on tilted samples was also performed which is shown in Figure 4.22 and Figure 4.23 for un-tilted and tilted tool sample, respectively. It shows that denser SiC particles concentration was observed on the tilted sample when compared to the un-tilted weld sample. Increase in SiC particle concentration was mainly caused by the coupling effects due to the tilting of the tool. Coupling effect contributes to increase particle concentration by ensuring material localization during the stirring process [14]. Tilting of the tool would also cause an increase in rounding and chipping effects which result in reduced SiC particles sizes and an increase in fine SiC particle concentration. Symmetrical distribution of SiC particles between the retreating side and the advancing side were also observed for the tilted welded sample. This shows that by tilting the tool during the welding process, a more balanced material flow between the advancing side and the retreating side was achieved.

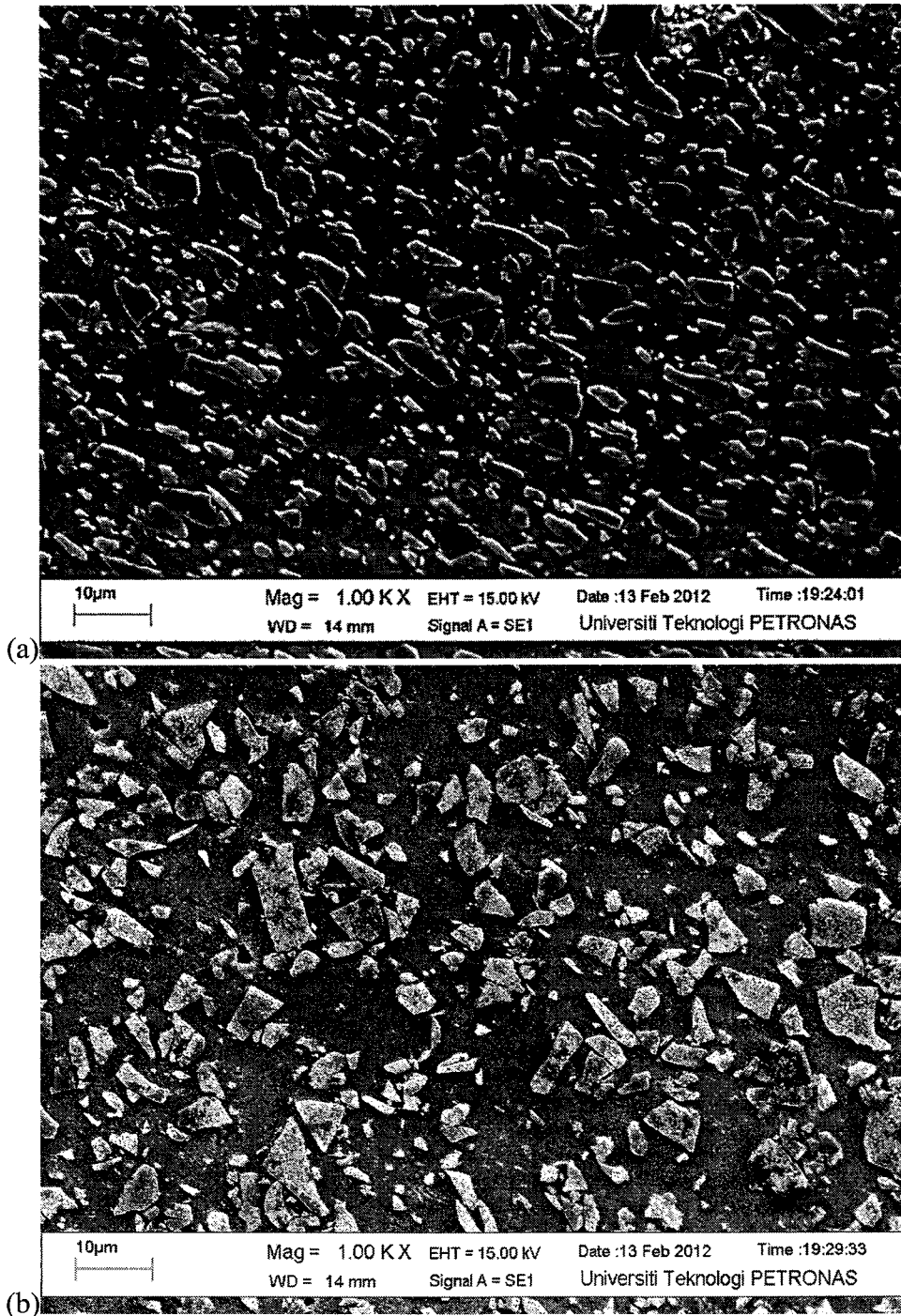


Figure 4. 22 (a) advancing side and (b) retreating side of the un-tilted welded sample

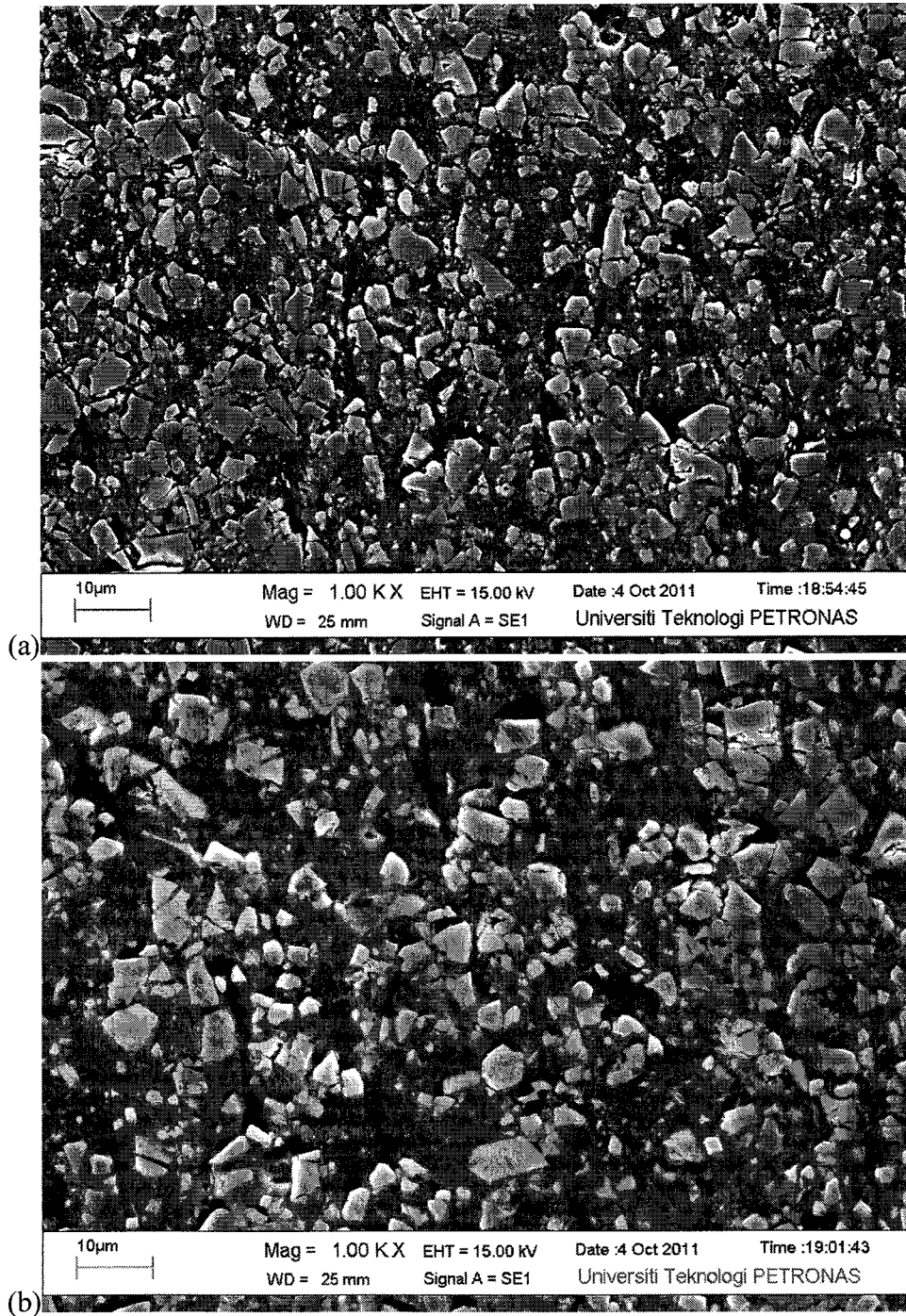


Figure 4. 23: (a) advancing side and (b) retreating side of the tilted welded sample

4.3.2.4 Comparison on weld zones microstructure

FSW weld zone can be divided into four separate sections, which is the parent metal (base metal), heat affected zone (HAZ), thermo mechanically affected zone (TMAZ) and the weld nugget. The location of these zones can be viewed in Figure 4.1. Weld nugget was also divided into two separate zones which are the retreating side (RS) and the advancing side (AS).

SEM analysis of the welded sample was conducted to determine microstructure changes on the weld zones. Similar microstructure changes between the weld zones were observed on all of the welded samples as shown in Figure 4.24 and Figure 4.25.

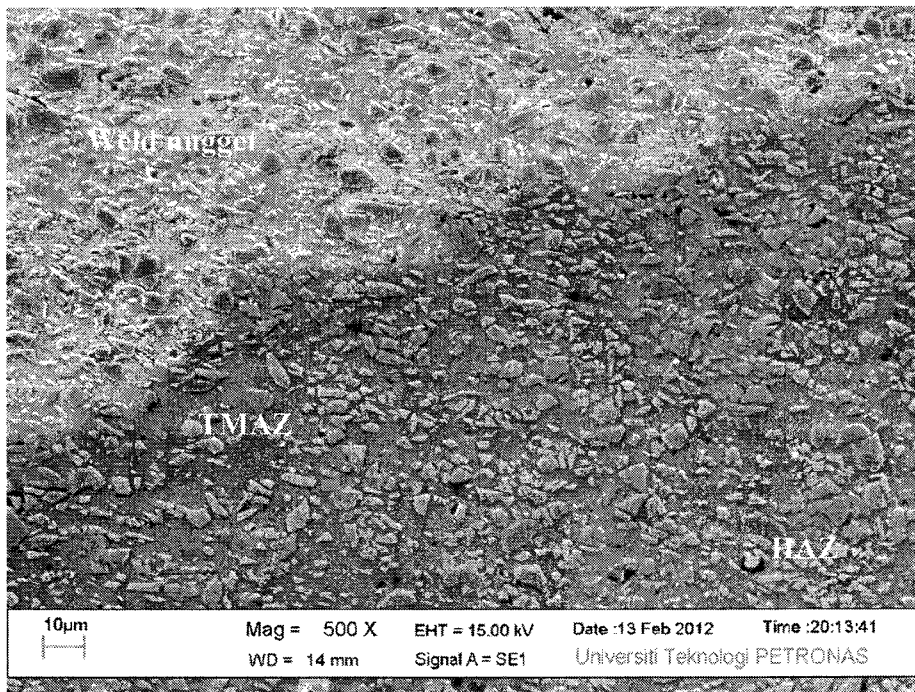


Figure 4. 24: Distribution of SiC particles in the weld regions for sample welded at tool rotation of 1200 rpm and tool traverse speed of 10 mm/min

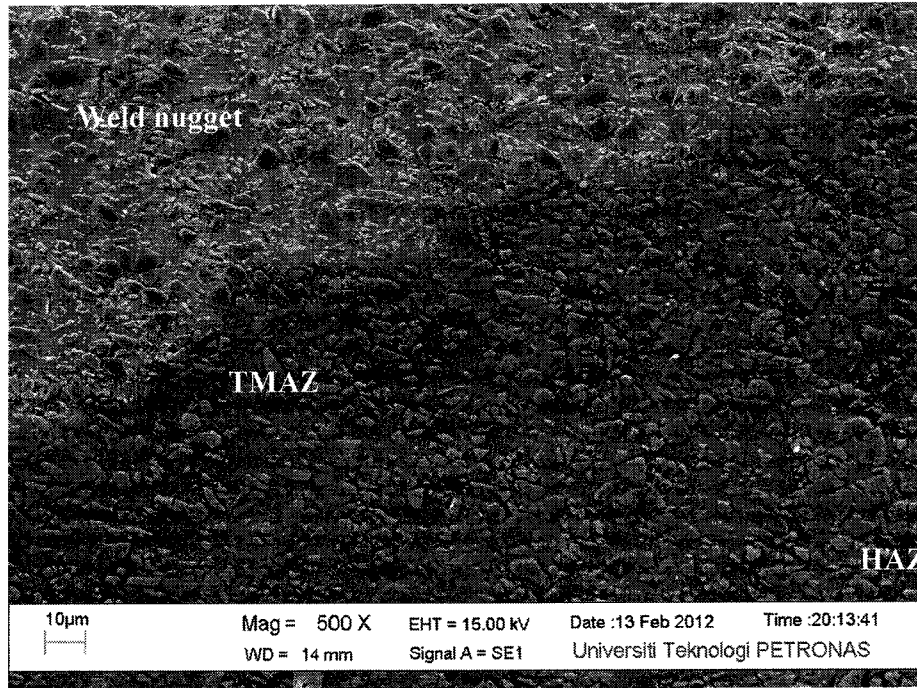


Figure 4. 25: Distribution of SiC particles in the weld regions for sample welded at tool rotation of 1200 rpm and tool traverse speed of 125 mm/min

SEM analysis conducted on the base metal showed random SiC particulate orientation as shown in Figure 4.26. When compared to TMAZ region and weld nugget, Figure 4.27 and Figure 4.28 respectively, a significant observation of particulate re-orientation was observed. It was also observed from the SEM micrograph that there is a re-concentration of SiC particulate within the weld nugget as shown in Figure 4.28. The weld nugget also showed better spread of fine and coarse SiC particulate compared to the other three zones. It was also observed that there was an increased quantity of fine SiC particulate in the weld nugget when compared to the other two regions (base metal and TMAZ region).

Figure 4.29 shows intact bonding interfaces between the weld nugget and the thermal mechanical affected zone (TMAZ). The SEM image in Figure 4.29 illustrates that the weld center has finer SiC particle when compared to the TMAZ region. The coarse particles in the weld nugget were also rounder and smaller. This was due to the knocking and chipping effect on the course SiC particle during the high velocity stirring.

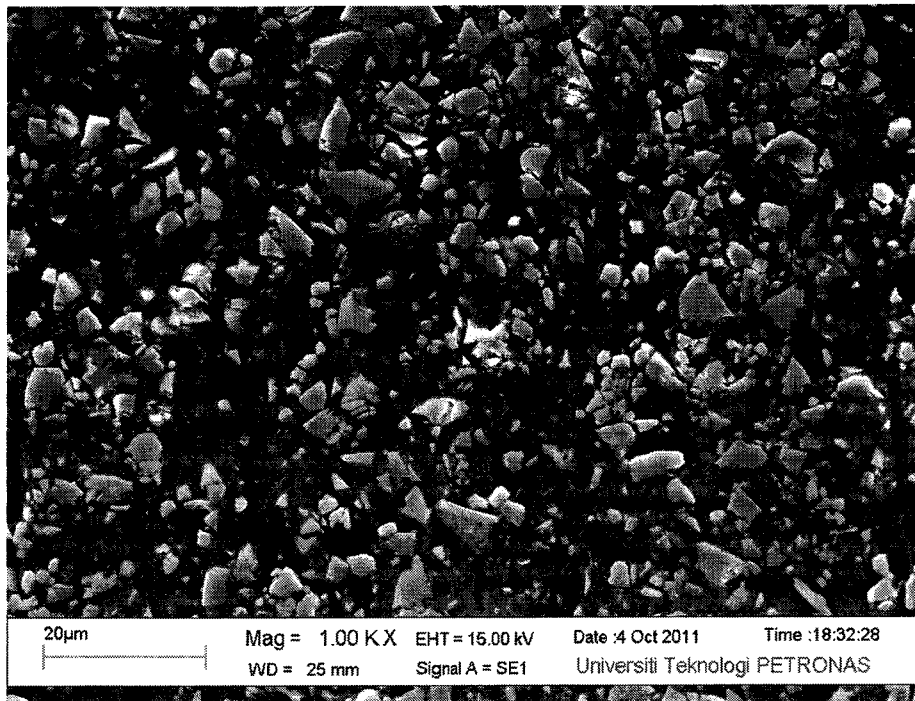


Figure 4. 26: Microstructure evaluations for friction stir welded sample in the Base metal

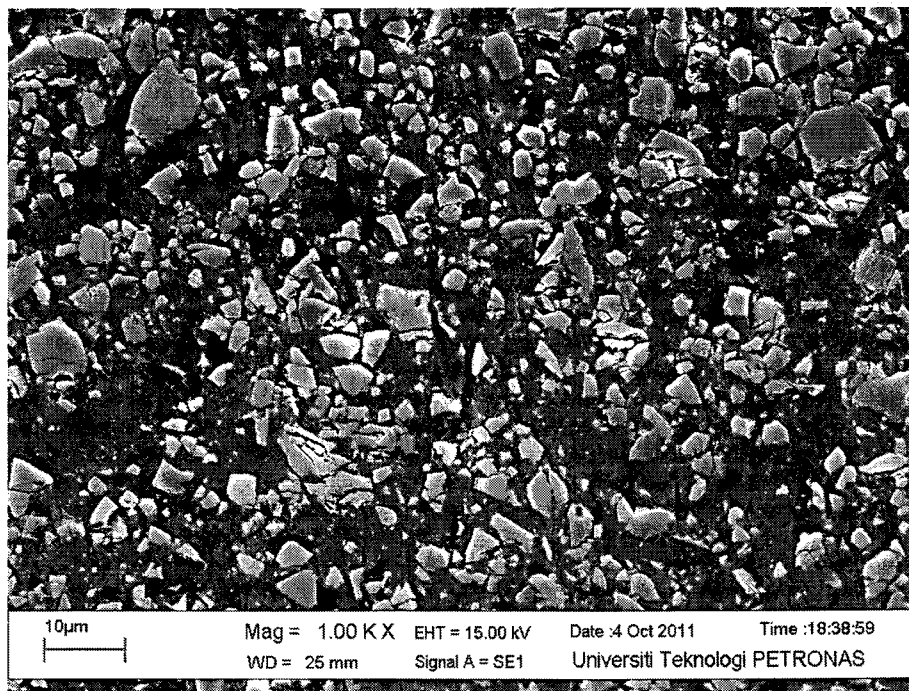


Figure 4. 27: Microstructure evaluations for friction stir welded sample in TMAZ region

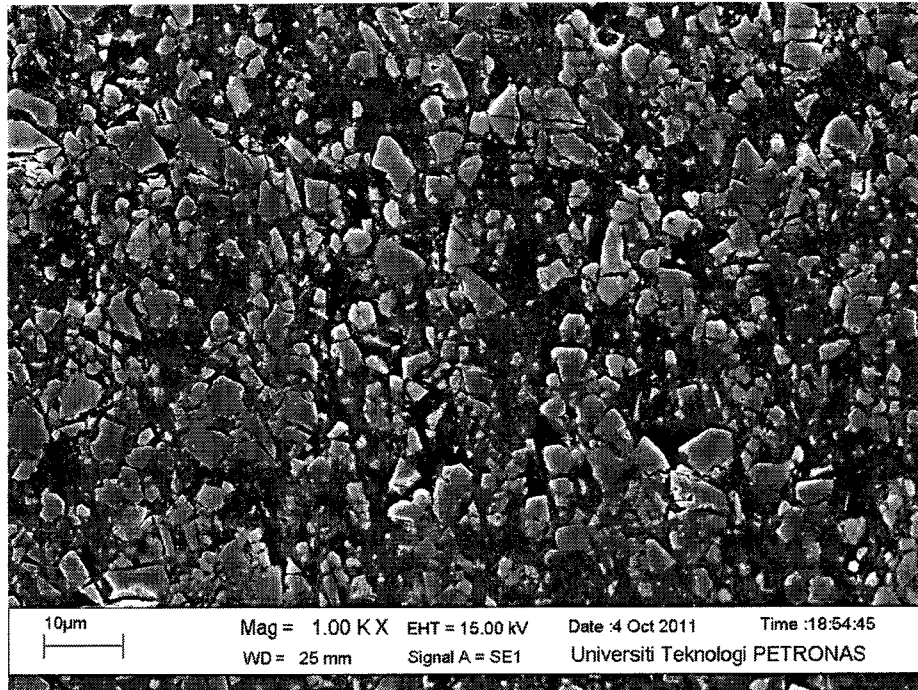


Figure 4. 28: Microstructure evaluations for friction stir welded sample in the weld nugget

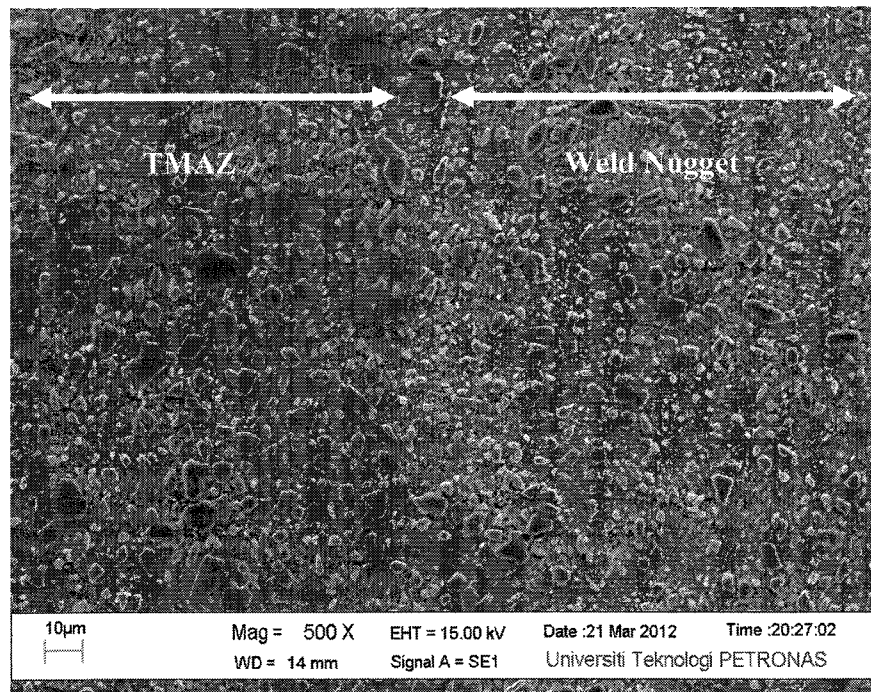


Figure 4. 29: Transition line between the weld nugget and TMAZ

A microstructure analysis was also conducted at a higher magnification to detect any deformities and also to analyze the interface between the SiC particle and the aluminum matrix. Weld microstructure observation showed formation of both fine and coarse SiC particles within the weld nugget. High rate of stirring action caused fine cracking on the course of SiC particles and knocking of the SiC particle edges were observed in the weld center as shown in Figure 4.30.

Figure 4.31 shows the development of pores on some of the coarse SiC particles. The formation of the pore may be related to the high stirring rate during the welding process due to the tool rotation. It is known that an increasing development of pores inside the weld nugget might reduce weld strength. Microstructure observation also proved that most of the pores occurred on the coarse SiC particles compared to fine SiC particle. Development of such pores can be reduced by increasing formation of fine SiC and decreasing the size of coarse SiC particulate sizes through knocking and chipping effect.

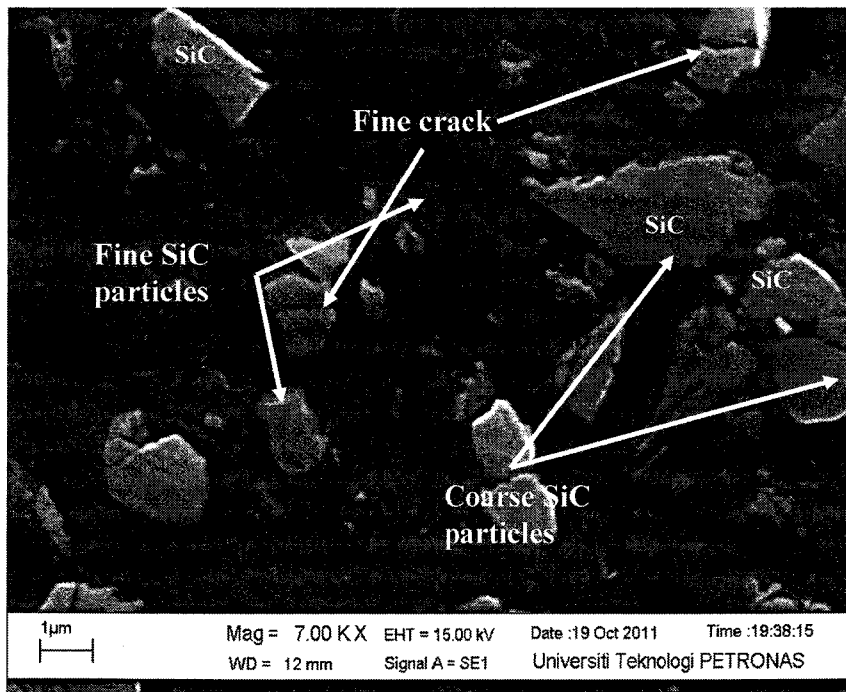


Figure 4. 30: Formation of fine cracks on the coarse SiC particulate

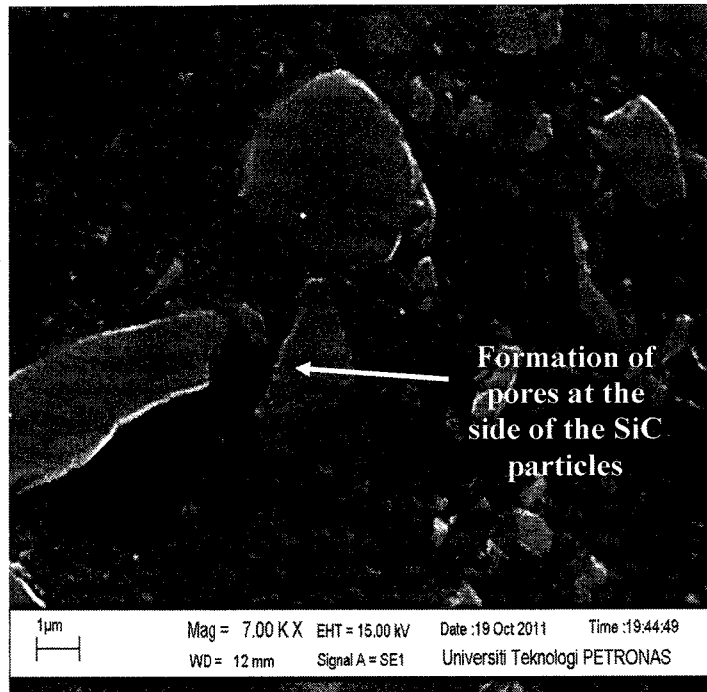


Figure 4. 31: Formation of pores at the interface between the aluminum matrix and the coarse SiC particulate

SEM micrograph in Figure 4.32, Figure 4.33 and Figure 4.34 also revealed difference in the particulate distribution within the welding nugget itself. Similar particulate distribution within the weld nugget was observed for most of the welded samples conducted using the MTS FSW machine. However some of the SEM micrograph analysis also shows that the advancing side (Figure 4.32) depicts a well spread SiC particulate with fewer coarse SiC particulate compared to the weld center (Figure 4.33) and the retreating side of the weld (Figure 4.34). SEM observation was also able to identify a higher amount of fine SiC particle spread in the advancing side compared to the weld center and the retreating side.

When compare to the advancing side, the retreating side shows a higher density of coarse SiC particulate and lesser density of fine SiC particulates distribution. Such result proves that the velocity or the movement of the plasticized material from the advancing side to the retreating side was not identical. It is understood that the advancing side had a better stirring action compared to the retreating side [47]. Such stirring action experienced in the advancing side caused it to have a better particle distribution and a more solubilized precipitation which enhanced the material strength. The denser fine SiC

particle spread within the advancing side was also caused by the movement of the plasticized material moving from the zone, around the tool and returning to the zone again [64].

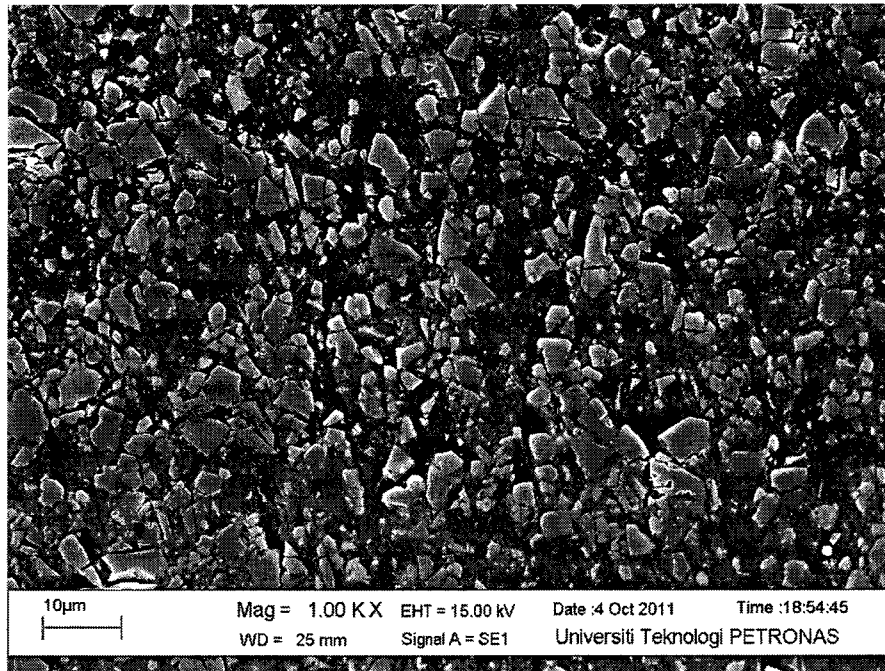


Figure 4. 32: Distribution of reinforcement particle in the advancing side

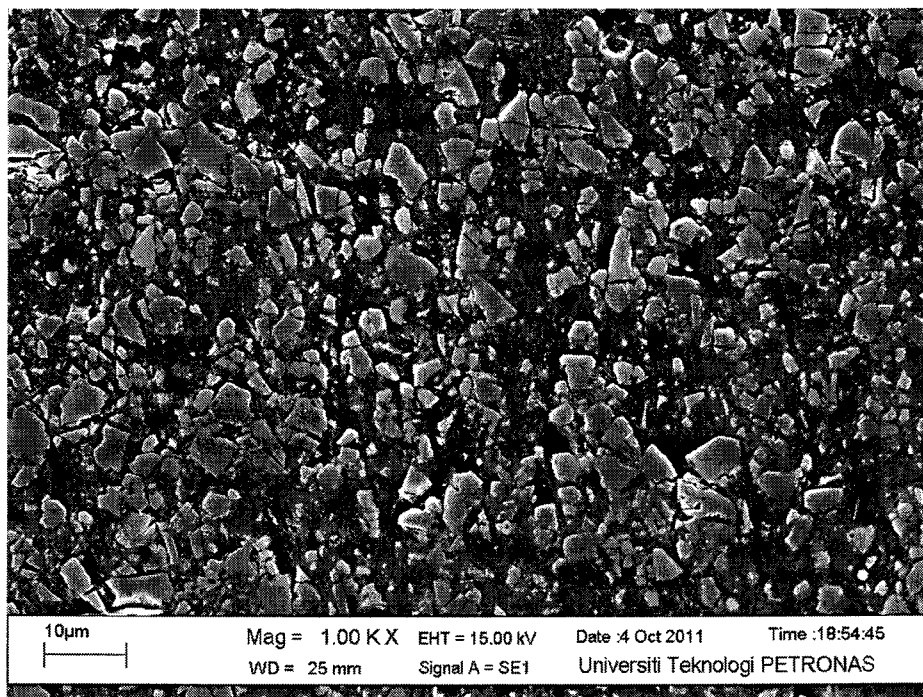


Figure 4. 33: Distribution of reinforcement particle near the center of the weld nugget

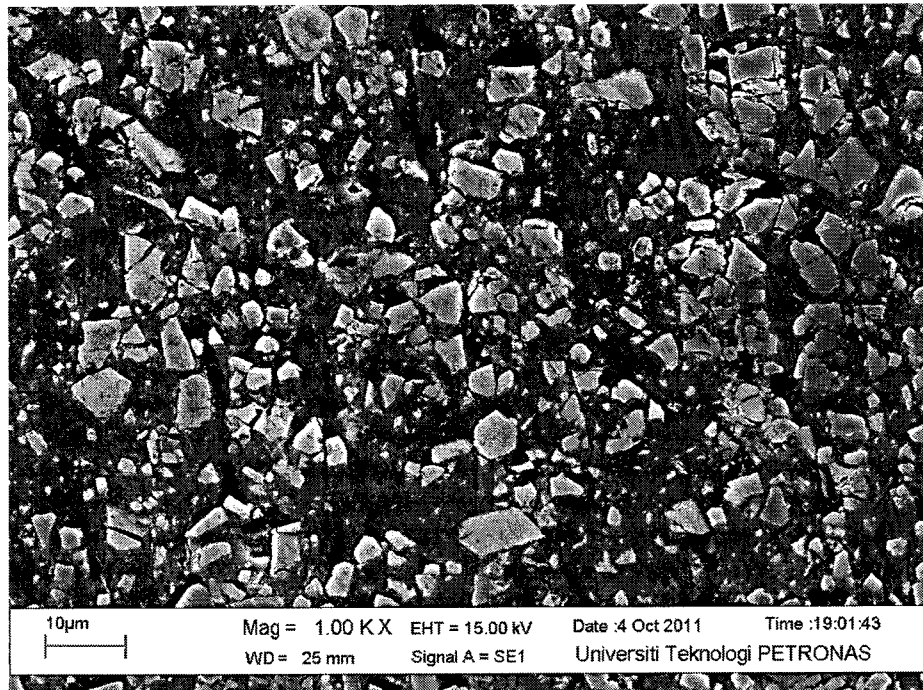
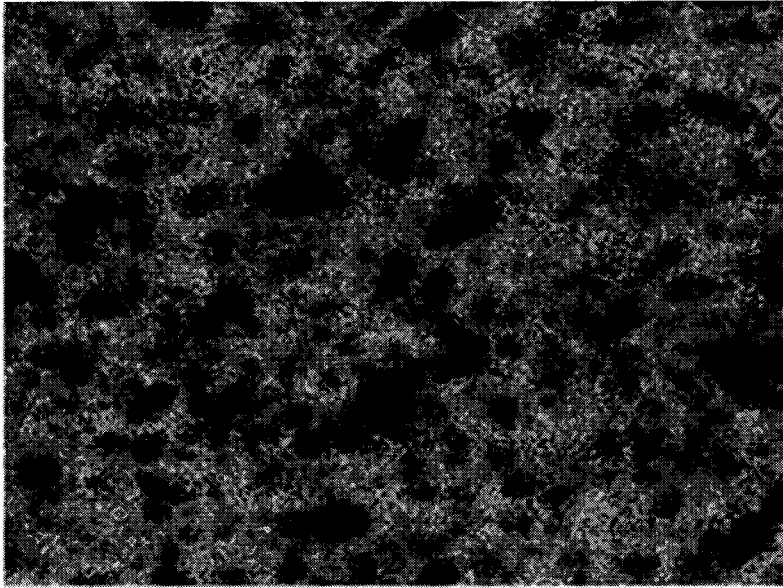


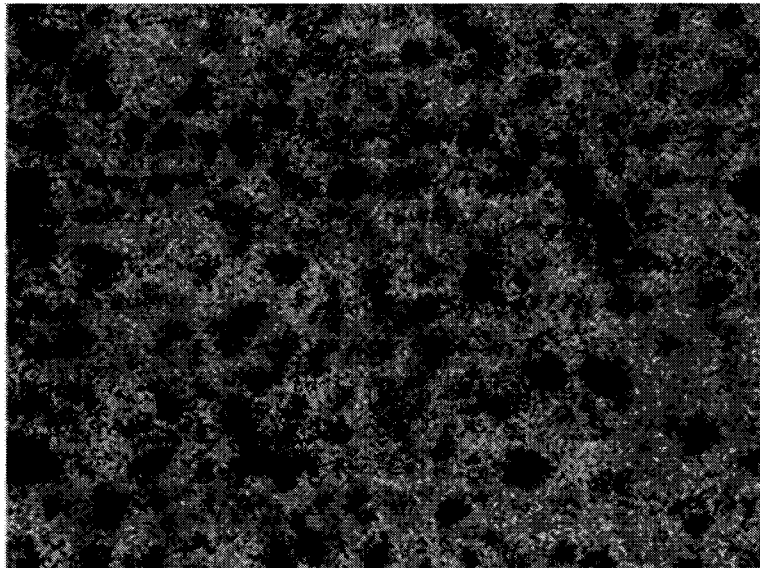
Figure 4. 34: Distribution of reinforcement particle in the retreating side

FESEM mapping further proved and enhanced the understanding of the SiC particulate distribution within the weld cross sections. To locate the distribution of hard SiC within the aluminum matrix mapping of aluminum and silicon element were compared. Mapping images in Figure 4.35 showed a more homogenous spread of SiC particulates in the advancing side of the weld when compared to the other two regions in the weld nugget (Figure 4.36 and Figure 4.37). The advancing side in Figure 4.35 exhibit a higher percentage of fine SiC particulates when compare to the other two regions. Such observation further supports SEM microstructure observation that was performed on the samples.



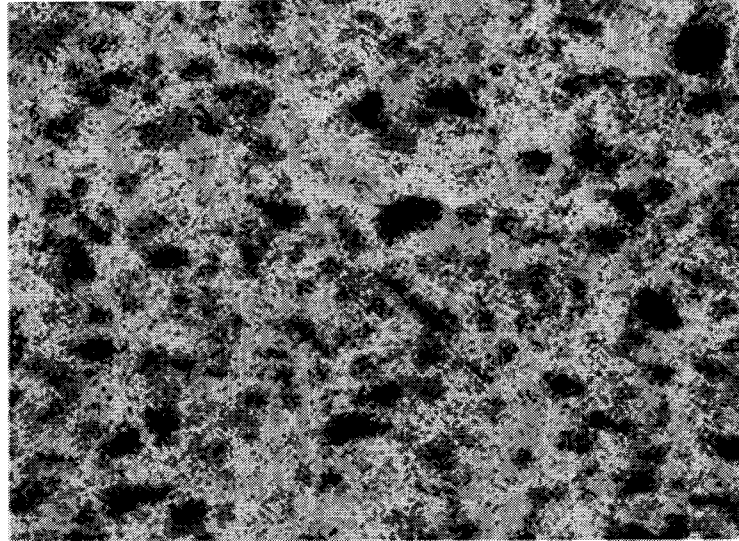
Al Ka1

Figure 4. 35: Mapping of aluminum distribution within the advancing side of the weld nugget



Al Ka1

Figure 4. 36: Mapping of aluminum distribution within the weld center of the weld nugget



Al Ka1

Figure 4. 37: Mapping of aluminum distribution within the retreating side of the weld nugget

Microstructure band of fine SiC particles was also identified within the welding zone. Such formation causes the material to have its distinctive onion like ring in its cross section. This structure is very obvious in the advancing side of the weld while it was not so visible in the retreating side. Electron micrograph depicts these structures in Figure 4.38 and an enlarged image in Figure 4.39 and Figure 4.40. Such observation was caused by the stir rate between the different sides of the tool where the advancing side experienced more stirring action when compared to the retreating side. Fine SiC particulate banding was attributed to smaller SiC particle size which was more prone to the stirring action when compared to larger particle sizes. Observation of higher concentration of banded structure in the advancing side was also attributed to a higher density of fine SiC particle when compared to the retreating side. The bands was initiated at the periphery of the tool pin and propagated towards the edge of the welding zone.

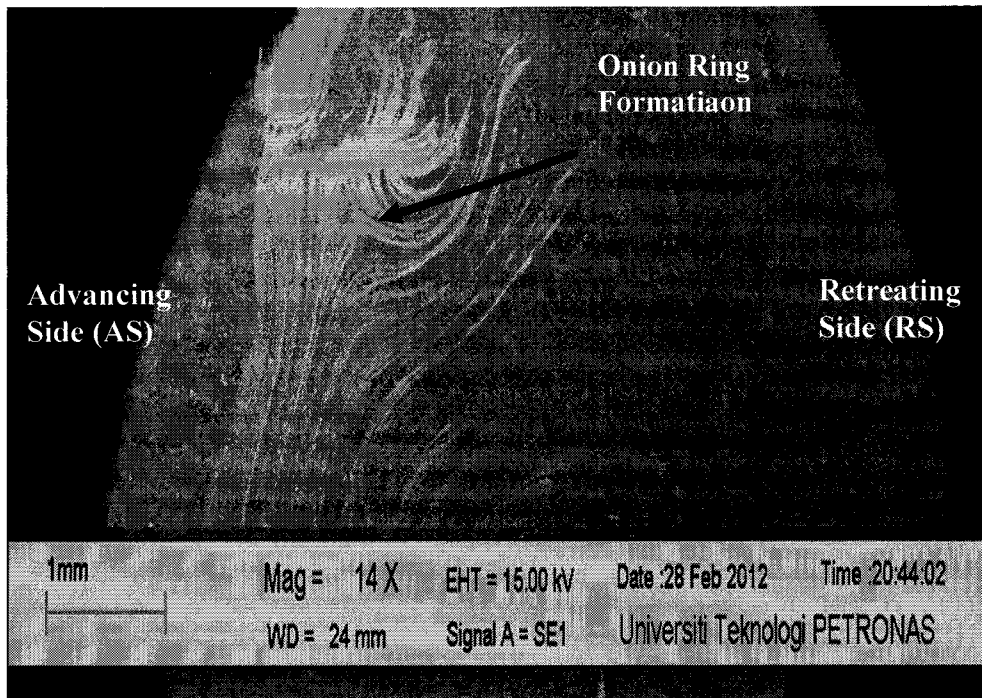


Figure 4. 38: Onion like rings within the weld zone

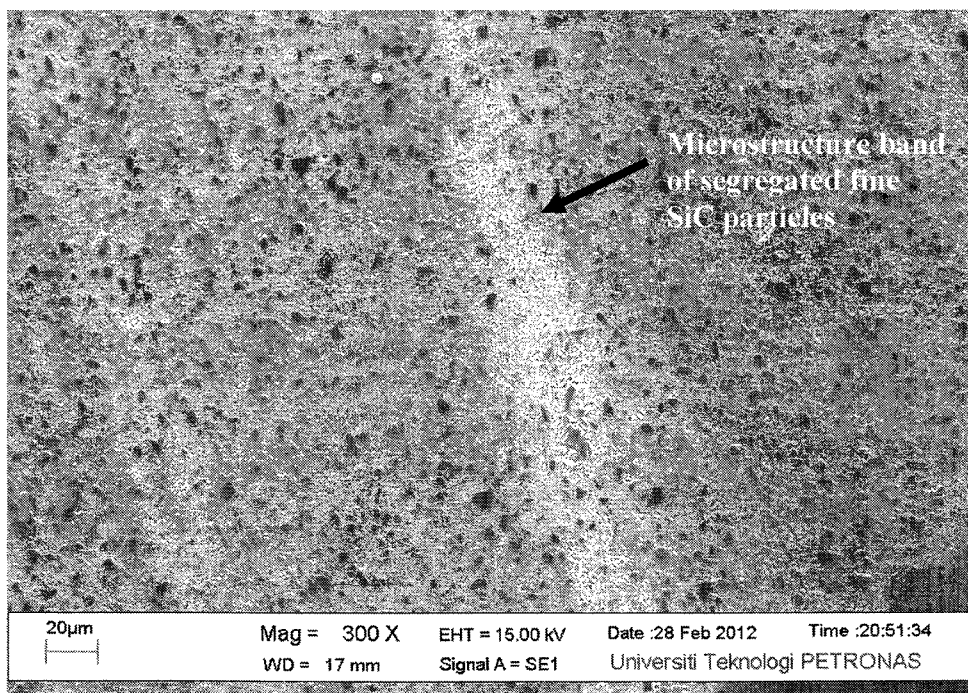


Figure 4. 39: Microstructure band of segregated fine SiC particle within the weld zone, magnification at 300X

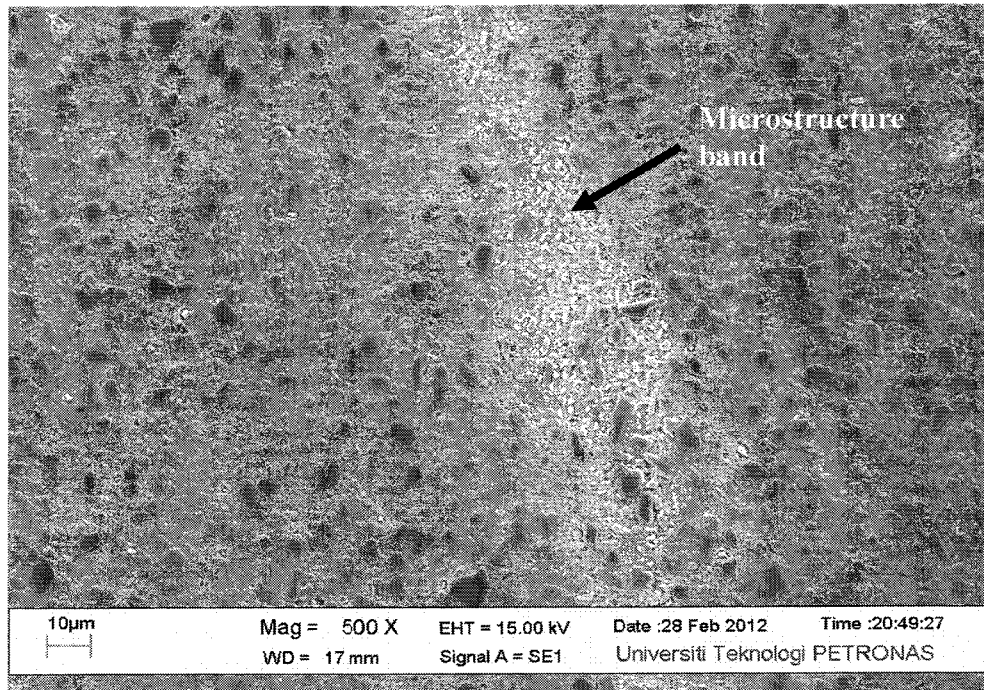


Figure 4. 40: Microstructure band of segregated fine SiC particle within the weld zone, magnification at 500X

4.3.3 Effect of welding parameter on mechanical properties

Tensile test showed variation in welding strength between various welding parameters as shown in Table 4.5. On average most of the welded samples had reasonably maintained material strength with lower elongation to failure percentage when compared to the base metal as shown in Figure 4.41 and Figure 4.42. Overall, sample 04 shows the best weld strength compared to other welded samples (Table 4.5).

The cause of failure may be due to defects within the weld nugget such as microscopic pores or even larger defects such as tunneling. Observation also showed that most of the failures occurred at the TMAZ interface near to the advancing side of the weld nugget as shown in Figure 4.47. Previous research done by Cavalierea *et al.* [36] on tensile test confirmed the welding failure within the mentioned interfaces. Some of the subsequent test also showed failures within weld nugget itself. Such failures might be resulted from post weld microstructure changes such as inhomogeneous distribution of reinforcement particles or formation microscopic pores. Most of the tensile tests also

showed a significant decrease in the percentage of elongation to failure. Reduction in the elongation to failure could be related to increasing brittleness of the weld nugget.

It is important to identify the effects of welding parameters on the weld strength. Optimum welding speeds and tool rotation is crucial in obtaining sound welding. For example, excessively low tool rotation might cause inadequate material mixing resulting in defects such as tunneling whereas overly high tool rotation would also cause similar effects. Besides tool rotation, an inadequate welding speed would cause insufficient heat dispersion resulting in low stirring rate, but unduly high welding speed would cause excessive heating that would cause grain (aluminum matrix) coarsening resulting in decreased material strength.

Table 4. 5 Tensile test results for MTS FSW machine

| Sample | Speed (mm/min) | RPM | TS (MPa) | Et % |
|--------|----------------|------|----------|------|
| 01 | 10 | 1200 | 223.17 | 1.21 |
| 02 | 100 | 1200 | n/a | n/a |
| 03 | 100 | 1200 | 226.00 | 1.31 |
| 04 | 100 | 900 | 256.63 | 0.33 |
| 05 | 150 | 900 | n/a | n/a |
| 06 | 125 | 900 | 218.41 | 0.6 |
| 07 | 125 | 1200 | 209.17 | 1.3 |
| 08 | 125 | 700 | 239.50 | 0.47 |

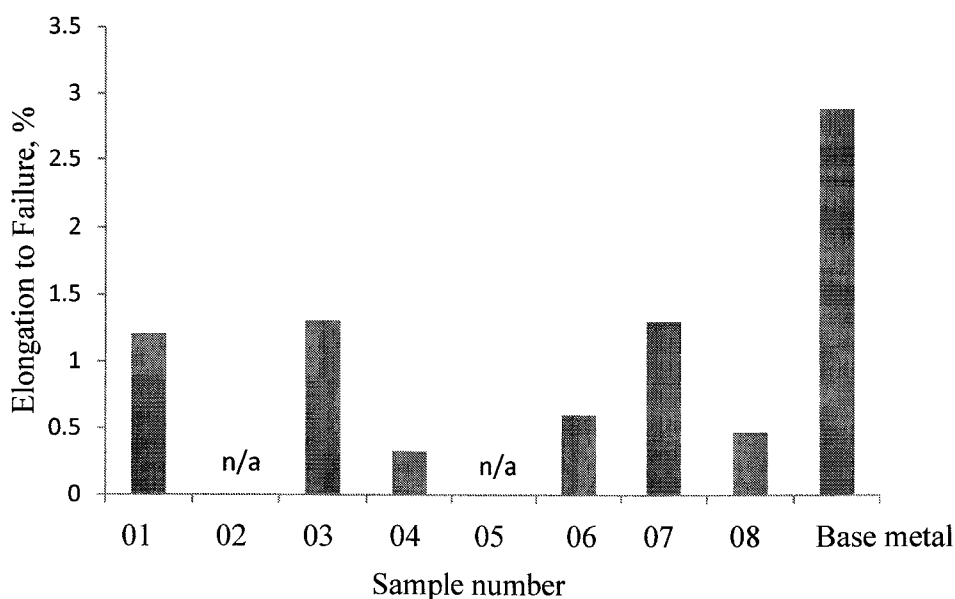


Figure 4. 41: Elongation to failure percentage from FSW using MTS FSW machine

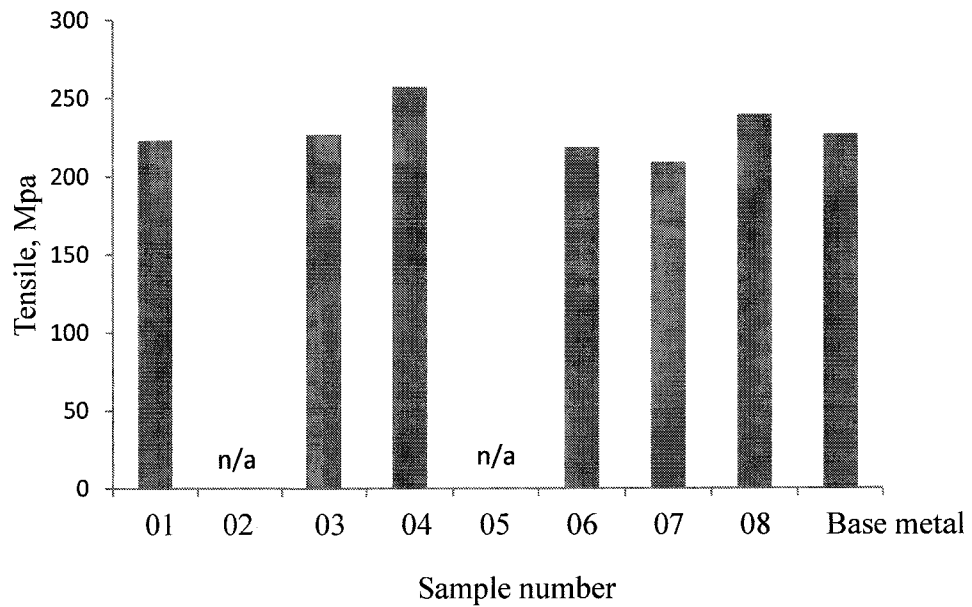


Figure 4. 42: Tensile test results from FSW using MTS FSW machine

4.3.3.1 Tool rotation

Analysis on the effect of tool rotation on the material's mechanical properties (tensile strength and elongation to failure) was conducted which is shown in Figure 4.43 and Figure 4.44. The welded samples have similar traversal speed of 125 mm/min with different tool rotations of 700 rpm, 900 rpm and 1200rpm. The result showed that an increase in the tool rotational speeds caused an increase in the material elongation to failure whereas a decreased in the joining strength. Decrease in material strength for sample welded at a higher tool rotation may be due to irregular distribution of SiC particle within the material microstructure (Figure 4.18). Microstructure irregularities were caused by detrimental high stirring effects such as microstructure band and inhomogeneous distribution of SiC particles within the weld nugget which induces stress within the material.

Sample analysis also shows that all samples with tool rotational speed of 1200rpm give better elongation to failure percentage when compared to samples with lower tool rotation. Such elongation to failure percentage increase for tool rotation of 1200 rpm was

detected in sample 01, 03 and 07, Table 4.5. However, such increase in elongation to failure does not ensure a similar improvement in material strength. Most of the samples that had a high elongation to failure percentage tend to have a lower tensile strength when compared with materials that have much lower elongation to failure percentage. Welded sample that have lower tool rotation such as sample 04 and 08 (Table 4.5) showed a definite increase in its tensile strength.

4.3.3.2 Tool traverse speed

An assessment was also performed to correlate the influence of tool traverse speed on the weld mechanical properties which is shown in Figure 4.45 and Figure 4.46. Samples with fixed tool rotation of 900 rpm and tool traversal speed of 100 mm/min, 125 mm/min and 150 mm/min were chosen for the test. The result showed that an increase of tool traverse speed from 100 mm/min to 125 mm/min, a drop in tensile strength from 256.68 MPa to 218.41 MPa was observed. Such observation can be supported through SEM analysis, where a more homogenous distribution of SiC particles was identified in the advancing side for the sample welded with tool traverse speed of 100 mm/min, Figure 4.19. It was also observed that as tool speed increased from 100 mm/min to 125 mm/min elongation to failure percentage was also seen to increase. As the speed progressed to 150 mm/min the tensile test was unable to be conducted due to the extensive tunnel like defect across the welding line observed in the welded sample.

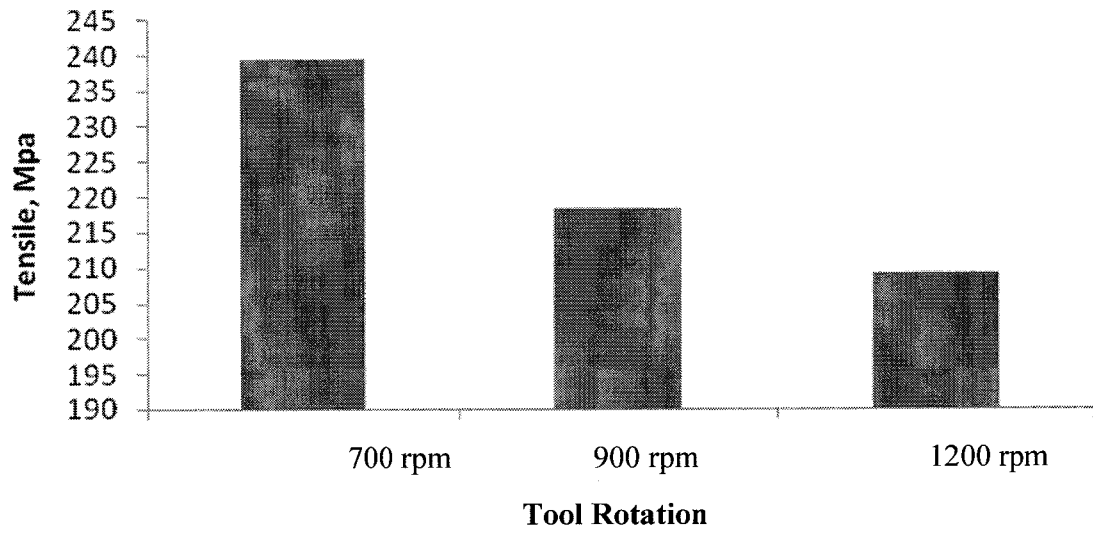


Figure 4. 43: Influence of tool rotation on tensile strength

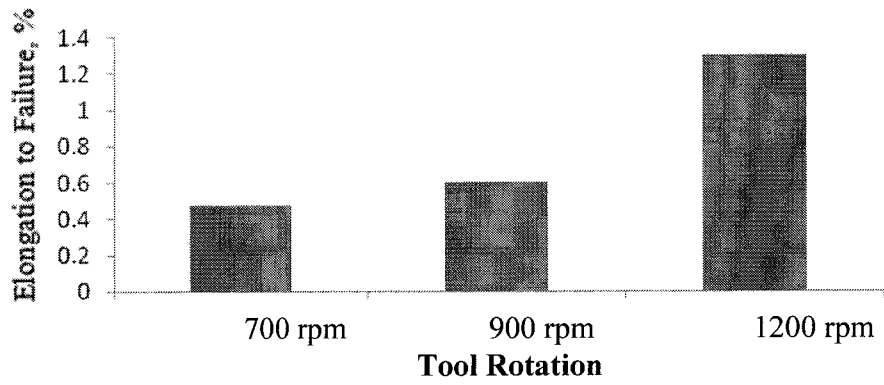


Figure 4. 44: Influence of tool rotation on elongation to failure percentage

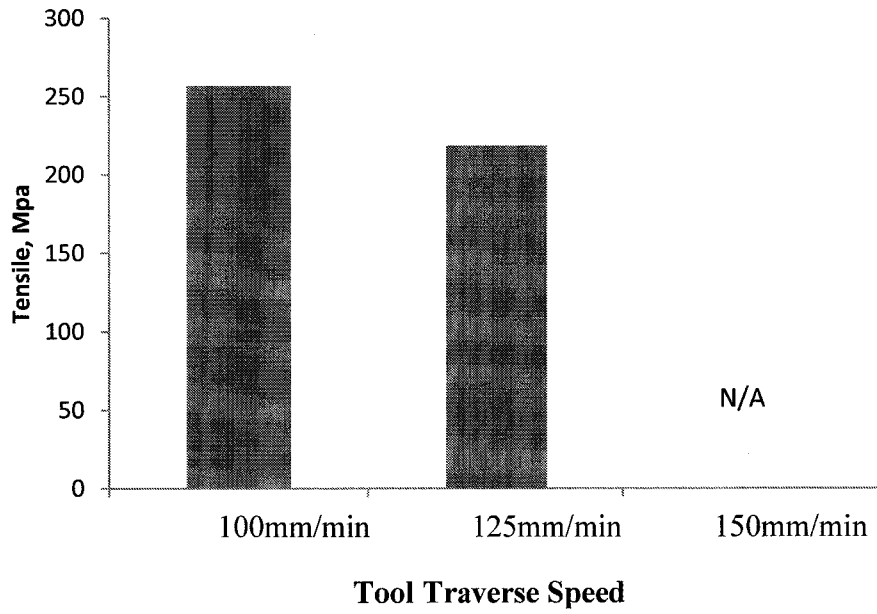


Figure 4. 45: Influence of tool traverse speed on tensile strength

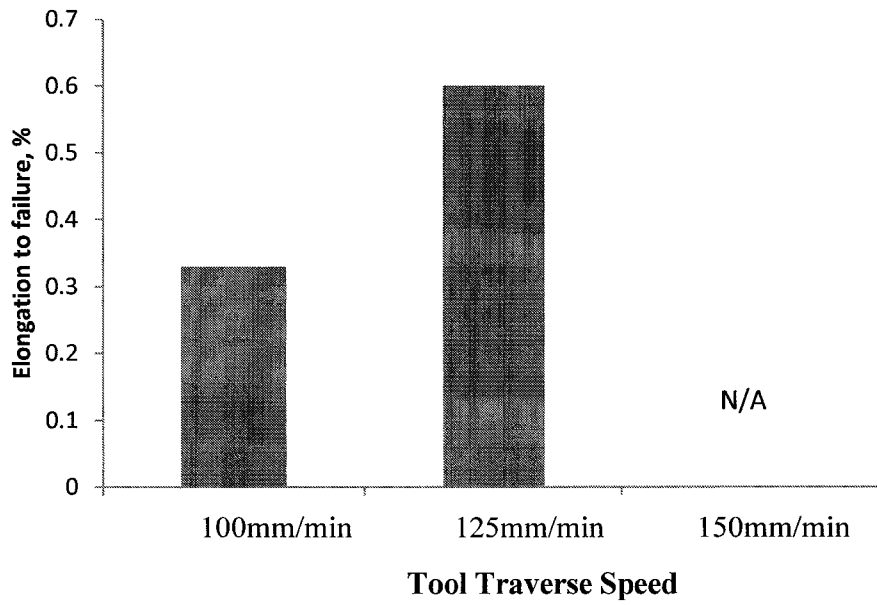


Figure 4. 46: Influence of tool traverse speed on elongation to failure percentage

4.3.3.3 Tool tilting

Un-tilted samples showed extensive defects within the weld nugget. The result showed that by using welding parameter with low tool traverse speed of 10 mm/min and high tool rotation of 1200 rpm (Figure 4.9 (a)), the un-tilted samples showed reasonable welding quality. As the tool speed was increased an extensive tunneling defect was observed within the weld nugget shown in Figure 4.9 (b). Such defect was due to inadequate localization of the stirred material during welding process. When compared to tilted FSW samples, extensive damages to the weld nugget were not seen. This was due to the coupling effects that tilted tool provided to ensure that the stirring material was contained during the welding process. Due to the problems identified, comparison between tilted samples and non-tilted samples was not possible.

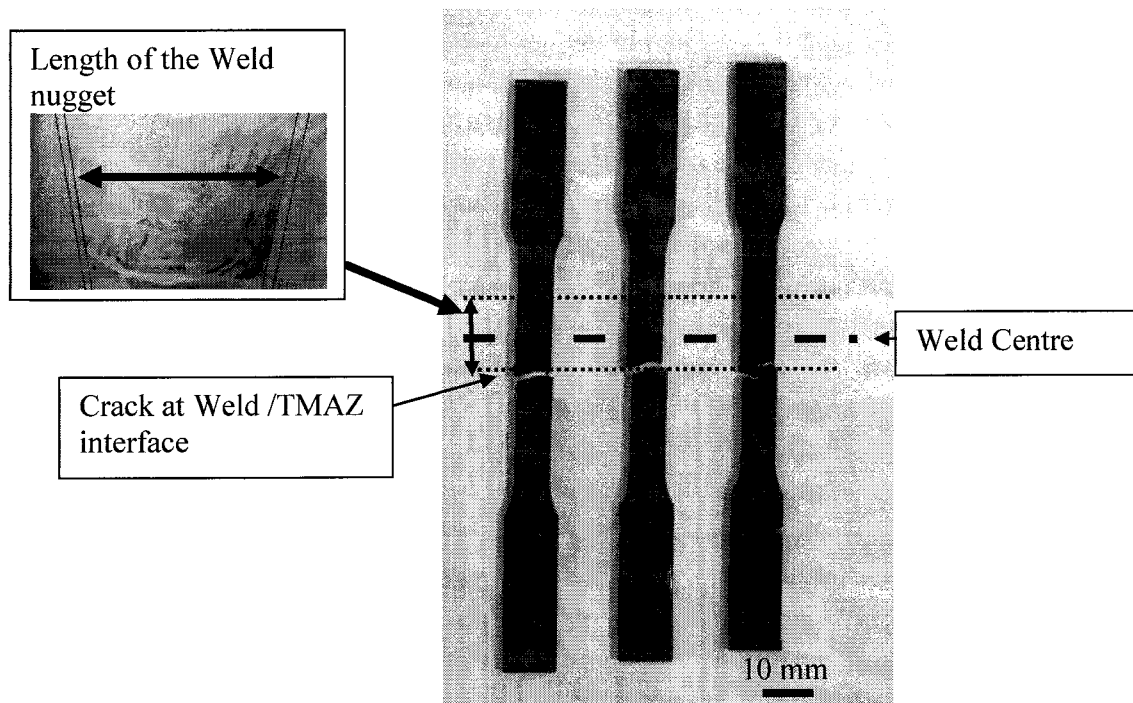


Figure 4. 47: Tensile Test Sample

4.4 Analysis of weld hardness

Overall hardness profile obtained from Vickers hardness test showed a significant increase in the weld zone when compared to the HAZ and the base metal. The location of the hardness test across the weld section can be viewed in Figure 4.48. Average hardness

readings were conducted among the welded sample shown in Table 4.6. Minimal change of hardness was observed from most of the welded samples. Obvious hardness changes were observed when comparing between tilted and untilted welded samples. Increase in weld hardness in tilted weld sample correlated with microstructure analysis which showed a more compacted and denser SiC particulate distribution. Denser SiC particulate in the tilted samples was due to the coupling effect caused by tool tilting during the welding process. In addition, weldment that was conducted using excessive tool traverse speed of 150 mm/min showed an almost similar weld hardness comparison to the base metal. Similar hardness result was due to reduce material mixing which maintained the material original property.

Most of the HAZ hardness test for the welded samples showed almost similar hardness with the base metal. However sample 01 showed a significant decrease in the hardness value compared to the other welded samples. This might be due excessive heating generated during the welding process which caused softening or annealing effect on the HAZ region.

Table 4. 6 Average hardness reading for MTS FSW machine welded samples

| Samples | Hardness value for weld nugget (HV) | Hardness value for HAZ (HV) |
|------------------------------------|-------------------------------------|-----------------------------|
| Base metal | 115 | - |
| 01(10mm/min, 1200rpm, un-tilted) | 127.13 | 101 |
| 02 (100mm/min, 1200rpm, un-tilted) | 111.3 | 116 |
| 03(100mm/min, 1200rpm, tilted) | 131 | 114 |
| 04(100mm/min, 900 rpm, tilted) | 128 | 112 |
| 05(150mm/min, 900 rpm, tilted) | 116.54 | 113 |
| 06(125 mm/min, 900 rpm, tilted) | 123.03 | 111 |
| 07(125 mm/min, 1200 rpm, tilted) | 123.05 | 114 |
| 08 (125mm/min, 700 rpm, tilted) | 127.2 | 113 |

Irregular hardness distribution was observed for most of the welded samples (Appendix A). However hardness test do show similar hardness trend for welded sample using low tool traverse speed (10 mm/min and 100 mm/min) and low tool rotation (700 rpm) as shown in Figure 4.49, Figure 4.50 and Figure 4.51. Hardness reading for such samples shows an unsymmetrical distribution between the advancing side and the retreating side which indicates hardness increase as it approaches the advancing side of the weld nugget.

Such observation was consistent with SEM micrograph analysis which indicated unsymmetrical circulation of the material flow inside the weld zone. SEM micrograph indicated a higher stir rate in the advancing side of the weld compared to the retreating side of the weld. Therefore such stir rate causes the advancing side to have higher hardness which was notable with homogenous spread of coarse and fine SiC particulate. Besides, the advancing side was also notable with its higher concentration of fine SiC particles. Higher amount of fine SiC particles tend to increase pinning effects within the aluminum matrix causing the material to get even harder [46,45]. Moreover, denser quantity of SiC particle in the advancing side of the weld was also attributed to the increase in hardness. Increasing SiC particulate concentration in the advancing side was attributed to majority deposition of the SiC particulate within the zone during the stirring process [64].

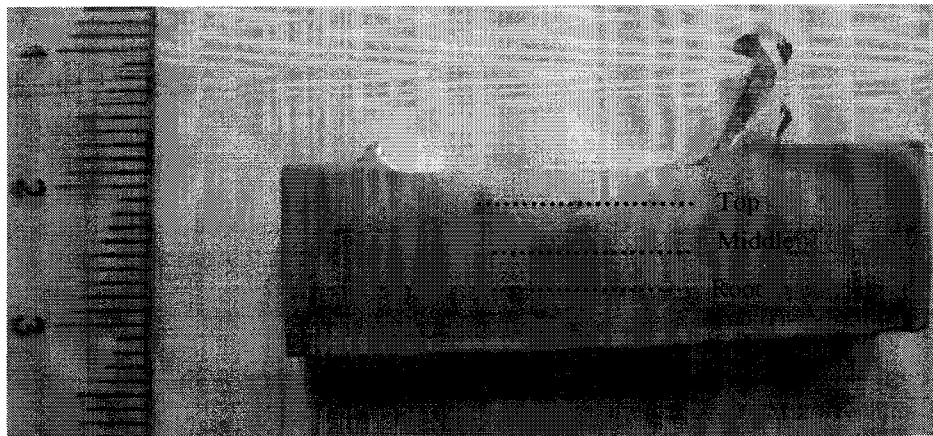


Figure 4.48: Three different locations of hardness

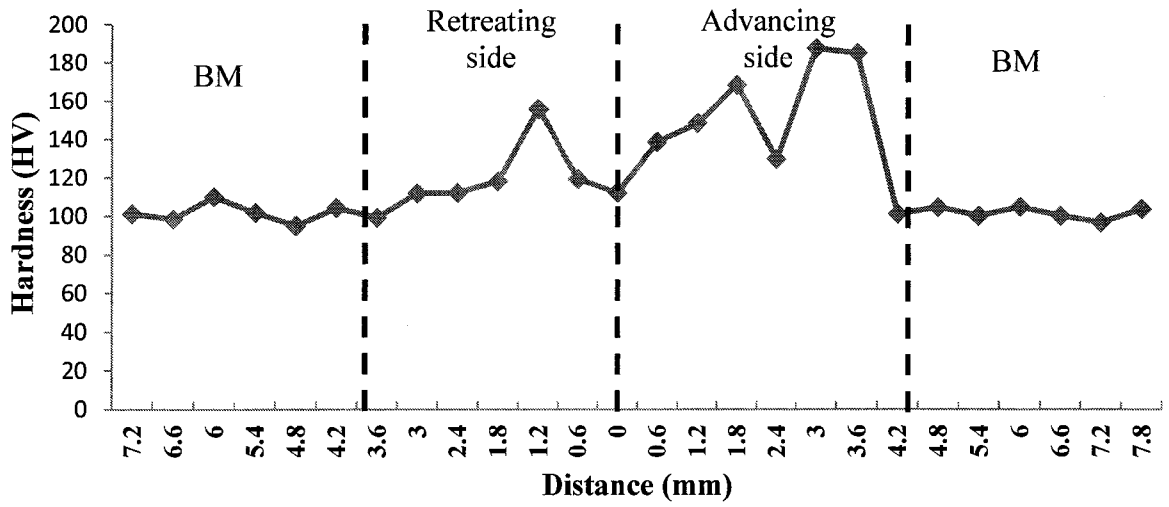


Figure 4. 49: Upper Section vickers hardness reading

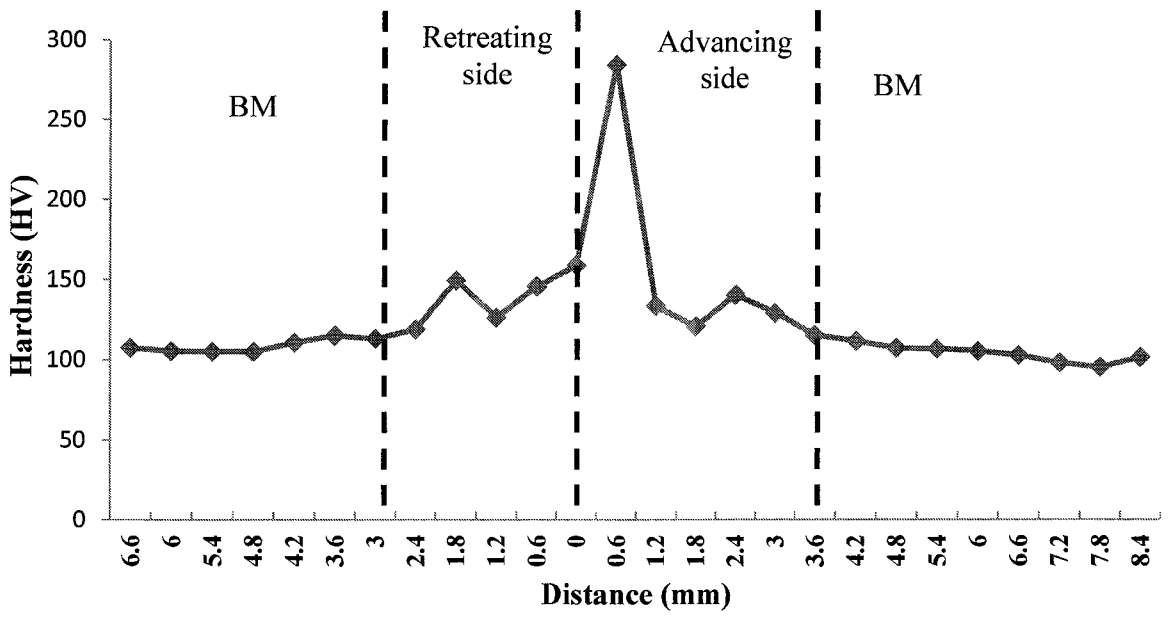


Figure 4. 50: Middle section vickers hardness reading

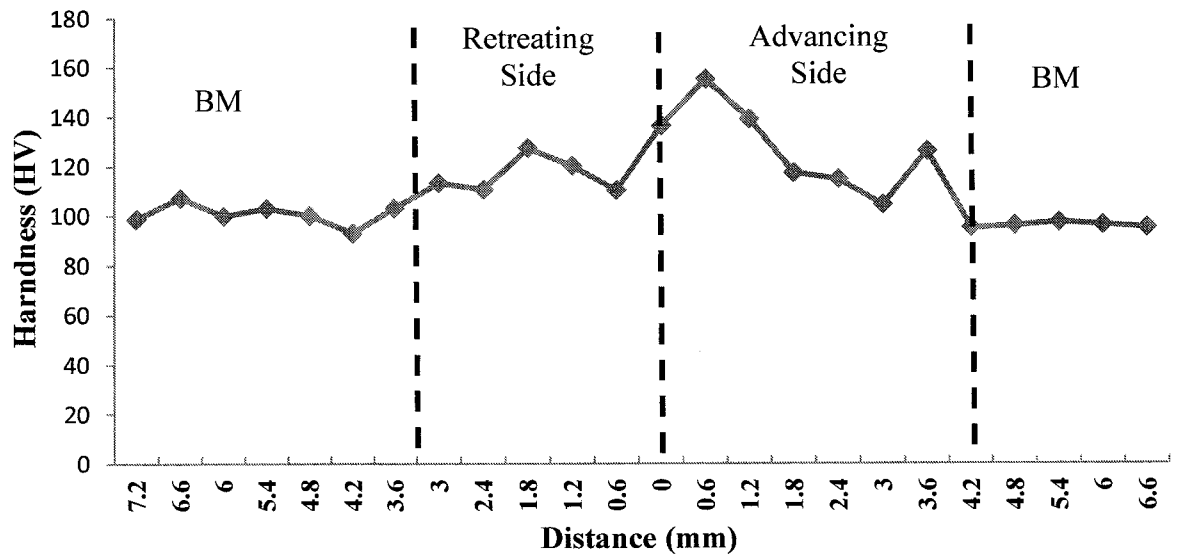


Figure 4. 51: Root section vickers hardness reading

4.5 Microstructure and mechanical comparison between CNC milling Bridgeport and MTS FSW machine

4.5.1 Weld Microstructure analyses

Samples with tool traverse speed of 10 mm/min and tool rotation of 1200 rpm were chosen for the comparison. Microstructure results are shown in the Figure 4.52. Both of the welded samples obtained by CNC milling Bridgeport and MTS FSW machine showed homogenous distribution of SiC particles. It was also observed that more distribution of fine SiC particles in the sample obtained by MTS FSW machine. Homogenous spread of SiC particles and an increased spread of fine SiC particles will caused pinning effects would result in better mechanical properties. These results showed that MTS FSW machine has better post weld macrostructure compare to the CNC milling Bridgeport welded sample. It was also observed that a higher concentration of SiC particles was seen for the welded sample using CNC milling Bridgeport.

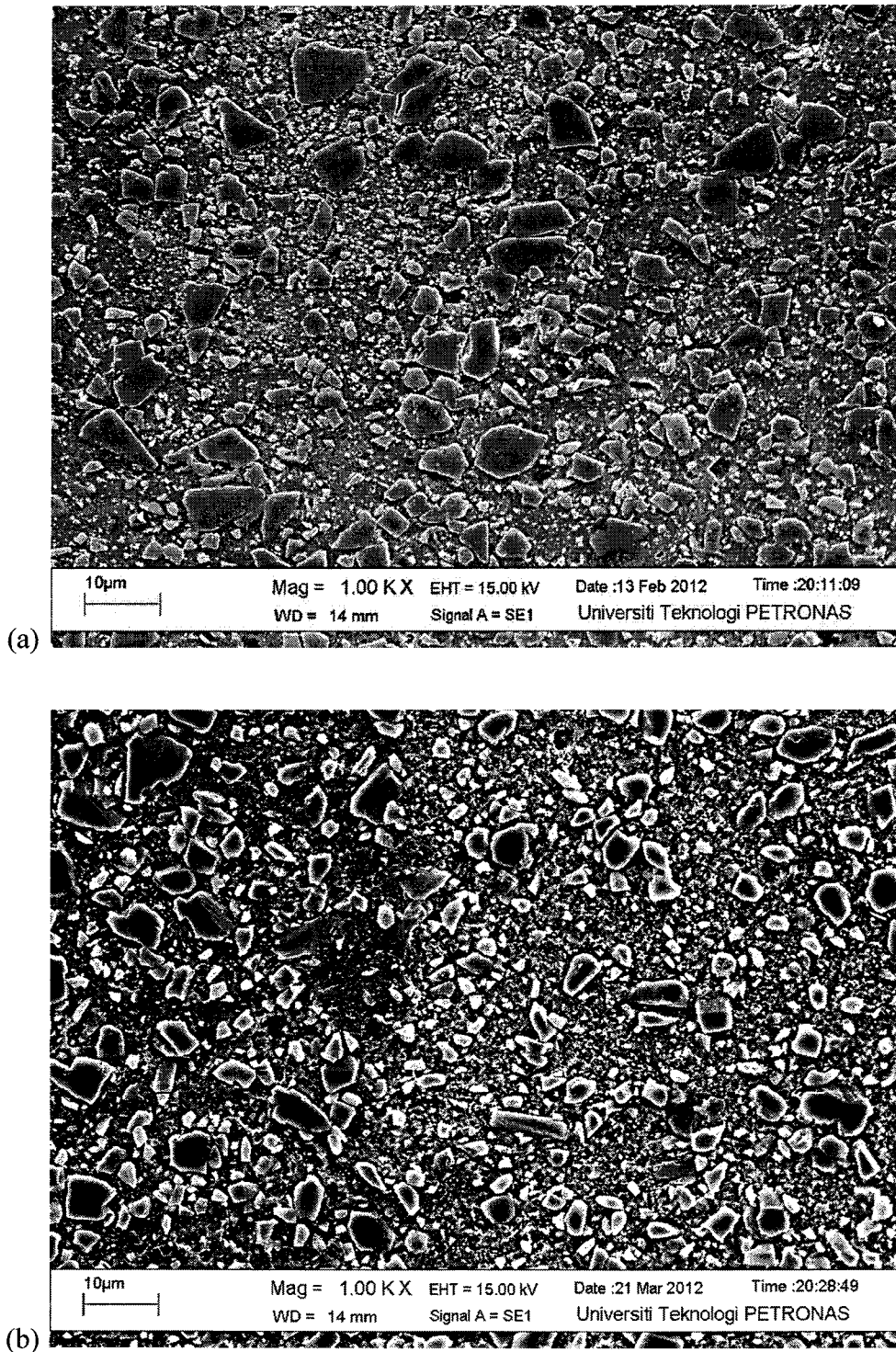


Figure 4. 52: (a) CNC milling Bridgeport and (b) MTS FSW welded sample

4.5.2 Weld mechanical results

Tensile test results between the two samples performed by CNC milling Bridgeport and MTS FSW machine are shown in Table 4.7. Overall the results show better tensile and elongation to failure value for the MTS FSW machine welded sample compared to the sample obtained by the CNC milling Bridgeport. These results confirmed to previous microstructure results which showed homogenous SiC particle distribution and higher fine SiC particle concentration in the sample obtained by MTS FSW machine welded sample.

Table 4. 7 Tensile Test comparison between MTS FSW machine welded sample and CNC milling Bridgeport Sample

| Sample | Tensile Strength (Mpa) | Elongation to failure percentage |
|------------------------------------|------------------------|----------------------------------|
| Sample 01 (MTS FSW machine) | 223.17 | 1.21 |
| Sample 02 (CNC milling Bridgeport) | 207.33 | 1.56 |

Hardness test conducted for both samples showed higher average hardness on the CNC milling Bridgeport sample compare to the sample obtained by MTS FSW machine. Hardness results are shown in the Table 4.8. Higher hardness reading in the CNC milling Bridgeport sample was due to high concentration of SiC particles observed in the microstructure analysis.

Table 4. 8 Hardness test comparison between MTS FSW machine welded sample and CNC milling Bridgeport sample

| Sample | Hardness Average (HV) |
|------------------------------------|-----------------------|
| Sample 01 (MTS FSW machine) | 111.13 |
| Sample 02 (CNC milling Bridgeport) | 116.8 |

It can be concluded that the MTS FSW machine showed better mechanical properties compare to the samples obtained by the CNC milling Bridgeport. Besides that,

the downturn in using CNC milling Bridgeport include the inability to hold to high machine loading and also to tilt the tool during the machining which further limit its application. Furthermore, such limitation also causes problems associated with visible defects in the weld nugget which have been discussed earlier.

4.5.3 FESEM Energy Dispersive X-ray Spectroscopy Results

EDX analysis showed similar chemical composition comparison between the samples done using CNC milling Bridgeport and MTS FSW machine which is shown in the Figure 4.53. Analysis on both samples also showed same chemical composition when compared to the base metal. The results showed welding conducted on both machines worked well below the melting temperature of the material.

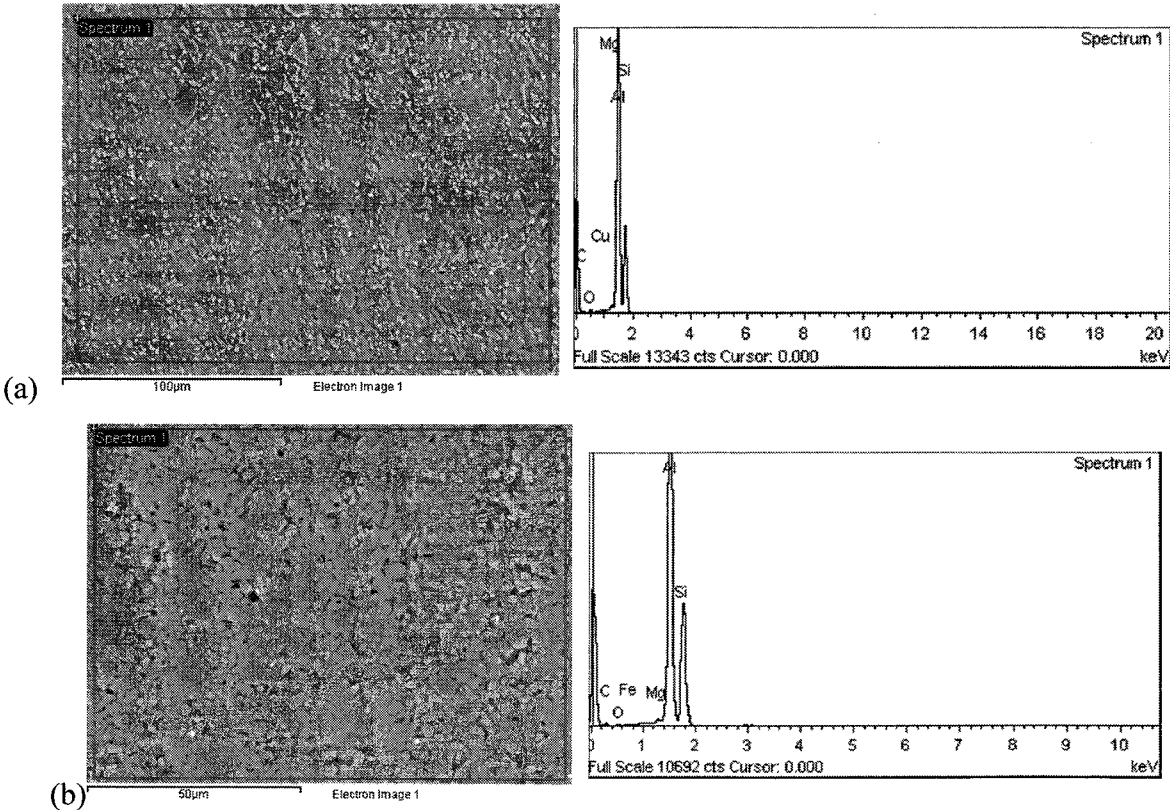


Figure 4. 53: EDX comparison between (a) CNC milling Bridgeport and (b) MTS FSW machine welded sample

4.5.4 XRD analyses of weld

XRD analysis was also performed to determine phase changes and development of stresses across the weld zones between the samples produced by the two mentioned welding machine. The examined weld zones were the base metal, HAZ, TMAZ and the weld nugget. Similar XRD results in the weld nugget were obtained from both samples where similar peaks and phase of SiC and Al were identified as shown in the Figure 4.54 and Figure 4.55.

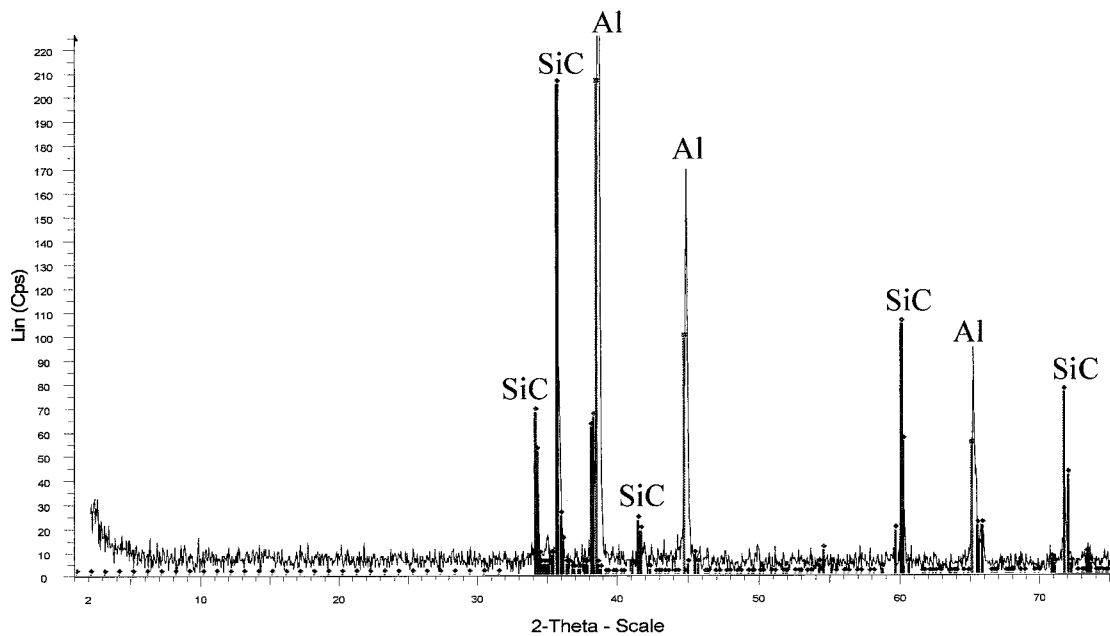


Figure 4. 54: XRD Peaks for CNC milling Bridgeport weld nugget sample

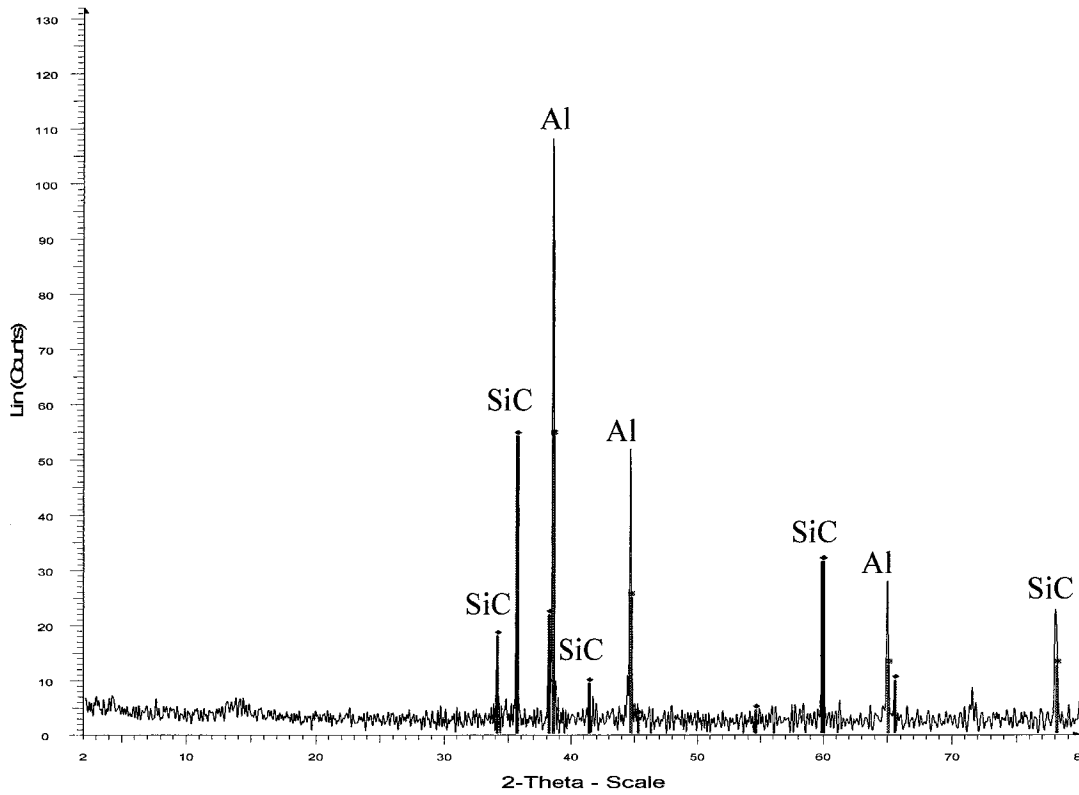


Figure 4. 55: XRD Peaks for MTS FSW machine weld nugget sample

Furthermore, based on the XRD results in Figure 4.56 and Figure 4.57, there were no evidence of phase changes across the weld zones from both of the welded samples. The results showed the FSW post weld samples maintained the material's original chemical composition. Among the potential cause of the unchanged material phase was the controlled welding temperature under the material melting point. It must be noted that welding temperature above the material melting point could cause decomposition of the material compound into new phase structure. So it can be seen that welding of AMMC using both machines maintained the welding temperature below the melting temperature which helped in retention of the material's original chemical properties.

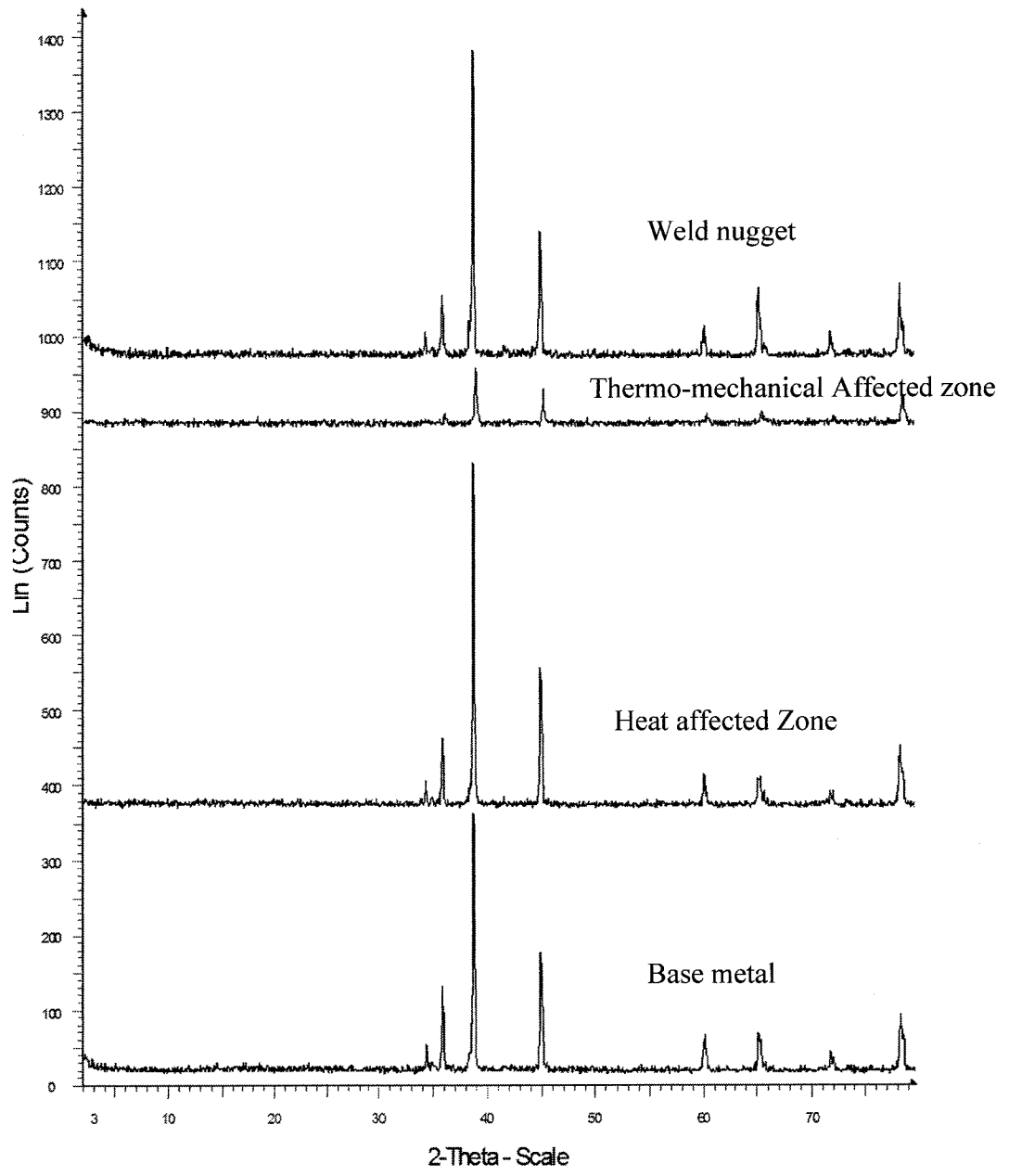


Figure 4. 56: Phase analysis on weld nugget, thermo-mechanical affected zone (TMAZ) and heat affected zone (HAZ) and base metal for CNC milling Bridgeport sample

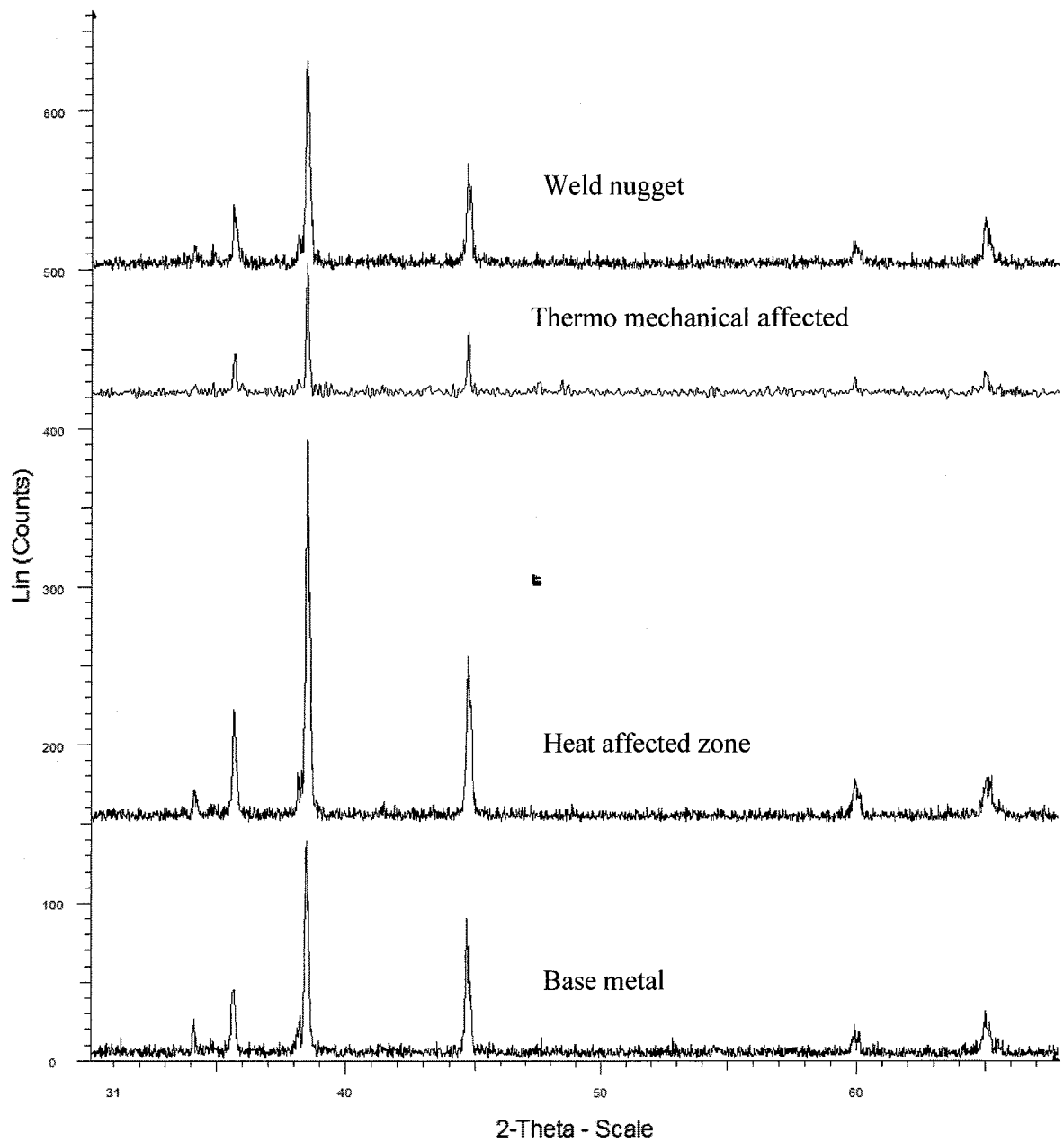


Figure 4. 57: Phase analysis on weld nugget, thermo-mechanical affected zone (TMAZ) and heat affected zone (HAZ) and base metal for MTS FSW machine

Lattice spacing analysis showed similar result for both samples as shown in Table 4.9 and Table 4.10. Results indicate insignificant amount of changes in lattice spacing while comparing the weld nugget to the base metal. XRD results show a higher space lattice reduction in the TMAZ region compare to other weld zones. The reduction of space lattice within the TMAZ indicates a slight compression within the region which was due to centrifugal forces during the stirring action. Peak intensity in the weld nugget and

TMAZ were also slightly lower compare to the HAZ and the base metal. Peak intensity reduction was caused by the partial phase dissolution within the weld nugget and the TMAZ. Phase dissolution occurred due to the effects of intense plastic deformation that arose during the welding process.

Table 4. 9 Lattice spacing analysis for CNC milling Bridgeport weld sample

| D-spacing (nm) | | |
|---------------------|---------------|----------|
| Cross section Zones | Aluminum Peak | SiC peak |
| Base Metal | 2.32175 | 2.50602 |
| HAZ | 2.32636 | 2.50064 |
| TMAZ | 2.31261 | 2.48994 |
| Weld Nugget | 2.32636 | 2.50602 |

Table 4. 10 Lattice spacing analysis for MTS FSW machine welded sample

| D-spacing (nm) | | |
|---------------------|---------------|----------|
| Cross section Zones | Aluminum Peak | SiC peak |
| Base Metal | 2.34008 | 2.5203 |
| HAZ | 2.33994 | 2.51938 |
| TMAZ | 2.33918 | 2.51941 |
| Weld Nugget | 2.34067 | 2.52180 |

4.6 Chapter Summary

The outcomes of the research work were presented in this chapter. The chapter begins with macrostructure and mechanical analysis on CNC milling Bridgeport followed by microstructure and mechanical analysis on MTS FSW machine welded samples. Finally, welded samples with the same welding parameters were compared from both machines.

The chemical composition of the weldment was analyzed using EDX techniques. SEM micrograph was used to characterize the weld microstructure. Microstructure analysis was carried out to detect welding defects and also to examine the density and distribution of SiC particles within the weld zones. Subsequently, mechanical testing was conducted on the base metal samples and the welded samples. Tensile test and Vickers micro-hardness tests were conducted to determine the mechanical property. XRD was also conducted to detect any phase changes and also to identify development of stress by considering the d-spacing.

CHAPTER 5

CONCLUSION AND RECOMMENDATIONS

5.1 Chapter overview

This chapter summarizes the findings of this research by providing overall conclusion of the thesis and suggestions for future research.

5.2 Conclusion

Several conclusions can be drawn from this study.

1. Friction stir welding on aluminum 6092/SiC/25p/T6 plate was successfully implemented using CNC milling Bridgeport and MTS FSW machine. Welding of AMMC plates using MTS FSW machine was more reliable compared to CNC milling Bridgeport. This was due to the capability of MTS FSW machine to hold high machine loading and tool tilting.
2. Microstructure analysis also shows different results when compared between CNC milling Bridgeport welded sample and MTS FSW machine welded sample. Result shows homogenous and higher amount of fine SiC particles distribution in the MTS FSW machine welded sample compared to the CNC milling Bridgeport sample. Better microstructure results in the MTS FSW machine was due to higher downward force exhibited from the machine when compared to the CNC milling Bridgeport. Superior microstructure properties resulted in increased weld strength and elongation to failure in the MTS FSW machine welded sample. However, these comparisons were only able to be conducted using lower tool traverse speed, higher tool rotation and un-tilted tool due the lower adaptability of the CNC milling Bridgeport to conduct FSW process.

3. Mechanical analyses show that welding through FSW reveals retained weld strength when compared to the base metal. Further testing also highlights an increased material hardness in the weld region when compared to the base metal. Hardness test also reveals an unsymmetrical hardness reading within the weld nugget. It shows a gradual increase of weld hardness when approaching the advancing side of the weld.
4. Microstructure examinations reveal that FSW causes extensive changes in the morphology of the material. Welding of the material through FSW causes redistribution and breaking of the SiC particulate (reinforcement material). An unsymmetrical distribution of SiC particulates was detected where the highest concentration of SiC particulates was found in the advancing side of the weld. XRD analysis reveals that the welding retained the material original phases but some stresses were induced on to the material especially within the TMAZ region.
5. Welding parameters also proved to be crucial in influencing the resultant weld properties. Macrostructure analysis shows the high influence of the weld parameters on the quality of the welding itself. Optimal welding parameters are crucial to supply adequate heat and stirring forces to ensure a defect free weld. The result showed that using lower tool speed and tool rotation guarantee adequate material mixing which contributes to a more homogenous spread of reinforcement particles within the weld nugget. Mechanical analysis shows that optimal welding strength is reached by using lower tool traversal and lower tool rotation. Vicker's hardness test showed that decrease in hardness value was attributed to increase in tool traverse speed and using un-tilted tool during the welding process.

5.3 Recommendations

It is recommended that further analysis should be performed to relate fine SiC particle dispersion with the dislocation density by using tunnel electron microscope (TEM). TEM micrograph technique could also be used to determine grain sizing in the weld nugget. Grain sizing analysis is critical in understanding the changes that FSW brings to the welded joint. Research work should also be carried out in correlating the tool geometry to the weld quality.

REFERENCE

- [1] Suraj Rawal, Metal Matrix Composite for Space Application, JOM 53 (4) (2001), pp 14-17.
- [2] S. Durante, G. Rutelli, F. Rabezzana, "Aluminum-based MMC machining with diamond-coated cutting tools", Surface and Coatings Technology 24th International Conference on Metallurgical Coatings and Thin Films, Volumes 94-95, pp.632-640, 1997.
- [3] Messler, Robert W. (1999). Principles of welding : processes: John Wiley & Sons, Inc.
- [4] Available: http://en.wikipedia.org/wiki/Friction_stir_welding, retrieved on 7th August 2012.
- [5] Nakata Kazuhiro, "New Material Need the Help of New Joining Technique" Trans.
- [6] C.B. Lin, C.K Mu, W.W. Wu, and C.H. Hung The Effect of Joint Design and Volume Fraction on Friction Welding Properties of A360/SiC (p) Composites Welding j. 78(100-108). 1999.
- [7] Alexander Evans, Christopher San Marchi, Andreas Mortensen (2003). Metal Matrix Composites in Industry: An Introduction and a Survey. Kluwer Academic Publishers.
- [8] Wayne M. Thomas, Edward D. Nicholas, James C. Needham, Michael G. Murch, Peter Temple-Smith, Christopher J. Dawes. (1995). US Patent 5, 460, 317.
- [9] Zhang, Y.N., Cao, X., Larose, S., Wanjara, "P. Review of tools for friction stir welding and processing", Canadian Metallurgical Quarterly 51 (3), pp. 250-261, 2012.
- [10] Wayne M. Thomas, Edward D. Nicholas, James C. Needham, Michael G. Murch, Peter Temple-Smith, Christopher J. Dawes. (1995). US Patent 5, 460, 317.

- [11] Hisaichi Ohnabea, Shoju Masakia, Masakazu Onozuka, Kaoru Miyaharab, Tadashi Sasab “Potential application of ceramic matrix composites to aero-engine Components”, *Composites: Part A Applied Science and Manufacturing* 30, pp. 489–496, 1999.
- [12] T.W. Nelson, H. Zhang, T. Haynes, in: *Proceedings of the Second Symposium on Friction Stir Welding*, Gothenburg, Sweden, June 2000.
- [13] R.A. Prado, L.E. Murr, D.J. Shindo, K.F. Sota, *Scripta Mater.* 45.2001. 75.
- [14] R.S. Mishraa, Z.Y. Ma, “Friction stir welding and processing”, *Materials Science and Engineering R* 50, pp. 1–78, 2005.
- [15] Lee, J.A., R.W. Carter and J. Ding. National Aeronautics and Space Administration. *Friction Stir Welding of Aluminum Metal Matrix Composites (MSFC Center Director’s Discretionary Fund Final Report, Project No. 98-09)*. Washington: GPO, 1998.
- [16] Benji Maruyama and Warren H. Hunt, Jr. *Discontinuously Reinforced Aluminum: Current Status and Future Direction*.
- [17] O. Lorrain, V. Favier², H. Zahrouni³, D. Lawrjaniec⁴ “Friction Stir Selding using Unthreaded Tools: Analysis of the Flow”, *Int J Mater Form* Vol. 3 Suppl 1, pp.1043-1046, 2010.
- [18] G.Buffa, J. Hua, R. Shiypuri, L. Fratini, “ Continuum based FEM model,” *Mater. Sci.Eng. A*419, pp. 381 – 388, 2006.
- [19] ZHANG Hong-wu, ZHANG Zhao, BIE Jun, ZHOU Lei and CHEN Jin-tao, “Effect of viscosity on material behavior in friction stir welding process”*Trans. Nonferrous Met.SOC. China* 16, pp.1045-1052, 2006.
- [20] Olivier Lorrain, Véronique Favier, Hamid Zahrounic, Didier Lawrjaniec, “Understanding the material flow path of friction stir welding process using unthreaded tools”,*Journal of Materials Processing Technology* 210 ,pp. 603–609, 2010.

- [21] Varuzan Kevorjikan, “Developments of Al MMC Composite for Automotive Industry”. Deformation and Structure of Metals and Alloys.(YAME). 2002.
- [22] Jacky C. Prucz, Samir N. Shoukry, Gergis W. William. (2005, August).“ Innovative Structural and Joining Concepts for Light weight Design of Heavy Vehicle Systems. US Department of Energy Freedom CAR and Vehicle Programs.” West Virginia University [Online.
- [23] Yan-hua Zhao T, San-bao Lin, Lin Wu, Fu-xing Qu,“The influence of pin geometry on bonding and mechanical properties in friction stir weld 2014 Al alloy”, Materials Letters 59,pp. 2948 – 2952, 2005.
- [24] 2012., Available: <http://www.freepatentsonline.com/6669075.html> retrieved on 7th August.
- [25] A. De2, H. K. D. H. Bhadeshia3 and T. DebRoy*1,"Review: friction stir welding tools",Science and Technology of Welding and Joining 2011 VOL 16 NO 4, pp 325-342, 2012.,
- [26] T.W. Nelson, H. Zhang, T. Haynes, in: Proceedings of the Second Symposium on Friction Stir Welding, Gothenburg, Sweden, June 2000.
- [27] Liu G, Murr LE, Niou CS, McClure JC, Vega FR. “Microstructural aspects of the friction-stir welding of 6061-T6 aluminum”. Scripta Mater 37(3), pp. 355–61,1997.
- [28] A.L. Etter, T. Baudin, N. Fredj, R. Penelle, “Recrystallization mechanisms in 5251 H14 and 5251O aluminum friction stir welds”, Materials Science and Engineering A 445–446, pp. 94–99, 2007.
- [29] D.M. Rodrigues, A. Loureiro, C. Leitao, R.M. Leal, B.M. Chaparro and P. Vilaça ,“Influence of friction stir welding parameters on the micro structural and mechanical properties of AA 6016-T4 thin welds”, Materials & Design. 30(6), pp. 1913-1921, 2008.

- [30] A.M Gaafer, T.S. Mahmoud, E.H. Mansour, “Microstructural and mechanical characteristic of AA7020-O Al plates joined by Friction Stir Welding” ,Materials Science and Engineering: A 527 (27-28), pp. 7424-7429,2010.
- [31] M. Jayaraman, R. Sivasubramanian , V. Balasubramanian ,“Establishing relationship between the base metal properties and friction stir welding process parameters of cast aluminium alloys”, IndiaMaterials and Design 31,pp. 4567–4576, 2010.
- [32] International, Rajiv S. Mishra (2007).Friction stir welding and processing: ASM.
- [33] L.M. Marzoli, A.v. Strombeck , J.F. Dos Santos , C. Gambaro , L.M. Volpone (2006), “Friction stir welding of an AA6061/Al₂O₃/20p reinforced alloy”, Composites Science and Technology 66 (2) 363-371.
- [34] Yang, Y. K., Dong, H., Cao, H., Chang, Y. A., and Kou, S.,“Liquation of Mg alloys in friction-stir spot welding”, Welding Journal 87, pp. 167-s - 177-s, 2008.
- [35] Available: http://en.wikipedia.org/wiki/Composite_material, retrieved on 7th August 2012.
- [36] Zhang, Y.N., Cao, X., Larose, S.,Wanjara, “P.Review of tools for friction stir welding and processing”, Canadian Metallurgical Quarterly 51 (3), pp. 250-261, 2012.
- [37] Yang, Y. K., Dong, H., Cao, H., Chang, Y. A., and Kou, S.,“Liquation of Mg alloys in friction-stir spot welding”, Welding Journal 87, pp. 167-s - 177-s, 2008.
- [38] Chen, Yong-Lai, Shaban, A., Yu, L. G., Wang, Hua Ming Fu-Xi Gan, Horst Weber, Zaiguang Li and Qingming Chen, “Laser beam welding of SiC-particle-reinforced aluminum metal matrix composite”, International Conference on Industrial Lasers, Proc. SPIE Vol. 3862,.
- [39] Available : <http://en.wikipedia.org/wiki/Liquation>, retrieved on 7th August 2012.
- [40] G. Cao and S. Kou, "Friction Stir Welding of 2219 Aluminum: Behavior of α (Al₂Cu) particles", supplement to the Welding Journal, pp 1-s - 8-s, 2005.

- [41] Chen, Yong-Lai, Shaban, A., Yu, L. G., Wang, Hua Ming Fu-Xi Gan, Horst Weber, Zaiguang Li and Qingming Chen, "Laser beam welding of SiC-particle-reinforced aluminum metal matrix composite", International Conference on Industrial Lasers, Proc. SPIE Vol. 3862,.
- [42] H. M. Wang, Y. L. Chen and L. G. Yu, "In-situ' weld-alloying/laser beam welding of SiCp/6061Al MMC", Materials Science and Engineering A293 (1-2), pp.1-6, 2000.
- [43] D. Storjohann, O.M. Barabash, S.S Babu, S.A. David , P. S. Sklad, E. E. Bloom "Fusion and Friction Stir Welding of Aluminum-Metal-Matrix Composite", Metallurgical and Materials 36 (11) 3237-3247, 2005.
- [44] Iuri Boromei, Lorella Ceschini, Alessandro Morri, Gian Luca Garagnani, "friction stir welding of aluminium based composites reinforced with al₂o₃ particles: effects on microstructure and charpy impact energy", Metallurgical Science and Technology.
- [45] Hu'seyin Uzun, "Friction stir welding of SiC particulate reinforced AA2124aluminium alloy matrix composite", Materials & Design Volume 28, Issue 5, pp.1440-1446, 2007.
- [46] L.H. Dai, L.F. Liu, Y.L. Bai, "Effect of particle size on the formation of adiabatic shear band in particle reinforced metal matrix composites", Materials Letters 58 pp.1773– 1776, 2004.
- [47] J.M. Root, D.P. Field, T.W. Nelson, "Crystallographic Texture in the Friction-Stir-Welded Metal Matrix Composite Al6061 with 10 volPct Al₂O₃", Metallurgical and Materials Transactions A: Physical Metallurgy and Materials Science 40(9),pp2109-2114, 2009.
- [48] P. Cavaliere a, G.L. Rossi, R. Di Sante , M. Moretti,"Thermoelasticity for the evaluation of fatigue behavior of 7005/Al₂O₃/10p metal matrix composite sheets joined by FSW", International Journal of Fatigue 30 (1) pp. 198-206, 2007.

- [49] Jian-Qing Su, Tracy W. Nelson , Colin J. Sterling, “Microstructure evolution during FSW/FSP of high strength aluminum alloys” *Materials Science and Engineering A* 405, pp. 277–286, 2005.
- [50] P. Cavalierea, R. Nobilea, F.W. Panellaa, A. Squillaceb, “Mechanical and microstructural behaviour of 2024–7075 aluminium alloy sheets joined by friction stir welding” *International Journal of Machine Tools & Manufacture* 46 , pp. 588–594, 2006.
- [51] A.H. Feng, B.L. Xiao, Z.Y. Ma, “Effect of microstructural evolution on mechanical properties of friction stir welded AA2009/SiCp composite” , *China Composites Science and Technology* (68), pp. 2141–2148, 2008.
- [52] Dinaharan, I., Murugan, N., “Effect of friction stir welding on microstructure, mechanical and wear properties of AA6061/ZrB 2 in situ cast composites”, *Materials Science and Engineering A* 543 , pp. 257-266, 2012.
- [53] H.L. Hao, D. R. Ni , H. Huang , D. Wang , B. L. Xiao , Z. R. Nie , Z. Y. Ma, "Effect of welding parameters on microstructure and mechanical properties of friction stir welded Al–Mg–Er alloy", *Materials Science & Engineering A* 559, 889–896, 2013.
- [54] X.G. Chen, M. da Silv, ,P. Gougeon, L. St-Georges “Microstructure and mechanical properties of friction stir welded AA6063–B4C metal matrix composites, ”*Materials Science and Engineering: A Volume 518, Issues 1–2* , pp. 174–184, 2009.
- [55] W.L. Stelwag Jr., and T.J. Lienert, “Friction stir welding of aluminum metal-matrix Composites”, Cooperative research program (CRP), Progress report PR0109, May 2001, (Edison Welding Institute Columbus, Ohio).
- [56] Govindaraju, M., Kandasamy, J., ManzoorHussain, M. and PrasadaRao, K. 2012. Some Aspects of Cross Butt Friction Stir Weldments of Rare Earth Magnesium Alloys: Novel Attempts in Friction Stir Welding. *Journal of Applied Sciences* 12(10): pp. 1043 – 1047,.

- [57] S. Gopalakrishnan, N. Murugan , “Prediction of tensile strength of friction stir Welded aluminium matrix TiCp particulate reinforced composite”,*Materials and Design*, 2010.
- [58] K. Elangovan, V. Balasubramanian, “Influences of pin profile and rotational speed of the tool on the formation of friction stir processing zone in AA2219 aluminium alloy”, *Materials Science and Engineering A* 459 pp. 7–18, 2007.
- [59] S. Gopalakrishnan, N. Murugan , “Prediction of tensile strength of friction stir Welded aluminium matrix TiCp particulate reinforced composite”,*Materials and Design*, 2010.
- [60] A Thangarasu, N. Murugan, I Dinaharan, and S. J Vijay, "microstructure and microhardness of AA1050/TiC surface composite fabricated using friction stir processing", *Sadhanā* (37), , pp. 579–586, 2012.
- [61] H.L. Hao, D. R. Ni , H. Huang , D.Wang , B. L. Xiao , Z. R. Nie , Z. Y.Ma, "Effect of welding parameters on microstructure and mechanical properties of friction stir welded Al–Mg–Er alloy", *Materials Science & Engineering A* 559, 889–896, 2013.
- [62] Yahya Bozkurt, Hu seyin Uzun, Serdar Salman, “Microstructure and mechanical properties of friction stir welded particulate reinforced AA2124/SiC/25p–T4 composite”, *Journal of Composite Materials* 0(0), pp. 1–9, 2011.
- [63] Chaitanya Sharma, Dheerendra Kumar Dwivedi, Pradeep Kumar, "Effect of welding parameters on microstructure and mechanical properties of friction stir welded joints of AA7039 aluminum alloy", *Materials and Design* 36 379–390, 2012.
- [64] Min-Su HAN, Seung-Jun LEE, Jae-Cheul PARK, Seok-Cheol KO, Yong-Bin WOO, Seong-Jong KIM, "Optimum condition by mechanical characteristic evaluation in friction stir welding for 5083-O Al alloy",*Trans. Nonferrous Met. Soc. China* 19, s17–s22, 2009.

- [65] S.J. Vijay, N. Murugan, "Influence of tool pin profile on the metallurgical and mechanical properties of friction stir welded Al-10 wt.% TiB₂ metal matrix composite", *Materials and Design* 31, pp. 3585–3589, 2010.
- [66] Olivier Lorrain, Véronique Favier, Hamid Zahrouni, Didier Lawrjaniec, "Understanding the material flow path of friction stir welding process using unthreaded tools", *Journal of Materials Processing Technology* 210, pp 603–609, 2010.
- [67] P. Janaki Ramulu, R. Ganesh Narayanan, Satish V. Kailas Influence of tool rotation speed and feed rate on the forming limit of friction stir welded AA6061-T6 sheets", *Journal of Mechanical Engineering Science*, 2012.
- [68] Yuh J. Chao, X. Qi, W. Tang, "Heat Transfer in Friction Stir Welding—Experimental and Numerical Studies", *Transactions of the ASME* 125, pp. 138-145, 2003.
- [69] Available:<http://machinedesign.com/article/a-better-way-to-cast-aluminum-1025>, retrieved on 20th September 2012.
- [70] C. Hamiltona, S. Dymekb, A. Sommersa, "A thermal model of friction stir welding in aluminum alloys", *International Journal of Machine Tools & Manufacture* 48, pp. 1120–1130, 2008.
- [71] A.P. Reynolds, "Flow visualization and simulation in FSW", *Scripta Materialia* 58 ,pp.338–342,2008.
- [72] A. Arora, A. Deand T. Deb Roy, "Toward optimum friction stir welding tool shoulder diameter", *Scripta Materialia* 64 pp. 9–12,2011.
- [73] M. Ericsson, R. Sandström, "influence of welding speed on the fatigue of friction stir welds, and comparison with MIG and TIG", *International Journal of Fatigue* 25, pp.1379–1387, 2003.

- [74] Storjohann, S.S. Babu, S.A. David and P. Sklad, "Friction stir welding of aluminum metal matrix composites". 4th International Symposium on Friction Stir Welding Utah-USA. 2003.
- [75] Available :<http://www.metalravne.com/selector/steels/utopmo2.html>. retrieved on 7th August 2012.
- [76] Ambient temperature, ISO/TTA 2:1997. Tensile test for discontinuously reinforce metal matrix composite at ambient.

APPENDIX A

Vicker's hardness test for welded samples

